AFIT/GE/ENG/93D-27

AD-A274 073

EVALUATION OF AN
ACOUSTIC CHARGE TRANSPORT (ACT) DEVICE
FOR ADAPTIVE INTERFERENCE SUPPRESSION
IN SPREAD SPECTRUM COMMUNICATIONS SYSTEMS

THESIS

Michael S. Mills, Captain, USAF

AFIT/GE/ENG/93D-27

93-31026

Approved for public release; distribution unlimited

93 12 22 139

Best
Available
Copy

The views expressed in this thesis are those of the author and do not reflect the official policy or position of the Department of Defense or the U.S. Government.

Accesion For	
NTIS CRA&I	✓
DTIC TAB	☐
Unannounced	☐
Justification	
By	
Distribution /	
Availability Codes	
Dist	Avail and / or Special
A-1	

EVALUATION OF
AN ACOUSTIC CHARGE TRANSPORT (ACT) DEVICE
FOR ADAPTIVE INTERFERENCE SUPPRESSION
IN SPREAD SPECTRUM COMMUNICATIONS SYSTEMS

THESIS

Presented to the Faculty of the Graduate School of Engineering

of the Air Force Institute of Technology

Air University

In Partial Fulfillment of the

Requirements for the Degree of

Master of Science in Electrical Engineering

Michael S. Mills, B.S.E.E.

Captain, USAF

December, 1993

Acknowledgments

I would like to thank Larry Gutman and Capt Carl Williams of the Systems Avionics Division of the Avionics Directorate at Wright Laboratories: Larry Gutman for providing the invigorating thesis topic and supplying information as to what he and his associates have already done with other versions of the ACT device related to this thesis topic; and Capt Williams for providing the spread spectrum generator needed for this thesis. I would also like to thank the above for making the CSEL facility available to me, even though I could not use it for my thesis effort.

I would like to thank my thesis committee for continually spurring me on to completion: Lt Col Robert Morrow, Maj Mark Mehalic, Dr. Victor M. Bright, all faculty members at AFIT; and Maj Robert Williams from the Mission Avionics Division, Avionics Directorate of Wright Labs. Special thanks to Victor Bright for introducing me to an associate of his at the Electronic Decisions Inc.(EDI), Div. of Comlinear Corp, Dr AJ Vigil. It was through this contact that I was able to obtain workable ACT devices without which this thesis could not have been conducted. The sacrifices of Dr Vigil to make many personal visits to AFIT to provide the ACT PTFs and valuable assistance is especially noteworthy and much appreciated. I would also like to thank Dr Vigil for inviting me to EDI so that I could use their facilities to obtain critical data in this research effort.

Finally, I would like to most of all thank my wife, Tamara, for being so longsuffering during this time. I would also like to thank my newborn son, Jonathan, for his cooperation in being born during the Thanksgiving break of my difficult Fall quarter.

ii

Table of Contents

iii

iv

List of Figures

List of Tables

AFIT/GE/ENG/93D-17

Abstract

Analytical results have shown that adaptive filtering can be a powerful tool for the rejection of narrowband interference in a direct sequence spread spectrum receiver. However, the complexity of adaptive filtering hardware has hindered the experimental validation of these results. This thesis describes a unique adaptive filter architecture for implementing the Widrow-Hoff Least-Mean-Square (LMS) algorithm using two state-of-the-art Acoustic Charge Transport (ACT) Programmable Transversal Filters (PTFs). Signal-to-noise ratio improvement measurements demonstrate the effectiveness of the adaptive filter for suppressing single- and dual-tone jammers at jammer-to-signal ratios (JSRs) of up to 30 dB. It is shown that the ACT adaptive interference rejection system can consistently produce 55 dB notch depths with 3-dB bandwidths as low as 300 kHz with minimal degradation to the spread spectrum signal. It is also shown that the adaptive system can eliminate single tone jammers at any frequency within the spread spectrum bandwidth at any of 10, 20, or 30 dB JSRs within 10-15 iterations of the adaptive algorithm. The only drawback with the adaptive system as tested is the amount of time taken to perform an iteration because of the requirement to update the PTF tap weights sequentially. Suggestions are given as to how this particular parameter of the adaptive interference system could be optimized.

EVALUATION OF AN

ACOUSTIC CHARGE TRANSPORT (ACT) DEVICE

FOR ADAPTIVE INTERFERENCE SUPPRESSION IN

SPREAD SPECTRUM COMMUNICATIONS SYSTEMS

I. Introduction

This chapter outlines a procedure for evaluating the performance of an Acoustic Charge Transport (ACT) technology implementation of a Programmable Transversal Filter (PTF). The chapter begins by introducing the problem electromagnetic conflict poses in disrupting secure and reliable communications and the role of PTFs in counteracting the interference threat. The objective, scope, and approach are then presented along with a listing of the necessary resources, both hardware and software, to accomplish the thesis objective. Finally, the chapter concludes with the organizational layout for the final thesis document.

1.1 Background

The purpose of any communication system is to transmit information or data with an acceptable probability of bit error or signal-to-noise ratio. In an ideal environment, a channel bandwidth approximately equal to the data rate is sufficient to transmit binary coded information. However, in a noisy, crowded, or hostile environment, a number of techniques may be implemented in order to increase the security and antijam characteristics of a communication system: power control techniques, spatial discrimination techniques, spread spectrum modulation, and interference suppression.

Increasing the power level of a communications transmitter, by either increasing the peak power or extending the duty cycle, to assure an inherent antijam capability (otherwise known as brute-force transmission), is a detriment in light of today's stealthy platforms. The need to hide one's signal is vital. What is preferable

is the technique of adaptive power control, in which the transmitter output power is automatically adjusted to the minimum signal-to-noise ratio required to maintain effective communications [1]. This technique provides jam resistance without degrading host low observable characteristics.

Spatial discrimination techniques include adaptive null steering antennas and high-gain directional antennas. Together, they mean placing nulls of the receivers antenna gain pattern in the direction of enemy jammers in order to avoid front end saturation of the receiver, and increasing the gain in the direction of the desired signal.

Spread spectrum communication is a technique whereby the bandwidth of the transmitted waveform is intentionally made wider (typically much wider) than is necessary to transmit the information over the channel. The advantage of spread spectrum is that it makes the system less sensitive to various interfering signals. These interfering signals might arise from intentional jamming, multipath, or multiple users coexisting on the same bandwidth, for example. A conventional communication system would typically not be able to function properly in the presence of such interference; hence, the need for spread spectrum [2].

Two common spread spectrum schemes are direct sequence (DS) and frequency hopping (FH). Direct sequence spreading, the focus of this research, is achieved by modulo-2 addition of a binary message sequence and a higher rate pseudorandom binary sequence. The result is a sequence at the pseudorandom sequence rate which is used to phase modulate a sinusoidal carrier signal. This technique spreads the energy of the signal over a large bandwidth so that it could be hidden in the noise levels of unintended receivers. Hence the signals have a low-probability-of-intercept while increasing the resistance to interference and jamming. Frequency hopping consists of hopping a narrowband signal, via frequency-shift keying using a large set of frequencies, over a large bandwidth with a pseudorandom pattern.

The inherent processing gain of a spread spectrum system will, in many cases, provide the system with a sufficient degree of interference rejection capability. However, at times the interfering signal is powerful enough so that even with the advantage that the system obtains by spreading the spectrum, communication becomes effectively impossible. In some of these cases, the interference immunity can be improved significantly

by using signal processing techniques which complement the spread spectrum modulation. If the interference is relatively narrowband compared with the bandwidth of the spread spectrum waveform, then the technique of interference suppression by the use of notch filters often results in a large improvement in system performance [3].

The spectral filtering techniques mentioned above most often make use of tapped delay line (or transversal) filter structures to implement the programmable notch filters. These PTFs can be implemented in a variety of device technologies such as surface acoustic wave (SAW) devices, charge-coupled devices (CCDs), high-speed digital signal processing (DSP) techniques (via VLSI or VHSIC circuits), or with a relatively new device technology called acoustic charge transport (ACT).

1.2 Objective

The objective of this research is to examine the effectiveness of using the ACT PTF for adaptive interference suppression of narrowband jammers in a direct sequence spread spectrum system. It is desirable to achieve a 1 MHz (or less) 3-dB notch bandwidth with 40-50 dB of suppression such that an acceptable signal-to-noise ratio (and hence, probability of bit error) is maintained in the reception of the transmitted messages. Also, the convergence of the adaptive filter should occur within the fewest number of iterations, consistent with application in real-time systems.

1.3 Scope and Assumptions

Since the single-tone or continuous-wave (CW) jammer is, perhaps, the easiest jamming signal to generate and is relatively effective in disrupting direct sequence signals, this study evaluates the capability of the ACT PTF for adaptive interference suppression of narrowband (tone) jammers. The following jamming signals scenarios are the focus of this report in their order of examination:

(i) fixed single tone

(ii) fixed multiple tones

(iii) narrowband Gaussian noise or narrowband FM signals

(iv) swept tone

(v) fixed tone plus swept tone

Of particular interest is the effectiveness of the ACT suppression filter in adapting to a CW jammer located at the center frequency of the direct sequence signal, since this is where the jammer achieves maximum effectiveness in disrupting communications. This is because at the center frequency, the maximum jammer energy passes through the receiver's reference bandwidth.

The performance criteria for this report will focus primarily on the qualitative signal-to-noise ratios instead of the quantitative probability of bit error (P_b) analysis due to the complexity of the system setup necessary to achieve the P_b results. Therefore, signal correlation, code despreading, and data detection will not be performed.

Crucial to the effectiveness of the interference suppression in the spread spectrum system is the adaptive algorithm used to update the tap weights in the PTF. This test environment will examine the se of the Widrow-Hoff Least-Mean-Square (LMS) adaptive algorithm and the linear random search algorithm. The LMS algorithm is the best known and most easily implemented algorithm in a class of algorithms which implement an iterative solution to the Wiener-Hopf equation without making use of any *a priori* statistical information about the received signal. (The Wiener-Hopf equation determines the optimal tap weight settings for the particular PTF function.) The random search algorithm is easily implemented when access to the input signal samples is not possible, and is, therefore, useful at times when the LMS algorithm is not.

1.4 Approach

The approach in this thesis is to first perform hardware benchtesting of the proposed setup and compare the results with the expected theoretical results. The literature is replete with data revealing the desired results.

To ascertain how well the ACT PTF performs in suppressing the narrowband jamming signals listed in Section 1.3, the following system and adaptive interference suppression (AIS) filter measurements are recorded:

- pre-detection jammer-to-signal (JSR) ratio

- post-detection JSR

- AIS filter convergence rate or number of iterations

- AIS filter frequency response after adaptation

1.5 Resources

- *ACT PTF from Electronic Decisions Inc (EDI), Div. of Comlinear Corp.*(2 ea.) - (127 tap, 6-bit tap weight resolution) with 2 ea. SMA connectors and RS-232C 25-pin parallel daisy-chain cable;

- *W.A.V.E. System Software from EDI* (along with 386/486 IBM PC with 4 Mbytes RAM and coprocessor): Used to implement adaptive algorithm for tap weight vector updates;

- *A/D Converter Card w/ BNC connection*: 12-bit resolution, Intelligent Instruments/Burr Brown PCI-20001C family of carrier boards; card ROM switch (hex CD40));

- *LRS-100 Spread Spectrum Generator*: Generates up to 20 Mcps DS/SS signal with a maximum 40 dB R_c/R_b ratio (processing gain); maximum R16 length m-sequence; BPSK/QPSK/Gold/Burst signal format options;

- *Marconi 2022 Signal Generators* (3 ea.): Two were used to generate tone jamming signals; one to generate the carrier for the DS/SS signal;

- *Power Supplies*: +12V/−5V (ACT-PTFs and adaptive module), and ± 5V (A/D converter/LPF patch);

- *HP 70000/HP 70206A Spectrum Analysis System*: Used to view frequency spectra at all points in the system;

- *HP 8753B Network Analyzer/HP 85046A S-Parameter Test Set*: Used to develop frequency responses of ACT PTF after adaptation;

- *Tektronix 7854 Oscilloscope*: Used to verify PN sequence and to view JSR in time-domain;

- *Tektronix 7854 Oscilloscope*: Used to verify PN sequence and to view JSR in time-domain;

- *HP 7470A/7450A Plotters*: Used to plot frequency spectra from HP 70206A Spectrum Analyzer;

- *HP 10514A Mixer (.2-500 MHz)*: Used to suppress-carrier modulate the BPSK baseband signal;

- *HP 355 C/D VHF Attenuators*: Used to adjust the JSR conveniently between 10, 20, 30 dB;

- *Various attenuators*: Used to balance the jamming and DS/SS signals to allow for the adjustable JSRs;

- *MCL 15542 Splitter/Combiners (4 ea.)*;

- *90 MHz Lowpass Filters (LPFs) (2 ea.)*.

1.6 Sequence of Presentation

Chapter 2 presents an overview of prior work accomplished in interference rejection techniques as applied to direct sequence spread spectrum systems. This overview encompasses progress made in various filtering techniques and adaptive algorithms, leading up to and providing a basis for this research. Chapter 3 contains the theoretical background necessary to grasp an understanding of the complexity of the problem. It begins with a brief overview of direct sequence systems and the properties of the pseudorandom codes that make it possible. This is followed by the fundamentals of adaptive algorithms, focusing primarily on the least-mean-square (LMS) and linear random search (LRS) algorithms. Chapter 4 is devoted to the characteristics of the programmable transversal filter, especially the qualities of the ACT PTF since this technology is the focus of the thesis. Chapter 5 presents the specific testing arrangement, procedures, and results for the adaptive interference system. Chapter 6 summarizes the results of this thesis and provides recommendations for further study in this area of research.

II. Interference Suppression Techniques:

A Literature Review

This chapter examines the published literature on the interference rejection problem as it relates to direct sequence spread spectrum communications. Although the particular implementation of an adaptive interference suppressor in this study focuses on the use of the acoustic charge transport (ACT) programmable transversal filter (PTF), the literature contains only work with other device types. Therefore, they will be examined for purposes of background into the interference rejection problem and for comparisons with other device implementations. Since most of the previous researchers have used the least-mean-square (LMS) adaptive algorithm, articles which implemented this algorithm will be favored; however, other filtering techniques and algorithms will be presented as well.

The application of adaptive algorithms to mitigate signal processing chores has been prevalent since the early-1960's when Bernard Widrow and associates applied them to antenna arrays [23]. Specific implementation of adaptive algorithms for interference suppression in direct sequence spread spectrum systems has been investigated since the mid- to late-1970's.

Hsu and Giordano [4] have laid down the foundational work in interference suppression in spread spectrum systems. They were the first to determine that due to the nearly flat spectral characteristics of the pseudorandom sequence (uncorrelated in the short term—meaning the sequence shifted by one bit with respect to itself is uncorrelated), a highly-correlated narrow-band interference signal can be filtered out by using linear prediction techniques. Their digital whitening techniques were implemented using a transversal filter whose coe..ricients were selected by either a Wiener algorithm or a maximum entropy algorithm, as seen in Figure 1. They found that for strong narrowband interference in a poor signal-to-noise ratio (SNR) condition, significant performance gains from digital whitening could be accomplished. In their study, the performance of the interference suppression was measured in terms of SNR improvement *with* whitening compared to the SNR *without* whitening. In their experiments, all signals were represented at baseband in terms of their low-pass equivalents. The interference was modeled as a sum of fixed amplitude and fixed frequency tones with random

2-1
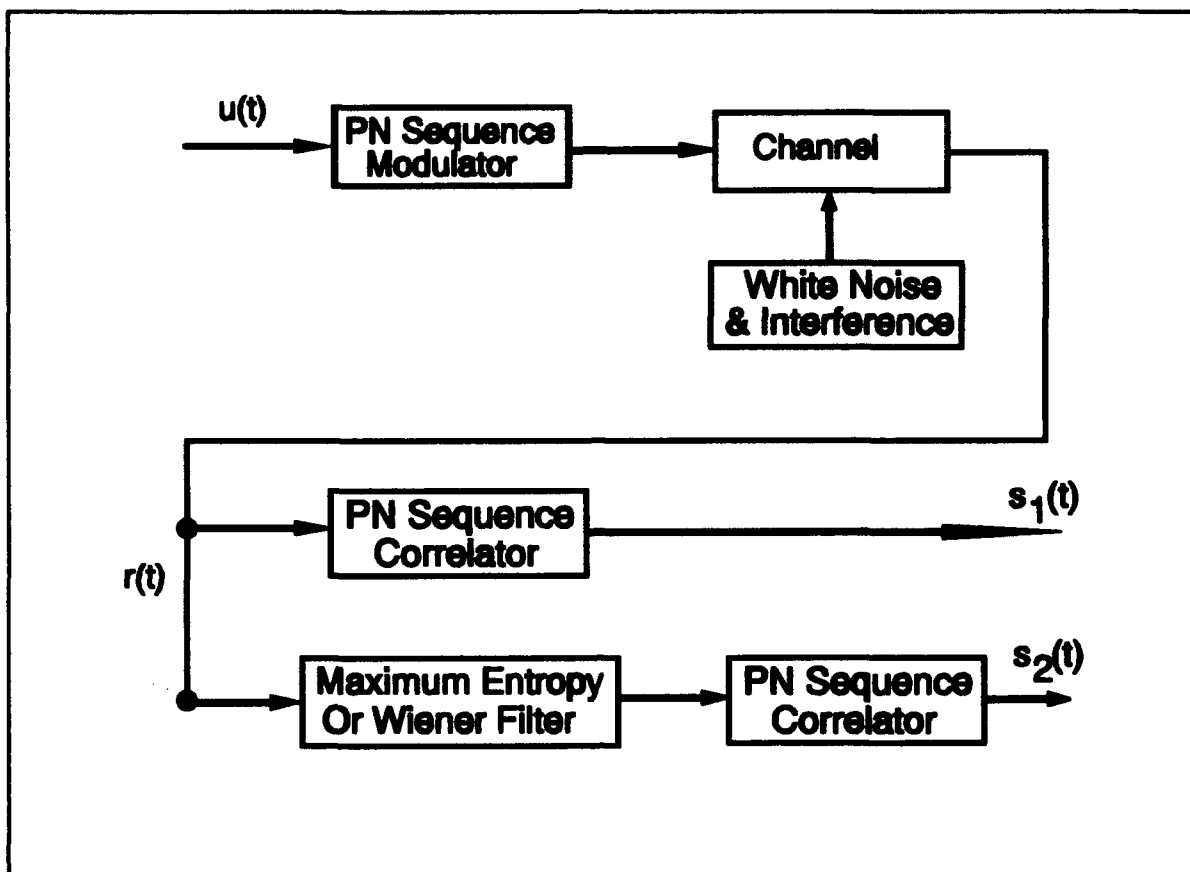
Figure 1 Hsu and Giordano's SS communications system model with interference suppression subsystems.

phases, as well as narrowband Gaussian interference. Both of their receiver models performed coherent detection and were assumed to be perfectly synchronized, with the digital whitening being done before correlation.

The Wiener filter was implemented recursively using a least-mean-square error criterion and a form of Levinson's algorithm in the actual computation. The maximum entropy whitening filter was based on an algorithm developed by Burg. The algorithm used a procedure for determining the prediction error filter coefficients directly from known data samples. An important feature of the Burg procedure is that no *a priori* estimate of the autocorrelation function is required.

Hsu and Giordano also established the theoretical SNR improvement calculations. The bandwidth of the interference for their experimentation was roughly one fifth of the bandwidth of the spread spectrum signal. They used either 10 or 100 tones uniformly spaced within the SS bandwidth.

Ketchum and Proakis [5] further improved the results of Hsu and Giordano by combining the interference rejection filter with its matched filter, resulting in an overall linear filter having a linear phase characteristic. In essence, the authors evaluated the effectiveness of the interference suppression as done in [4], but they further defined the performance of the SS receiver as measured in terms of the probability of error, which was obtained by applying a Gaussian assumption on the total residual noise and interference followed by Monte Carlo simulation. Figure 2 contains their probability of bit error results for a 4-tap filter with the matched filter and without the matched filter.
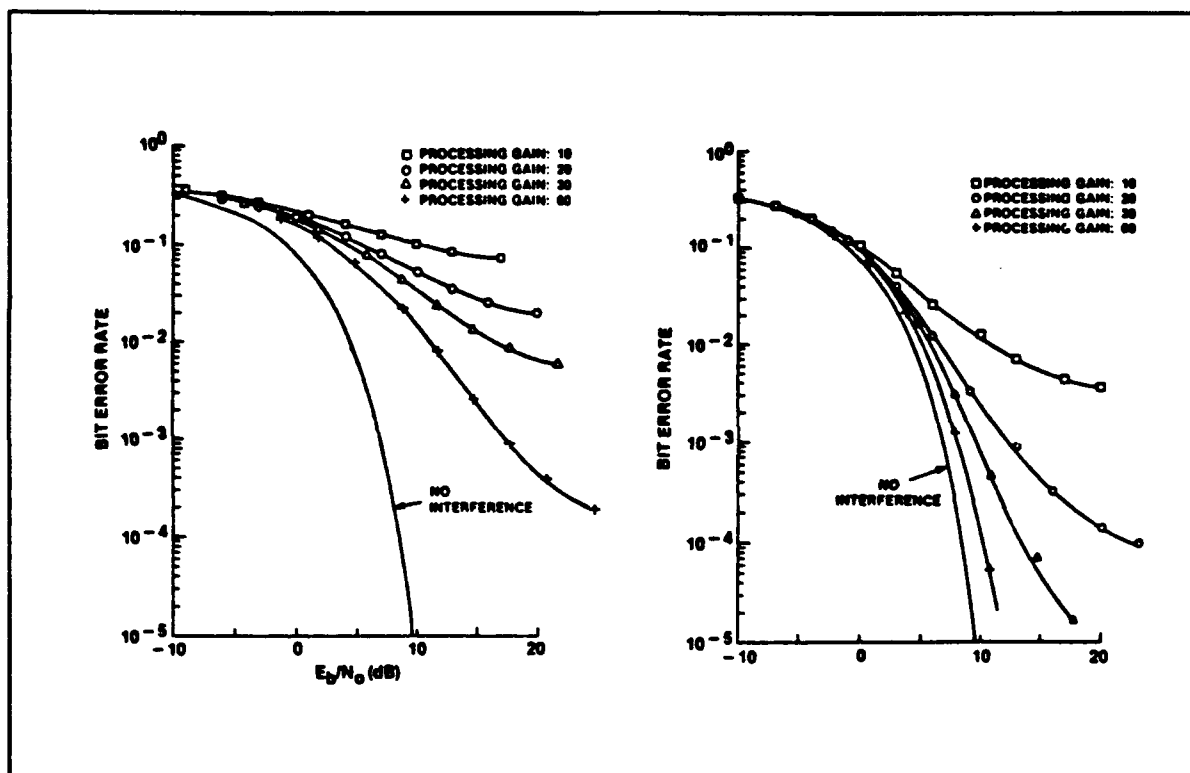
Figure 2 Bit error probability under the Gaussian assumption for 4-tap predictor (a) with no matched filter, (b) with matched filter [5].

Ketchum and Proakis also evaluated a number of algorithms for estimating and suppressing the narrowband interference. The algorithms were classified into two general categories. One was based on performing a spectral analysis on the received signal using the fast Fourier transform (FFT) algorithm. Depending on the spectral estimate obtained, a transversal filter was designed to suppress the interference. The

algorithms in the authors' second category were based on linear prediction, as was the case in [4]. An important aspect in their investigation was the size of the interference suppression filter (in terms of number of taps) required to handle multiple-band interference. They found that if the filter order (number of taps) is increased the frequency response improves, in terms of providing a deeper notch at the interfering tone frequencies and less attenuation in the frequency range between notches. They also demonstrated that a prediction filter having a number of coefficients (or taps) that is fewer than twice the number of interfering bands does nothing to suppress the interference.

Li and Milstein [6] examined two similar forms of estimation-type interference rejection filters. They compared the results of a transversal filter with two-sided taps versus the prediction error filters (with one-sided taps) previously described in [4,5]. Figure 3 reveals the differences in these two filter configurations. Whereas the linear prediction filter uses past signal samples to estimate the current input, the two-sided transversal filter uses "future" samples as well as past samples to estimate the current input. They found in this study that in most cases, the two-sided structure worked better than the one-sided structure in terms of the signal-to-noise improvement factor, especially if the frequency of the jamming tone is near the carrier frequency of the spread spectrum signal. The authors reported a couple of key conditions that should be met when using a prediction filter for interference rejection specifically for direct sequence signals. One is that the sample interval, T, should be equal to the chip duration. They also indicated that the period of the PN sequence should be sufficiently long so that the PN signal samples at different taps are approximately uncorrelated. They also found that the SNR improvement factor for the two-sided filter increased as the number of taps increased or as the input interference-to-signal power ratio J/S increased.

Another point that Li and Milstein made was that if the Widrow-Hoff LMS algorithm is used, because of the symmetry of the two-sided transversal filter, the samples on the $-k$th and kth taps could be added together first and then multiplied by the weight a_k. Because the number of variable weights is halved, the number of multiplications is reduced, achieving a simpler implementation.
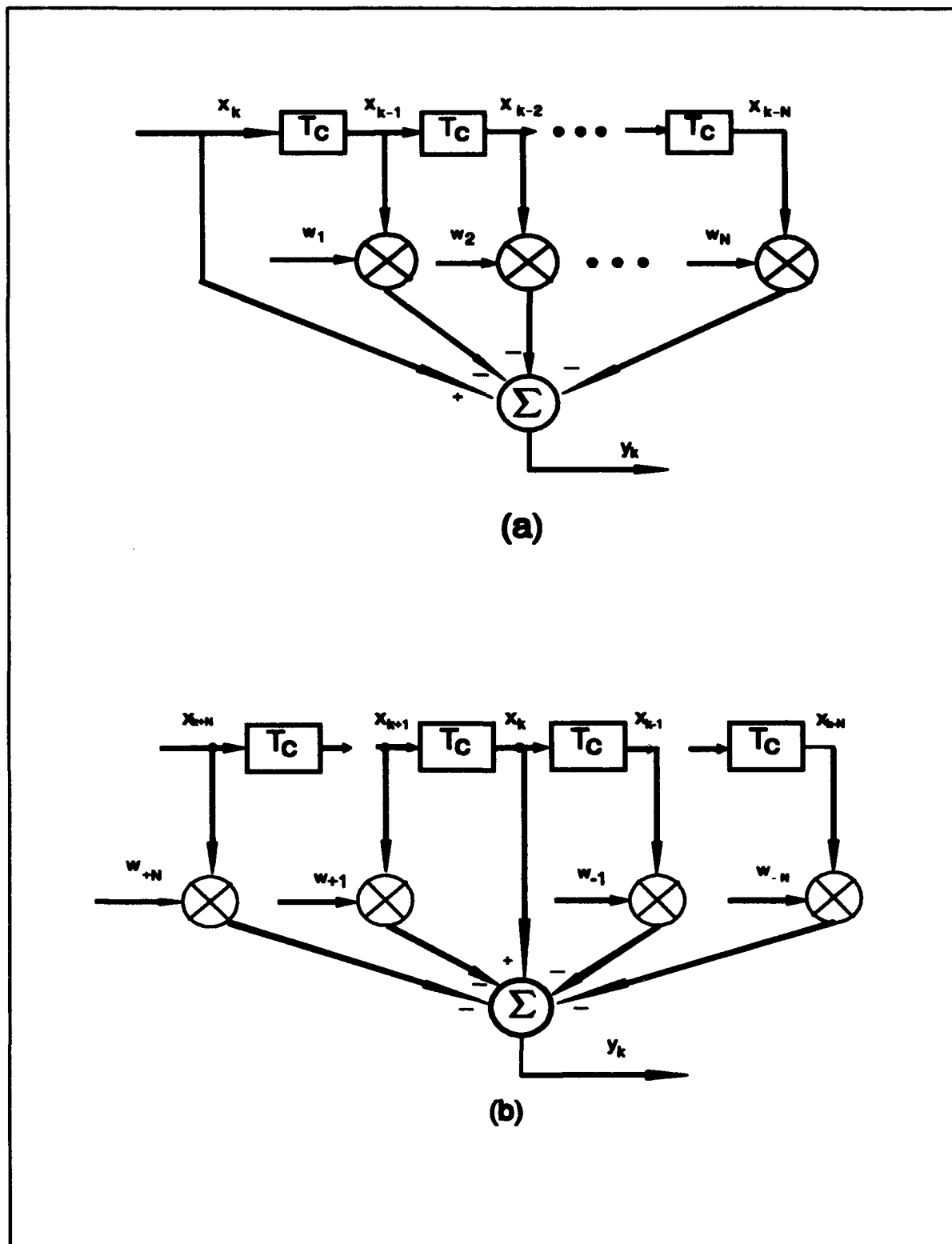
Figure 3 Transversal filter structures: (a) one-sided predictive filter, (b) two-sided interpolating filter.

Iltis and Milstein in [7] performed a stricter performance analysis of the narrowband interference rejection techniques already mentioned in [4-6]. They presented analytical expressions for the *exact* bit error rates for two direct sequence spread spectrum systems under the conditions of either tone or narrowband Gaussian interference.

Of particular relevance to this thesis effort is the work of Saulnier [8-11]. He has performed hardware implementations of interference suppression filters using three different transversal filter structures: charge transfer device (CTD), digital filter techniques, and surface acoustic wave (SAW) device. These three implementations were of the estimation-type adaptive filter. He has also examined the transform domain approach using FFTs.
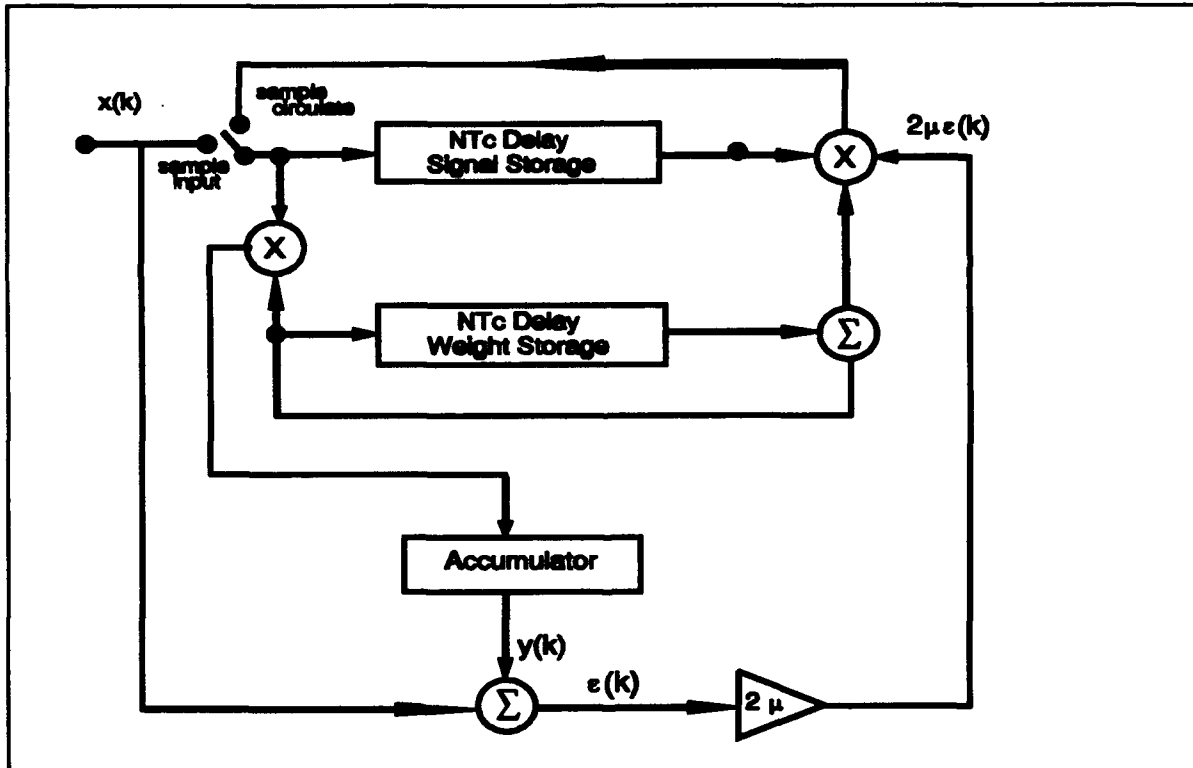
Figure 4 Block diagram of the "burst processing" adaptive LMS filter.

In [8] Saulnier, along with Das and Milstein, designed a CTD-based adaptive filter. The adaptive filter architecture implemented the Widrow-Hoff LMS algorithm using only two multipliers; a technique that could be used regardless of the filter order. This hardware simplification was achieved through the use of a "burst

processing" technique (Figure 4). A two-sided version of the adaptive filter constructed with the CTD's was used to suppress a single tone jammer where probability of error measurements demonstrated the effectiveness of the configuration. The test system configuration not only specified 16 tap weights, but also a 26.3 kHz sampling frequency and chip rate, and a 7-bit PN code.

The authors' motivation for using the burst processing technique stemmed from the cost and complexity of the required four-quadrant multipliers necessary to perform the $2N$ multiplications and the N storage elements required of an Nth order filter. The burst processing technique may also be employed if a software implementation of the LMS is chosen and access to the individual delayed signal samples is not possible. The authors show that this technique does not compromise the convergence time of the adaptive process; however, it does require N times the bandwidth of the conventional LMS hardware configuration. With the burst processing arrangement, a transversal filter is actually not needed; however, two identical wideband delay lines are required. The authors also warned that intersymbol interference (ISI) caused by the correlation inherent in the PN code is present in an interference suppression subsystem when the PN code length is shorter than the order of the filter.

Saulnier, Das, and Milstein followed this work with an identical setup with a digital hardware implementation instead of the CTD [9]. However, in this effort there was a variation on the type of jamming signals tested, such as single-tones, swept-tones, and narrowband Gaussian noise. Again, several important aspects of their test arrangement included processing the code at baseband, and obtaining chip and bit synchronization directly from the code generator. The authors also embark on a discussion between the selected convergence value, μ, in the LMS algorithm and the PN code balance of 1's and 0's since they affect filter transfer function. They also concluded that a small value of μ works best with a slowly swept frequency tone and, likewise, a larger μ is appropriate for faster swept tones.

Saulnier, Grant, and Das recently performed a hardware experimentation using a SAW-based adaptive filter to perform the interference suppression [10]. The primary advantage of using the SAW-based transversal filter is the availability of higher bandwidths and operating frequencies (correlation of the DS signal at RF). The

paper discussed the design and performance of an 8-tap LMS adaptive filter constructed using a SAW tapped-delay line with a carrier frequency of 300 MHz. The difference in this study is that a direct hardware implementation of the LMS algorithm was accomplished, as opposed to using the burst processing technique, or other similar implementation of the LMS algorithm.

Most of the references mentioned so far primarily conducted interference suppression in the time-domain using the estimation-type predictive or two-sided filter configurations. However, throughout the 1980's, work has been accomplished in the frequency-domain, otherwise known as transform-domain interference excisors [2,3,11-14]. Another paper conducts a comparison between implementations in the time and frequency domains [15]. In addition, two thorough review papers cover many of the areas of interest within the interference rejection domain of spread spectrum communications [2,3].

Regarding research at the Air Force Institute of Technology (AFIT), in 1982 2nd Lt Michael Shepard submitted a thesis on the performance of a PN spread spectrum receiver preceded by an adaptive interference suppression (AIS) filter [16]. Shepard simulated a SAW PTF operating in the 200-300 MHz band. The simulation included the modeling of the SAW device, filter tap weights, Applebaum and power inversion adaptive algorithms, and the filter fabrication and circuitry errors. In addition, the desired and interfering signals were generated in the simulator, passed through the AIS filter, and demodulated by a simulated matched filter. The system performance was determined by measuring the improvement in pre-detection signal-to-jammer ratio (SJR) and post-detection signal-to-jammer plus noise ratio (SJNR) provided by the AIS filter, and by computing the AIS filter convergence rate. Shepard was able to show that the filter provided sufficient null depth (up to 60 dB); however, the minimum obtained 3-dB notch bandwidth was only as low as 8 MHz. Also, his interference suppression configuration used two SAW PTFs; one for interference monitoring and one for interference suppression, as seen in Figure 5.

In 1984, Way developed a simulation program to implement a 19-tap interference suppression filter to DS/SS signals [17]. Way implemented a different adaptive algorithm: a "soft-constraint" version of the least-
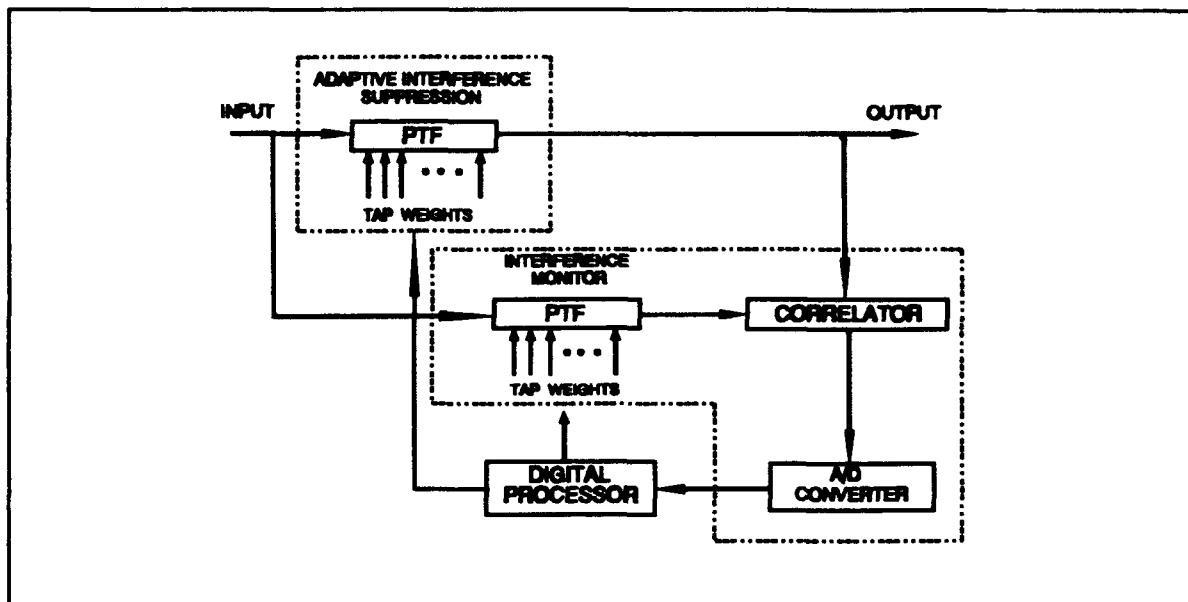
Figure 5 Shepards' simulated adaptive configuration using two PTF's.

mean-square (LMS) algorithm. He examined the filter's effectiveness versus single-tone jammers and frequency hopping tone jammers. He likewise evaluated the performance of the filter via SNR improvement.

In 1990, Mikulanicz provided a performance evaluation of a 128-tap ACT PTF [18]. While he intended to evaluate its effectiveness for interference suppression in DS/SS systems, he incurred difficulties, and resorted to applying the device as a matched filter for PN maximal-length codes. He also demonstrated the effectiveness in creating assorted FIR bandpass filter responses using the rectangular, Hamming, and Hanning window distributions. It is noted that the version of ACT PTF used in Mikulanicz' research has been significantly upgraded for the current research effort.

III. Theoretical Developments

3.1 Direct Sequence Spread Spectrum (DS/SS) Systems

A spread spectrum (SS) system is a system that produces a signal with a bandwidth much wider than the original message bandwidth. SS techniques have made possible the development of interference resistant communications with multiple access capability while having low-probability-of-intercept (LPI). There are a variety of types of SS systems with different modulation formats:

(1) direct sequence, which is usually a form of phase-shift keying;

(2) frequency hopping, in which a narrowband frequency-shift keyed signal is hopped over a wide band with pseudorandom carrier frequency selection;

(3) time hopping, which is similar to frequency hopping except the PN sequence selects the transmission time (slot) within consecutive time frames (usually of low duty cycle or bursts); and

(4) hybrid systems, combining any of the three main types.

Direct sequence spreading, the focus of this research, is achieved by modulo-2 addition of a binary message sequence and a higher rate pseudorandom binary sequence. The result is a sequence at the pseudorandom sequence rate which is used to suppress-carrier modulate an RF carrier signal (e.g. binary phase-shift-keyed (BPSK), or quadrature phase-shift-keyed (QPSK) formats). The signal is identified as suppressed-carrier because the spectral density of the modulated signal has no identifiable carrier present, although the spectrum is centered at ω_c. This technique spreads the energy of the signal over a large bandwidth so that it could be hidden in the noise levels of unintended receivers. Hence the signals have a low-probability-of-intercept while increasing the resistance to interference from co-existing users of the frequency band, multipath, and jamming.

3.1.1 Spread Spectrum System Model

The principal components of a DS modulated SS system are illustrated in Figure 6, where $d(t)$ is the digital data or message sequence (± 1), P, is the transmitted signal power, $c(t)$ is the PN code sequence (or

"chip" sequence with values ± 1), and ω_o is the carrier frequency (rad/sec). Multiplication of the bipolar data sequence with the bipolar PN sequence is equivalent to a modulo-2 addition (or exclusive-OR) of the sequences when the data or code sample value of "+1" is represented as a binary "0" and the value of "–1" as a binary "1". This higher rate sequence (at the PN code rate) is then multiplied by a carrier resulting in a phase shift of 0 or π radians and is expressed as

$$s(t) = \sqrt{2P_s}\, d(t)c(t)\cos\omega_c t \tag{1}$$

The rate of the PN code is typically on the order of megachips per second (or more), while the rate of the message waveform is often on the order of kilobits per second or lower, depending on the desired amount of processing gain (defined below) needed when a physical constraint is imposed on the maximum PN code rate. As a result of this modulation, the power in the transmitted signal is spread in frequency over a bandwidth corresponding to the PN clock frequency.
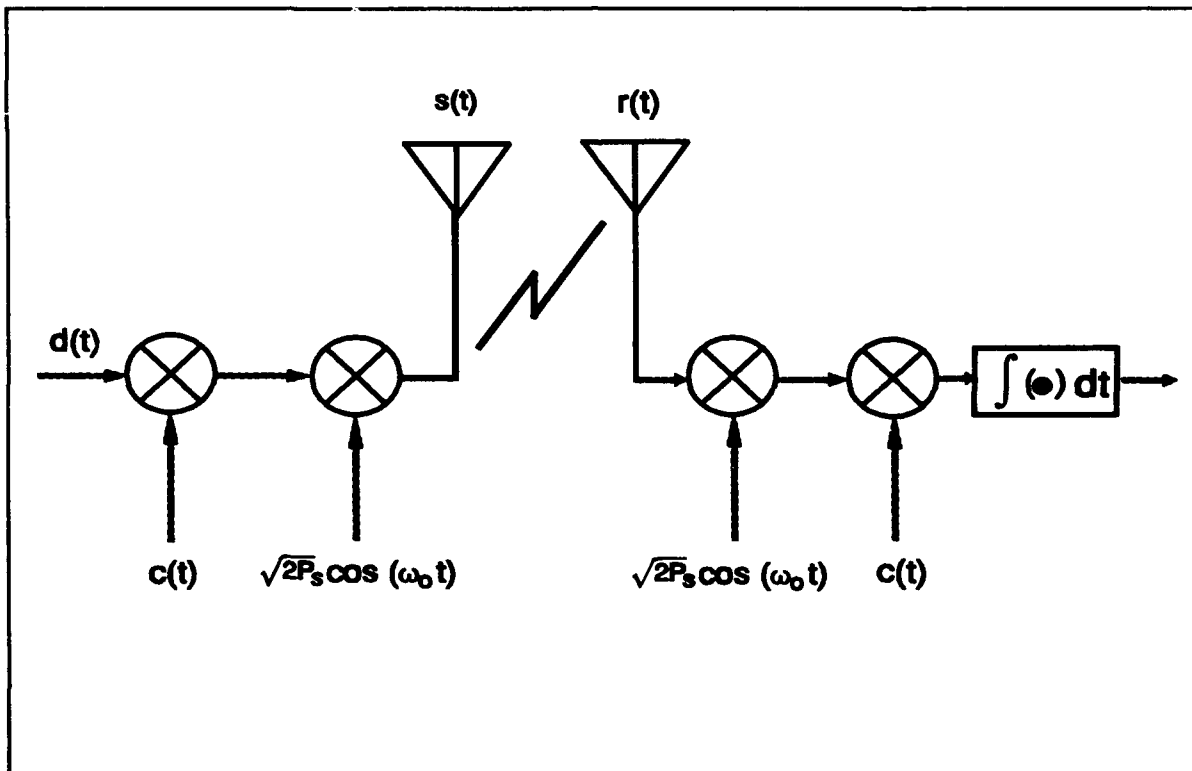
Figure 6 Direct sequence spread spectrum communications system model.

3-2

The receiver has a replica of the transmitted PN code, $c_{rep}(t)$, which, when mixed with the incoming signal, serves to despread the wideband signal to its original message bandwidth, giving:

$$r(t) = \sqrt{2P_s}d(t)c(t)c_{rep}(t)\cos\omega_c t = \sqrt{2P_s}d(t)\cos\omega_c t \qquad (2)$$

The despread signal is then demodulated by mixing the (still) RF signal with a local oscillator at ω_c yielding

$$r_1(t) = \sqrt{2P_s}d(t)\cos\omega_c t \sqrt{2P_s}\cos\omega_c t = P_s d(t) \qquad (3)$$

The message sequence is then passed through a correlator to perform detection in accordance with traditional digital communication systems.

An important parameter that is useful for specifying the performance of a SS signal in the presence of interference is known as the processing gain [20]. This processing gain, G_p, is usually defined as the ratio of the RF signal bandwidth, W_{SS}, to the message bit rate, R_b. Another definition of the processing gain of DS/SS systems is the ratio of the chip rate of the PN code to the data bit rate. The former definition gives a value that is factor of two larger than the latter definition, so care must taken to state which formula is referenced. Obviously from these definitions, the larger the processing gain, the greater the advantage versus interfering signals. This processing gain is either achieved by increasing the chip rate or reducing the data rate, or both.

The performance of the DS/SS signal in terms of signal-to-noise ratio (SNR) can be expressed using the processing gain, G_p, such that

$$SNR_{recv\ out} = G_p SNR_{recv\ in} \qquad (4)$$

At the output of the correlator/matched filter, the bit error probability of the system in the presence of only additive white Gaussian noise (AWGN) is the same as that of a BPSK signal *without* spread spectrum,

3-3

$$P_e = Q\left(\sqrt{\frac{2E_b}{N_o}}\right) ; \quad \text{where } Q(x) = \int_x^{\infty} \frac{1}{\sqrt{2\pi}} \exp\left(-\frac{z^2}{2}\right) dz \qquad (5)$$

and E_b is the data bit energy and $N_o/2$ is the two-sided noise power spectral density (PSD). In effect, what Equations (4) and (5) suggest is that a spread spectrum signal can be transmitted at a lower peak signal power than traditional BPSK signals (by an amount equal to the processing gain) and still maintain the same probability of error. The effect of a tone interferer on the output SNR of the receiver and the bit error probability are examined in a later section.

3.1.2 Characteristics of PN Sequences

The terms pseudorandom (PR) or pseudonoise (PN) are given to a class of linear code sequence which generates sample statistics similar to a random noise-like waveform. However, the sequences are actually both deterministic and periodic. A completely random sequence is neither deterministic nor periodic; e.g., the outcome of successive coin tosses. The type of PN code most often used in DS-SS systems is the maximal sequence or m-sequence. By definition, the maximal code is the longest code that can be generated with a particular shift register (delay element) of a given length [19]. For a binary n-stage feedback shift-register generator, as shown in Figure 7, the maximal length sequence is $2^n - 1$ chips. The m-sequence exhibits a number of randomness properties important to SS systems [19]:

(1) *Balance Property*. For every m-sequence, the number of ones exceeds the number of zeros by exactly one. This balance of ones and zeros eliminates the dc component by an amount proportional to the length of the code. A carrier modulated by the code will therefore be suppressed by a factor of $1/(2^n - 1)$.

(2) *Shift-and-Add Property*. A phase-shifted replica of a maximal linear code modulo-2 added to itself results in the same sequence but with a different phase shift.

(3) *Run-Length Distribution*. The distribution of runs of p consecutive ones or zeros in a maximal sequence of length $2^n - 1$ is defined by $2^{n-(p+2)}$. This means that in every period, one-half of the runs are of
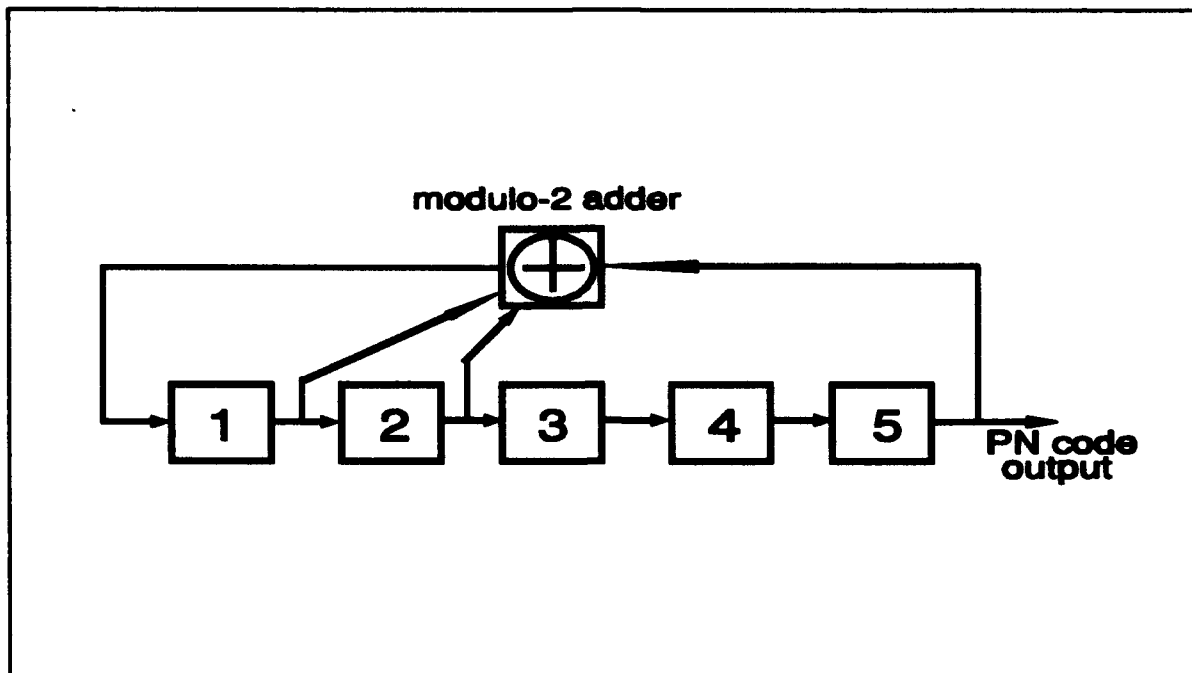
Figure 7 PN (5,4,2,1) maximal code generator

length 1, one-fourth are of length 2, one-eighth are of length 3, and so forth.

(4) *State Exhaustion.* All possible n-states except the all-zero state are generated by an n-stage binary shift register generator with maximal feedback connections. For instance, a 2-stage with maximal feedback taps on both stages will sequence through the states 11, 01, and 10 before repeating states.

(5) *Autocorrelation Property.* The autocorrelation of an m-sequence for all values of phase shift greater than or equal to ± 1 chip is equal to -1 and increases linearly from -1 to the peak value of $2^n - 1$ for phase shifts less than ± 1 chip. The autocorrelation property is of particular importance when examining the spectral characteristics of the DS/SS signal.

3.1.3 Spectral Characteristics of PN Sequences

The time-averaged autocorrelation of the periodic PN sequence of length N, when taken alone, can be represented as

$$R_{PN}(\tau) = \lim_{T \to \infty} \frac{1}{T} \int_{-T/2}^{T/2} c^*(t)c(t+\tau)dt \qquad (6)$$

where τ is the amount of time shift. From the balance property it is clear that when $|\tau| > T_c$, the average value of the autocorrelation is approximately zero (actually $-1/2^n$) because of the equal probability of ± 1 chips. Since PN codes are periodic, the limiting operation can be dropped. Therefore, the autocorrelation over one period of the code is

$$R_{PN}(\tau) = \int_{-T/2}^{T/2} c^*(t)c(t+\tau)dt. \qquad (7)$$

This autocorrelation is periodic when the time-shift equals

$$\tau = (2^n - 1)T_c = NT_c. \qquad (8)$$

The autocorrelation is then given by:

$$R_{PN}(\tau) = \begin{cases} \left(-\dfrac{|\tau|}{T_c} + 1\right)N & for\,|\tau| \le T_c \\ -2^{-n} & for\,|\tau| > T_c \end{cases} \qquad (9)$$

and is illustrated in Figure 8. In the spread spectrum receiver detection process, the peak allows acquisition and synchronization for despreading and eventual demodulation.

The power spectral density, $S_{PN}(\omega)$, of the PN sequence is obtained by taking the Fourier transform of the autocorrelation function, $R_{PN}(\tau)$.

$$\mathscr{F}\left[R_{PN}(\tau)\right] = \int_{-\infty}^{\infty} R_{PN}(\tau)e^{-j\omega\tau}d\tau \qquad (10)$$

Realizing that a vertical shift of the triangular peak by $-1/2^n$ would only affect the dc component, $R_{PN}(\tau)$ can be approximated as:

$$R_{PN}(\tau) = \Lambda\left(\frac{\tau}{T_c}\right) \qquad (11)$$

where

$$\Lambda \left(\frac{\tau}{T_c} \right) = \begin{cases} 1 - \dfrac{|\tau|}{T_c}, & \text{for } |\tau| \leq T_c \\ 0, & \text{for } |\tau| > T_c \end{cases} \tag{12}$$

Substituting the above equation into the Fourier transform for $R_{PN}(\tau)$ yields

$$\mathscr{F}\left[R_{PN}(\tau) \right] = \int_{-\infty}^{\infty} \Lambda \left(\frac{\tau}{T_c} \right) e^{-j\omega\tau} d\tau \tag{13}$$

$$= T_c \text{sinc}^2(T_c f)$$

The PSD, $S_{PN}(\omega)$, is shown in Figure 8(c).

3.1.4 Effect of Tone Interference on Spread Spectrum Performance

As was mentioned in Chapter 1, the tone jammer is the most damaging signal to the effective operation of a DS/SS system and is easily generated by the enemy. However, the effects of the jammer are minimized by the inherent operation of the spread spectrum link. Mixing a locally generated replica of the PN sequence in the receiver with any incoming interfering signal serves to spread the energy of the interferer proportional to the amount of the processing gain of the SS system. It is difficult to apply a broadband jammer with enough energy spread across the spectrum bandwidth to counteract this phenomena. Henceforth, the narrower the input interfering signal is at the input of the spread spectrum receiver, the greater the probability that its energy will pass through the system bandwidth of the spread spectrum receiver. Likewise, as was stated in Chapter 1, a tone jammer is most effective at the carrier frequency of the spread spectrum signal for the reasons just mentioned. Therefore, the analysis of the effects of a tone jammer with regard to the JSR and P_e quantities of the received SS signal will be examined under this worst-case scenario.

In considering the effect of a single tone interferer at the carrier frequency of the transmitted SS signal, it is assumed that the jammer power, J, is much greater than the Gaussian noise, *i.e.*
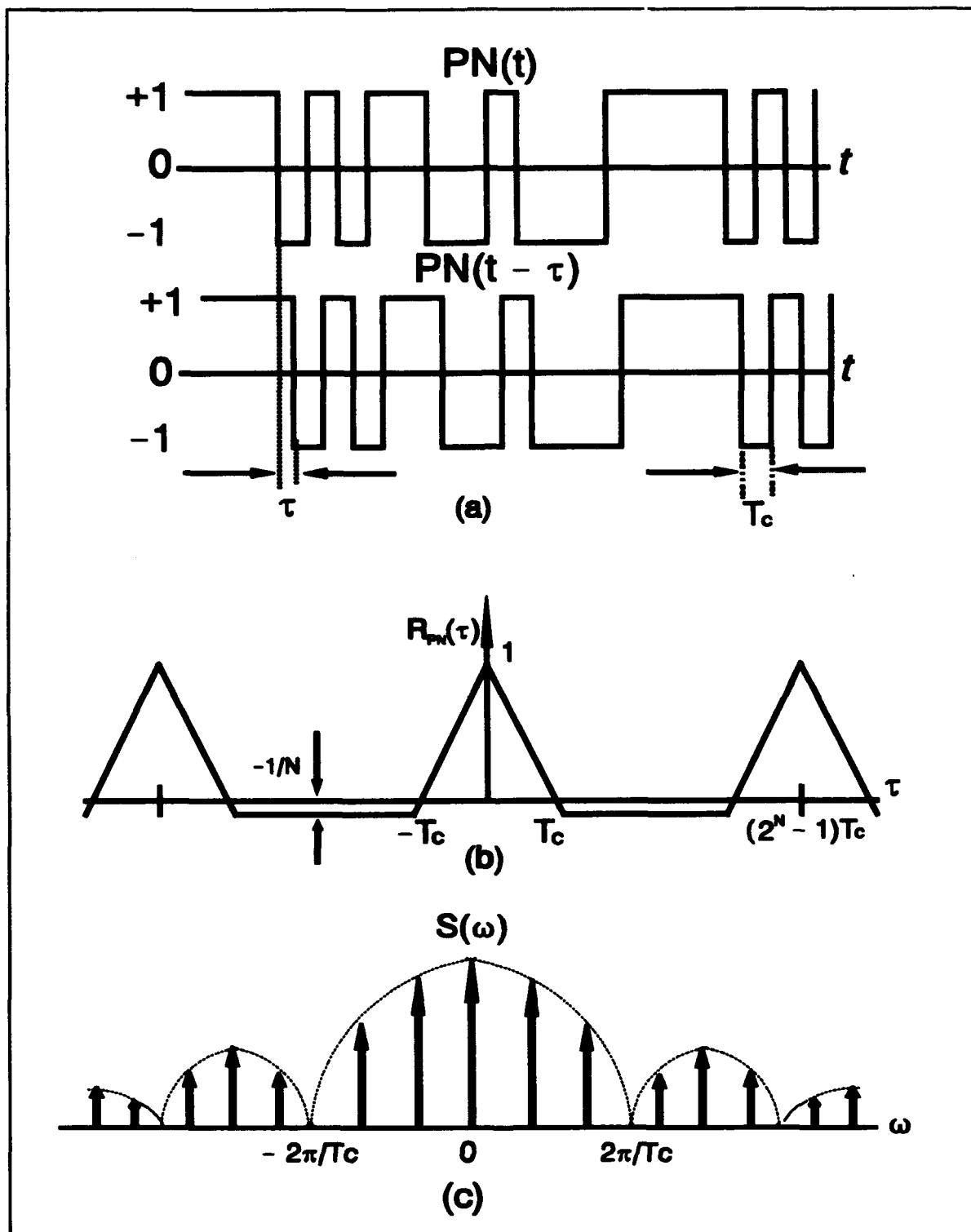
Figure 8 Modulation/demodulation of a PN sequence: (a) performing the autocorrelation of a PN sequence, (b) plot of the autocorrelation, and (c) the spectral representation (PSD).

3-8

$$J_o > \frac{N_o}{2} ; \quad \text{so that} \quad J + N \approx J \tag{14}$$

where J_o is the PSD of the jammer. The jamming signal is expressed as

$$J(t) = \sqrt{2P_J} \cos(\omega_c t + \theta) \tag{15}$$

where θ is the phase of the jammer with respect to the phase of the carrier. A more general expression for the jamming signal would be

$$J(t) = \sqrt{2P_J} \cos[(\omega_c + \Delta\omega)t + \theta] \tag{16}$$

where $\Delta\omega$ is the frequency offset from the carrier. At this frequency, the signal input to the receiver will be approximately

$$r_s(t) = \sqrt{2P_s} d(t)c(t)\cos\omega_c t + \sqrt{2P_J} \cos(\omega_c t + \theta) \tag{17}$$

After despreading, recognizing that $c^2(t) = 1$, and carrier demodulation, the signal becomes

$$r_1(t) = P_s d(t)[1 + \cos 2\omega_c t] + \sqrt{P_s P_J} c(t)[1 + \cos 2\omega_c t]\cos\theta - \sqrt{P_s P_J}\sin 2\omega_c t \sin\theta \tag{18}$$

The output of the correlator, which eliminates the double-frequency components, is

$$r_o(t) = P_s d(t) + \sqrt{P_s P_J} c(t)\cos\theta \tag{19}$$

Notice that the SS signal is collapsed to a narrowband signal, while the interfering signal is expanded by multiplication with the high bit-rate PN sequence, $c(t)$, to a wideband signal. The interfering signal's new PSD is of the following form [31]:

$$S_{JJ}(f) = \frac{P_s P_J \overline{\cos^2\theta}}{2f_c} \text{sinc}^2(f/f_c) \tag{20}$$

where $f_c = 1/T_c$ (where T_c = chip interval). After correlating with the integration period equal to the data bit interval T_b (which acts as a low-pass filter)

3-9

$$S_{JJ}(f) = \frac{P_s P_J \overline{\cos^2\theta}}{2f_c} \tag{21}$$

Using the expression for probability of bit error, P_e, given in Equation (5) and replacing $N_o/2$ with $S_{JJ}(f)$ yields

$$P_e = Q\left(\sqrt{\frac{2E_b f_c}{P_J \overline{\cos^2\theta}}}\right) \tag{22}$$

Since $E_b = P_s T_b$, and $f_c = 1/T_c$, P_e can be simplified as

$$P_e = Q\left(\sqrt{\frac{2T_b P_s}{T_c P_J \overline{\cos^2\theta}}}\right) = Q\left(\sqrt{\frac{4P_s G_p}{P_J}}\right) \tag{23}$$

where $\overline{\cos^2\theta} = 1/2$ because of its random phase over the range $[0, 2\pi]$ with respect to the phase of the carrier.

The effect of the tone jammer at the output of the SS receiver can also be expressed in terms of the SNR [20]:

$$SNR_o = \frac{P_s}{\dfrac{N_o}{2T_b} + \dfrac{P_J}{G_p}} = \frac{P_s G_p}{\dfrac{N_o G_p}{2T_b} + P_J} \tag{24}$$

Neglecting the noise term, this yields

$$SNR_o = \frac{P_s G_p}{P_J} \tag{25}$$

Stated another way, the term $(E_b/J_o)_{reqd}$ is the bit energy per jammer noise PSD required to maintain a link at a specified error probability [32]. It can be formulated as follows:

$$\left(\frac{E_b}{J_o}\right)_{reqd} = \left(\frac{P_s T_b}{P_J/W_{SS}}\right)_{reqd} = \frac{W_{SS}/R_b}{(P_J/P_s)_{reqd}} = \frac{G_p}{(P_J/P_s)_{reqd}} \tag{26}$$

3.1.5 Spread Spectrum System Performance with Interference Suppression Subsystem

The performance of a DS/SS system with an interference suppression filter subsystem in place to reject narrowband jammers can be measured according to one of two criteria: SNR improvement and, additionally, average probability of bit error, P_e. The SNR improvement factor, defined as the ratio of the SNR with the suppression filter in the system to the SNR of the system operating without the rejection filter, provides a good qualitative indication of system performance while the P_e provides a good quantitative description [3].

3.1.5.1 Derivation of the SNR Improvement Factor

The SNR improvement has been calculated by Li and Milstein [6] with both the predictive (one-sided) adaptive filter and the two-sided adaptive filter. The formulation leading to the final results will not be given here. The results are important for comparison purposes.

It can be shown that the SNR improvement factor, G_1, for the prediction error filter under single-tone jamming, and with the optimum tap weights obtained (i.e. convergence of the chosen adaptive algorithm) is given by [6]:

$$G_1 = \frac{J + \sigma_n^2}{2(S + \sigma_n^2)\cfrac{\left[L + \cfrac{2(S + \sigma_n^2)}{J}\right]\cfrac{\sin(L\Omega T)}{\sin(\Omega T)}\cos[(L + 1)\Omega T]}{\left[L + \cfrac{2(S + \sigma_n^2)}{J}\right]^2 - \cfrac{\sin^2(L\Omega T)}{\sin^2(\Omega T)}} + \sigma_n^2} \tag{27}$$

where S = signal power, J = jammer power, σ_n^2 = power due to thermal noise, L = number of taps in the PTF, T = sampling interval = chip duration, and Ω = angular frequency of the jamming tone.   If we assume $\sigma_n^2 = 0$ (a reasonable approximation for laboratory results), then the following simplification can be made

$$G_1 = \left[1 + \frac{J}{2S}\left(L + \frac{\sin(L\Omega T)}{\sin(\Omega T)}\right)\right] \cdot \frac{L + \frac{2S}{J} - \frac{\sin(L\Omega T)}{\sin(\Omega T)}}{L + \frac{2S}{J} - \frac{\sin(L\Omega T)}{\sin(\Omega T)} \cos[(L + 1)\Omega T]} \tag{28}$$

For the two-sided transversal filter, the SNR improvement factor, G_2, is as follows [6]:

$$G_2 = \frac{(S/N)_{out}}{(S/N)_{in}} = \frac{J + \sigma_n^2}{\frac{J}{1 + \frac{J}{2(S + \sigma_n^2)}\left[2N - 1 + \frac{\sin[(2N + 1)\Omega T]}{\sin(\Omega T)}\right]} + \sigma_n^2} \tag{29}$$

where $2N$ = the total number of taps; N on each side of the center tap. Again, if we make the assumption that $\sigma_n^2 = 0$, then

$$G_2 = 1 + \frac{J}{2S}\left[2N - 1 + \frac{\sin[(2N + 1)\Omega T]}{\sin(\Omega T)}\right] \tag{30}$$

From (30), we see that G_2 increases with an increase in the number of taps or as the input interference-to-signal power ratio J/S increases. Also note that G_2 is dependent upon ΩT. The transfer function, $H(\omega)$, of the transversal filter with the optimal tap weights established, can be reviewed in [6] but will not be given here. This transfer function yields insight into the interference rejection process.

The final results for the probability of bit error, P_b, will also not be given here since it will not be measured in the experimentation of this thesis. Interested readers may see [7,21] for details.

3.2 Adaptive Processes

This section will examine the pertinent adaptive processes that will support the work in this thesis. It will begin with a short introduction on what an adaptive system is and its benefits, followed by the fundamental linear equations that characterize the adaptation, and conclude with a look at the least-mean-square algorithm, which will be used in this study. Most of what is developed here follows Widrow and Stearns development [22,23] and enhanced by Haykin [24] when appropriate.

3.2.1 General Description of the Adaptive Process

According to one of the foremost authorities on adaptive processes, Bernard Widrow, an automated adaptive system is one "whose structure is alterable or adjustable in such a way that its behavior or performance (according to some desired criterion) improves through contact with its environment [22]." Widrow and Stearns describe a simple example of this with the automatic gain control (AGC) used in radio and television receivers. In this example, the function of the circuit is to adjust the sensitivity of the receiver inversely as the average incoming signal strength. The receiver is thus able to adapt to a wide range of input levels and to produce a much narrower range of output levels.

Adaptive systems, although of varied methods of operation, usually have the following characteristics in common [22]:

1. They can automatically adapt or self-optimize in light of changing (nonstationary) environments and changing system requirements.

2. They can be trained to perform specific filtering and decision-making tasks. In a sense, adaptive systems can be "programmed" by a training process.

3. Because of the above, adaptive systems do not require elaborate synthesis procedures. Instead, they tend to be "self-designing".

4. They can extrapolate a model of behavior to deal with new situations after having been trained on a finite and often smaller number of training signals.

5. To a limited extent, they can repair themselves; that is, they can adapt around certain kinds of internal defects.

6. They can usually be described as nonlinear systems with time-varying parameters.

The most important characteristic of the adaptive system is its time-varying and self-adjusting performance. The need for such performance may readily be seen by realizing that if a system is of fixed design which is considered optimal, the implications are that the designer has foreseen all possible input conditions, at least statistically, and knows what the system is to do under each of these conditions.

3-13

In many instances, the complete range of input conditions may not be known sufficiently or the conditions may change from time to time. In such circumstances, an adaptive system that continually seeks the optimum within an allowed class of possibilities, using an orderly search process, would give superior performance compared with a system of fixed design.

The adaptive system is inherently difficult to analyze in conventional terms, because of their nonlinear and time-varying characteristics. In essence, if a signal is applied to the input to determine its response characteristics, the system adapts to this specific input and thereby changes its own form.

Adaptive systems can be classified into two schemes: open-loop and closed-loop. The open-loop adaptive process (or non-iterative process) involves making measurements of the input, applying this information to a formula or to a computational algorithm, and using the results to set the adjustments of the adaptive system. Closed-loop adaptation, on the other hand, involves automatic experimentation with these adjustments and knowledge of their outcome in order to optimize a measured system performance. The latter process may be called adaptation by "performance feedback" and is therefore iterative in nature. The closed-loop scheme will be implemented in this thesis.

The performance feedback process is diagrammed in Figure 9. One can call the input signal x and define a "desired response" signal d, which is assumed to represent the desired output of the adaptive system. The error signal, e, is the difference between the desired output signal and the actual output signal, y, of the adaptive system. Using the error signal, an adaptive algorithm adjusts the structure of the adaptive system, thus altering its response characteristics by minimizing some measure of the error, thereby closing the performance loop.

In the prediction application of an adaptive system of Figure 10(a), the desired signal is the input signal, s, and a delayed version of the latter is sent to the adaptive processor, which must therefore try to "predict" the current input signal in order to have y cancel d and drive e toward zero. Figure 10(b) shows the adaptive processor in an interference-canceling configuration. Here the signal, s, is corrupted by additive noise, n. A distorted but correlated version of the noise, n', is also available. The goal of the adaptive processor in this case
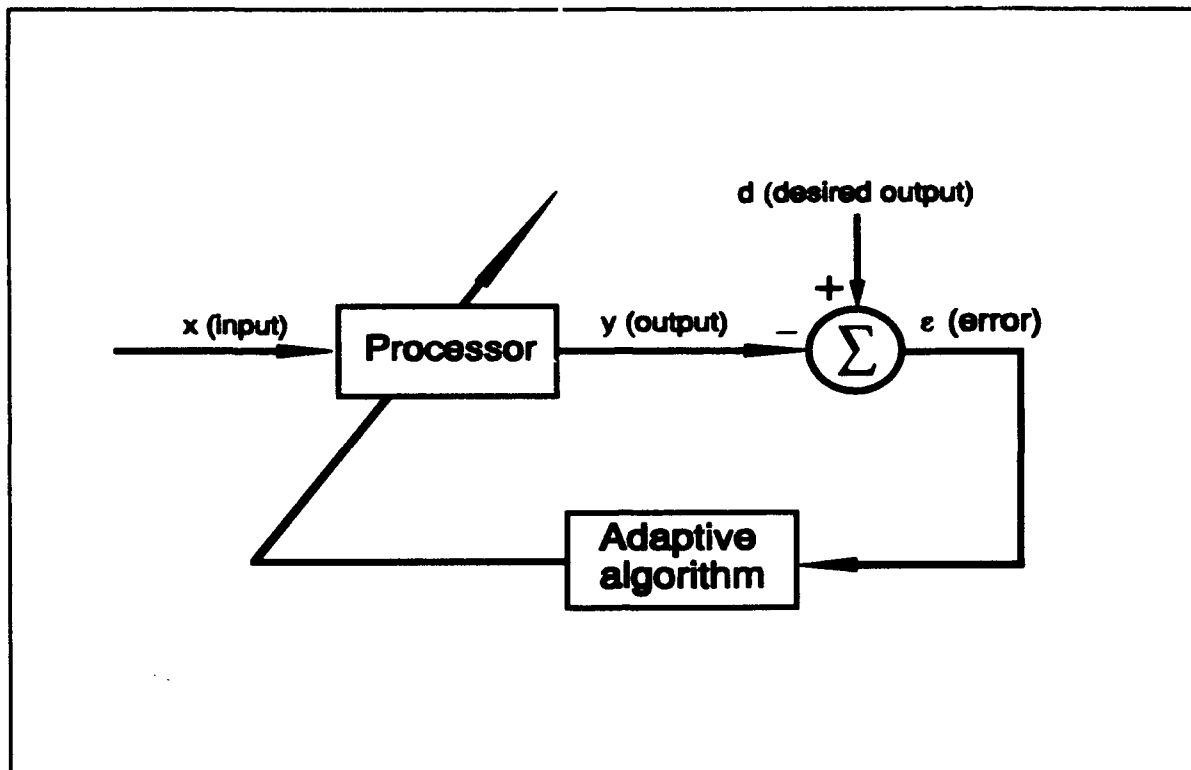
Figure 9 Adaptive system in the closed-loop configuration.

is to produce an output, y, that closely resembles n, so that the overall output, e, will closely resemble s. The key element that allows this adaptive structure to achieve its goal is the fact that s and n are uncorrelated, whereas n and n' are correlated. If these conditions are violated, the adaptive filter may cancel the signal s in place of (or in addition to) the noise or could fail to cancel the noise altogether [23].

3.2.2 Mathematical Description of Adaptive Processes

The adaptive linear combiner, or non-recursive adaptive filter, is fundamental to adaptive signal processing, and is the single most important element in "learning" systems and adaptive processes in general (see Figure 11) [22]. In essence, it is a time-varying, non-recursive digital filter. The combiner is called "linear" because for a fixed setting of the tap weights its output is a linear combination of the input components. In other words, with fixed tap settings it is merely a finite-impulse response (FIR) filter. When the adaptive processor

3-15
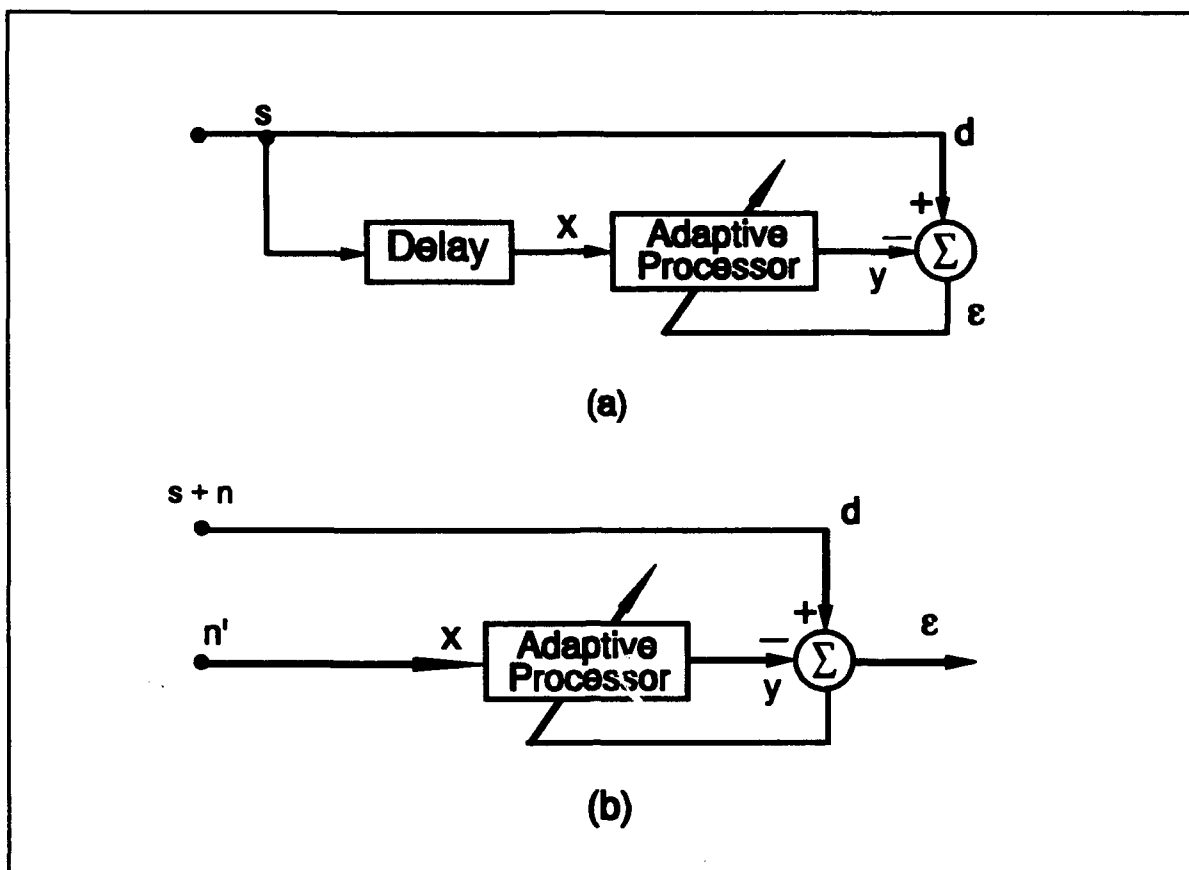
Figure 10 Adaptive processor in (a) predictive filter configuration, and (b) interference canceling configuration.

is implemented with an adaptive linear combiner and unit delay elements, the structure is called an adaptive

transversal filter or tapped-delay line.

The elements x_k through x_{k-L} are $L + 1$ sequential samples of the same signal source and are interpreted

as a single-input case (versus a possible multiple input case; *i.e.* adaptive antenna arrays). The input vector for

the single-input case depicted in Figure 11 is:

$$X_k = [x_k \quad x_{k-1} \quad \cdots \quad x_{k-L}]^T \tag{31}$$

The T stands for transpose, so X_k is actually a column vector. Again the subscript k is used as a time index. For

this single-input case, the elements are sequential samples taken at points k, $k-1$,..., going back in time through

the sequence of data samples. One obtain the input-output relationships for Figure 11 as follows:

3-16
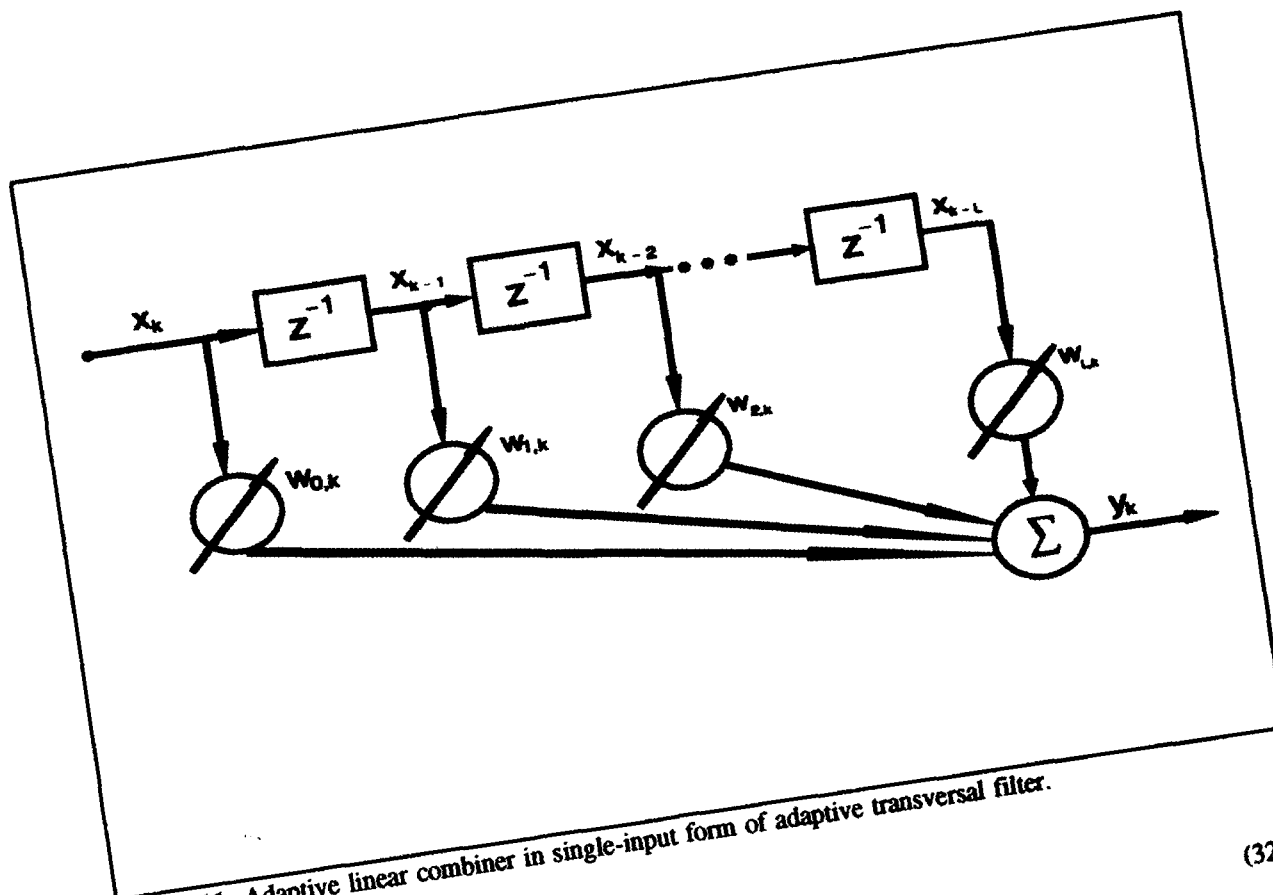
Figure 11 Adaptive linear combiner in single-input form of adaptive transversal filter.

$$(32)$$

$$y_k = \sum_{l=0}^{L} w_{lk} x_{k-l}$$

Corresponding with Equation (31), a weight (or coefficient) vector can be expressed as

$$(33)$$

$$W_k = [w_{0,k} \quad w_{1,k} \quad \cdots \quad w_{L,k}]^T$$

With this definition Equation (32) can be expressed in a single relationship using vector notation:

$$(34)$$

$$y_k = X_k^T W_k = W_k^T X_k$$

With this description of the operation of the adaptive linear combiner, one can proceed to a discussion of how it adapts; that is, of the effect of changing the vector W_k as the time index, k, changes.

The weight vector of the linear combiner is adjusted to cause the output, y_k, to agree as closely as possible with the desired response signal. This is accomplished by comparing the output with the desired response to obtain an "error" signal and then adjusting or optimizing the weight vector to minimize this signal.

3-17

In most practical instances, the adaptive process is oriented toward minimizing the mean-square value, or power, of the error signal. The source of the desired response signal, d_k, depends on the application of the adaptive combiner. Often considerable ingenuity is required to find a suitable signal, since if the actual desired response were available, one would generally not need the adaptive system.

The error signal with time index k is

$$e_k = d_k - y_k \tag{35}$$

Substituting in the value from Equation (34) yields

$$e_k = d_k - X_k^T W = d_k - W^T X_k \tag{36}$$

where the subscript k is dropped so that an analysis can be accomplished at a particular point in time with the taps weights frozen. Squaring Equation (36) to obtain the instantaneous squared error,

$$e_k^2 = d_k^2 + W^T X_k X_k^T W - 2d_k X_k^T W \tag{37}$$

If one assumes that e_k, d_k, and X_k are statistically stationary, and taking the expected value of Equation (37) over k,

$$E[e_k^2] = E[d_k^2] + W^T E[X_k X_k^T] W - 2E[d_k X_k^T] W \tag{38}$$

The mean-square-error function can be more conveniently expressed as follows. Let $\mathbf{R}$ be defined as the square matrix

$$R = E[X_k X_k^T] = E \begin{bmatrix} x_k^2 & x_k x_{k-1} & \cdots & x_k x_{k-L} \\ x_{k-1} x_k & x_{k-1}^2 & \cdots & x_{k-1} x_{k-L} \\ \vdots & \vdots & \vdots & \vdots \\ x_{k-L} x_k & x_{k-L} x_{k-1} & \cdots & x_{k-L}^2 \end{bmatrix} \tag{39}$$

This matrix is designated the *input correlation matrix*. The main diagonal terms are the mean-squares of the input components, and the cross terms are the cross-correlations among the input components. Let $\mathbf{P}$ be similarly

3-18

defined as the column vector

$$P = E[d_k X_k] = E[d_k x_k \quad d_k x_{k-1} \quad \cdots \quad d_k x_{k-L}]^T \qquad (40)$$

This vector is the set of cross-correlations between the desired response and the input components. Letting the mean-square error (MSE) in Equation (38) be designated by ξ and expressing it in terms of Equations (39) and (40):

$$\xi = E[\epsilon_k^2] = E[d_k^2] + W^T R W - 2 P^T W \qquad (41)$$

The mean-square error ξ is precisely a quadratic function of the components of the weight vector W when the input components and desired response input are stationary stochastic variables. A portion of a two-dimensional mean-square-error function is illustrated in Figure 12. The bowl-shaped quadratic error function, or performance surface, formed in this manner is a paraboloid (or hyper-paraboloid if there are more than two weights). The point at the "bottom of the bowl" is projected onto the weight-vector plane as W^*, the optimal weight vector or point of minimum mean-square error.

Many useful adaptive processes that cause the weight vector to seek the minimum of the performance surface do so by gradient methods [22]. The gradient of the mean-square-error performance surface, designated $\nabla(\xi)$ or simply ∇, can be obtained by differentiating Equation (41) to obtain the column vector

$$\nabla \triangle \frac{\partial \xi}{\partial W} = \left[\frac{\partial \xi}{\partial w_0} \quad \frac{\partial \xi}{\partial w_1} \quad \cdots \quad \frac{\partial \xi}{\partial w_L} \right]^T$$
$$= 2 R W - 2 P \qquad (42)$$

where R and P are given by Equations (39) and (40), respectively. To obtain the minimum mean-square error the weight vector W is set at its optimal value W^*, where the gradient is zero:

$$\nabla = 0 = 2 R W^* - 2 P \qquad (43)$$

Assuming that R is nonsingular, the optimal weight vector W^*, sometimes called the Wiener weight vector, is found from Equation (43) to be
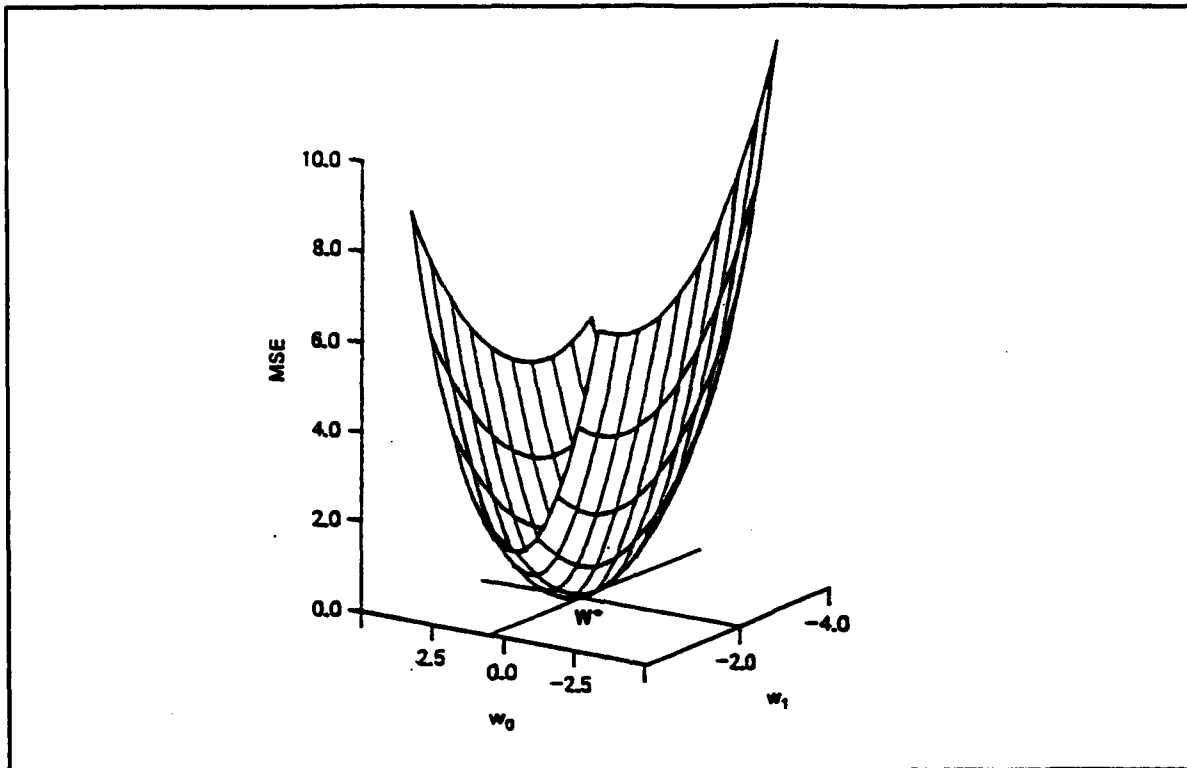
Figure 12 Portion of a two-dimensional quadratic performance surface [22].

$$W^* = R^{-1}P \qquad (44)$$

This equation is an expression of the Wiener-Hopf equation in matrix form [22]. The minimum mean-square error is now obtained by substituting W^* from Equation (44) for W in Equation (41):

$$\begin{aligned} \xi_{min} &= E[d_k^2] + W^{*T}RW^* - 2P^TW^* \\ &= E[d_k^2] + [R^{-1}P]^TRR^{-1}P - 2P^TR^{-1}P \end{aligned} \qquad (45)$$

Simplifying this result using three rules from linear algebra: $AA^{-1} = I$; $[AB]^T = B^TA^T$; and, for symmetrical matrices, $R^T = R$; $[R^{-1}]^T = R^{-1}$, Equation (45) becomes

$$\xi_{min} = E[d_k^2] - P^TR^{-1}P = E[d_k^2] - P^TW^* \qquad (46)$$

A useful and important statistical condition exists between the error signal and the components of the input signal vector when $W = W^*$, namely,

$$E[\varepsilon_k X_k]_{W-W^*} = P - P = 0 \qquad (47)$$

This result of Wiener filter theory states that when the impulse response of a filter is optimized, the error signal is uncorrelated with (orthogonal to) the input signals. Hence, one can conclude that the two criteria: "minimum mean-squared error" and "orthogonality between error and input" yield identical optimum filters [22,24].

3.2.3 The Least-Mean-Square Algorithm

I now discuss the algorithm for adjusting the weights and descending on the performance surface to the minimum mean-square error. I will exclusively use the least-mean-square (LMS) algorithm in this thesis effort. The LMS algorithm is important because of its simplicity and ease of computation; it does not require off-line gradient estimations or repetitions of data, nor does it require the matrix inversion (R^{-1}) [24]. Thus, it is perhaps the most universally applicable adaptive algorithm in use today [23].

Again, when using the adaptive linear combiner structure explained earlier, one has, as in Equation (36)

$$\varepsilon_k = d_k - X_k^T W_k \qquad (48)$$

To develop an adaptive algorithm, one would normally estimate the gradient of $\xi = E[\varepsilon_k^2]$ by taking differences between short-term averages of ε_k^2. Instead, to develop the LMS algorithm, ε_k^2 is taken itself as an estimate of ξ_k. Then, at each iteration in the adaptive process, a gradient estimate is obtained for which one can specify a steepest-descent type of adaptive algorithm [22]

$$\begin{aligned} W_{k+1} &= W_k - \mu \nabla_k \\ &= W_k + 2\mu \varepsilon_k X_k \end{aligned} \qquad (49)$$

This is the LMS algorithm. Actually, Equations (48) and (49) completely describe the LMS algorithm. [24]. From Equation (49), one sees that given an input signal x_k and a desired signal d_k, the implementation of the LMS adaptive algorithm requires only the selection of the convergence parameter μ [23]. This convergence factor, or gain constant, regulates the speed and stability of adaptation, and is hence plays a pivotal role in

determining the performance of the system. In terms of convergence and stability, a large μ could result in an adaptive process that never converges to the minimum mean-square error (MMSE) solution. If μ is too small, the coefficient vector adaptation is slow, and therefore the system may not react rapidly enough to cope with changing signal statistics [23].

Since the weight changes at each iteration are based on imperfect gradient estimates, one would expect the adaptive process to be noisy. Overall, the LMS algorithm is attractive because it can be implemented in a practical system without squaring, averaging, or differentiating and is elegant in its simplicity and efficiency. In fact, the efficiency of the LMS algorithm has been shown to approach a theoretical limit for adaptive algorithms when the eigenvalues of the R-matrix are equal or nearly equal [22].

As with all adaptive algorithms, a primary concern with the LMS algorithm is its convergence to the optimum weight vector solution, where $E[\epsilon_k^2]$ is minimized [22]. It is found that convergence is guaranteed only if

$$\frac{1}{\lambda_{max}} > \mu > 0 \qquad (50)$$

where λ_{max} is the largest eigenvalue; that is, the largest diagonal element in Λ, the eigenvalue matrix. For the transversal filter structure, the convergence of the weight-vector mean is assured when

$$0 < \mu < \frac{1}{(L + 1)S} \qquad (51)$$

where S is the signal power and L is the filter order or number of taps. In practice, μ is generally restricted to a small fraction of this stable range in order to smooth the noisy instantaneous gradient estimate [23]. As an aside, there is no known unconditional proof of convergence of the LMS algorithm [22].

There are other adaptive algorithms one could apply to the interference rejection problem, but they have certain trade-offs when comparing to the LMS algorithm. For instance, the recursive least-squares (RLS), another popular algorithm, is capable of realizing a rate of convergence that is much faster than the LMS algorithm. However, the price paid is the increase in computational complexity [24]. However, the random search algorithm

will be examined because of its application in unique situations; *e.g.*, the input delayed signal samples are not available or when a parameter other than the tap weights is the variable.

3.2.4 *The Random Search Algorithms [30]*

Besides the method of steepest-descent in searching the quadratic performance surface for the optimal solution to minimizing the mean-square error, which is a systematic technique employed by the LMS and other such algorithms, the minimal mean-square error solution may also be found by random search techniques. Random searching seeks to improve performance by making random changes in system parameters; for my case, random changes in the tap weight vector. A simple algorithm based on this method is called *random search by "natural selection"*.

In random search by natural selection, a random change is made in the weight vector of the adaptive processor (*i.e.* PTF). The mean-square error is measured before and after the change and the measurements compared. If the change causes the error to be lower, it is accepted. If it does not, it is rejected, and a new random change is tried. This procedure can be described algebraically as follows:

$$W_{k+1} = W_k + \frac{1}{2}[1 + \text{sgn}\{\xi(W_k) - \xi(W_k + U_k)\}]U_k \qquad (52)$$

where U_k is a random vector; $\xi(W_k)$ is an estimate of mean-square error based on N samples of ϵ_k with $W = W_k$; $\xi(W_k + U_k)$ is an estimate of mean-square error based on N samples of ϵ_k with $W = W_k + U_k$; and sgn(z) is +1 for $z \geq 0$ and −1 for $z < 0$.

This algorithm, although easy to implement, has the drawback that nothing is learned when a trial change is rejected and forgotten. For this reason, a more efficient "linear" random search algorithm (LRS) is available. In this algorithm, a small random change U_k is tentatively added to the weight vector at the beginning of each iteration. The corresponding change in mean-square error performance is observed. A permanent weight vector change, proportional to the product of the change in performance and the initial tentative change, is then made. This procedure can be expressed algebraically as follows [22]:

$$W_{k+1} = W_k + \frac{\mu}{\sigma^2}[\xi(W_k) - \xi(W_k + U_k)]U_k \qquad (53)$$

where U_k is a random vector from a random vector generator designed to have a covariance of $\sigma^2 I$; $\xi(W_k)$ and $\xi(W_k + U_k)$ are as defined above; and the terms μ and σ^2 are design constants affecting stability and rate of adaptation.

The LRS algorithm is "linear" because the weight change is proportional to the change in mean-square error, and in this respect it differs from the random search by natural selection as described in Equation (52). The latter algorithm is simpler to implement but does not perform as well in terms of reaching convergence. It is difficult to treat mathematically.

3.2.5 Comparison Between the LMS and LRS Algorithms

As a brief comparison, it is noted that both algorithms are easily implemented in adaptive systems. The LRS algorithm is much less efficient than the LMS in terms of data usage, and it has a higher misadjustment for a given speed of convergence. Misadjustment is the amount of the average excess mean-square error beyond the minimum mean-square error divided by the minimum mean-square error. The LMS algorithm, however, is restricted in use to the adaptive linear combiner of Figure 9 where the inputs X_k and d_k are known, while the LRS algorithm is more general in its use. For example, it can be used in adaptive systems that where the input signals are unavailable or where the adjustment parameters are not signal weights [22]. For example, Figure 13 demonstrates the relative performances of the algorithms presented as a "learning" curve, which expresses the value of the mean-square error as time progresses (in this case in the number of data samples). Figure 13 further reveals the superior speed of convergence and efficiency of the LMS algorithm. Also note that while individual sample functions of the LRS are noisy, the ensemble average of 32 sample functions is not nearly as noisy.
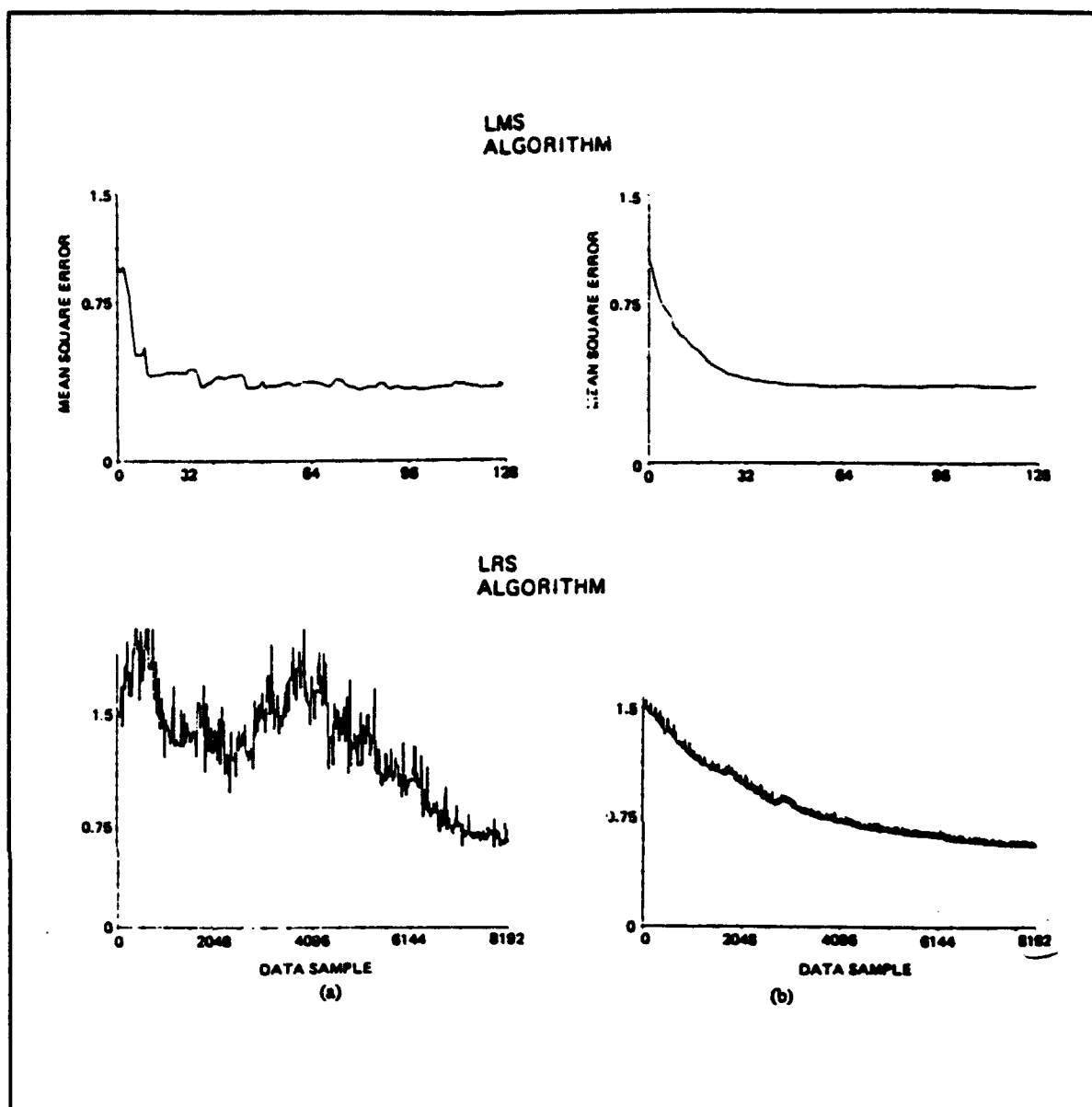
Figure 13 Results of a fixed-delay modeling experiment with theoretical total misadjustment at 9.375 percent. (a) individual learning curves, (b) ensemble averages of 32 learning curves [30].

IV Programmable Transversal Filters and the ACT Technology

4.1 Transversal Filter Fundamentals [25,26]

Since the programmable transversal filter is the primary object of consideration in this thesis, it is appropriate to take a rather detailed look at the ACT PTF used in this study and compare its characteristics with those of other competing technologies such as surface acoustic wave (SAW), charge-coupled device (CCD), and digital or VHSIC (very high-speed integrated circuit) implementations of the PTF. The transversal filter was introduced in the discussion on adaptive filtering by default since it is the device that the adaptive algorithm adjusts to achieve the minimum mean-square-error. In general, a transversal filter may be realized in any technology which can provide good delay lines, tapping and weighting mechanisms, and a means for summing the weighted replicas. Analytically, the transversal filter has an impulse response which is specified by the sequence of tap weights, and since many algorithms used for signal processing result in a specified impulse response, a transversal filter often represents the most direct path from theory to hardware. In many applications it is necessary, or at least desirable, to change or adapt the impulse response with time; thus, a programmable transversal filter (PTF) is a valuable component [26].

Parameters that must be considered when selecting a PTF are bandwidth, number of taps, dynamic range, accuracy, linearity, programming rate, power/size/weight, and, of course, cost and availability [25,26]. Some of these characteristics will be examined in the comparison of device technologies.

If a signal and the taps are both discrete in time, then a difference equation applies; this applies to digital and CCD filters. If the signal is continuous but the taps discrete, as is the case with SAW tapped-delay lines and ACT devices, then a difference-differential equation applies. If the tapping mechanism as well as the signal are continuous, then a differential equation is the proper model; this is the case for a SAW convolver.

In order to implement a transversal filter in a given technology, it is first of all necessary that the technology offer low-loss, low-distortion delay lines. The measure of utility of a delay line is its time-bandwidth product (TBP), which is a measure of the information capacity or the measure of the complexity of the

waveform which can be stored in the delay line [26]. For a PTF, this is also a measure of the complexity of the impulse response.

The availability of high-quality delay lines is a necessary but not sufficient condition for implementation of PTFs. Signal attenuation, reflections from taps, and unintentional filtering by tapping structures result, even in fixed-response transversal filters [26]. For PTFs it becomes even more difficult because the tapping circuitry must now be active, rather than passive.

Concerning TBP, two obvious constraints on a PTF are that the overall delay be at least as long as the duration of the longest desired impulse response, and that the passband of the device not substantially reshape the signal spectrum. These constraints, of course, imply that the TBP of the structure is consistent with the waveform complexity of the impulse response [26].

Dynamic range is a measure of the instantaneous range (*i.e.*, without signal renormalization) over which signals can be used with a component [26]. In any device, the low end of its dynamic range is limited by noise, and the high end by nonlinearities that cause limiting or produce spurious signals [25]. Although a variety of definitions exist, the spurious-free dynamic range will be discussed in this application.

4.2 PTF Device Alternatives [25]

A quick discussion will be provided for each PTF technology type; the ACT device will be examined more extensively. Bottom-line comparisons to the ACT technology will be the chief interest here.

4.2.1 ACT Technology

ACT was first demonstrated by M.J. Hoskins and B.J. Hunsinger at the University of Illinois in 1982. Figure 14 is a cross-sectional view of a simplified ACT delay line and is used here to describe the basic ACT principle of operation.

A surface acoustic wave generated by a high-Q unidirectional transducer (UDT) propagates through a conductive region of a depleted n-doped GaAs epitaxial layer. This region is the acoustic charge transport
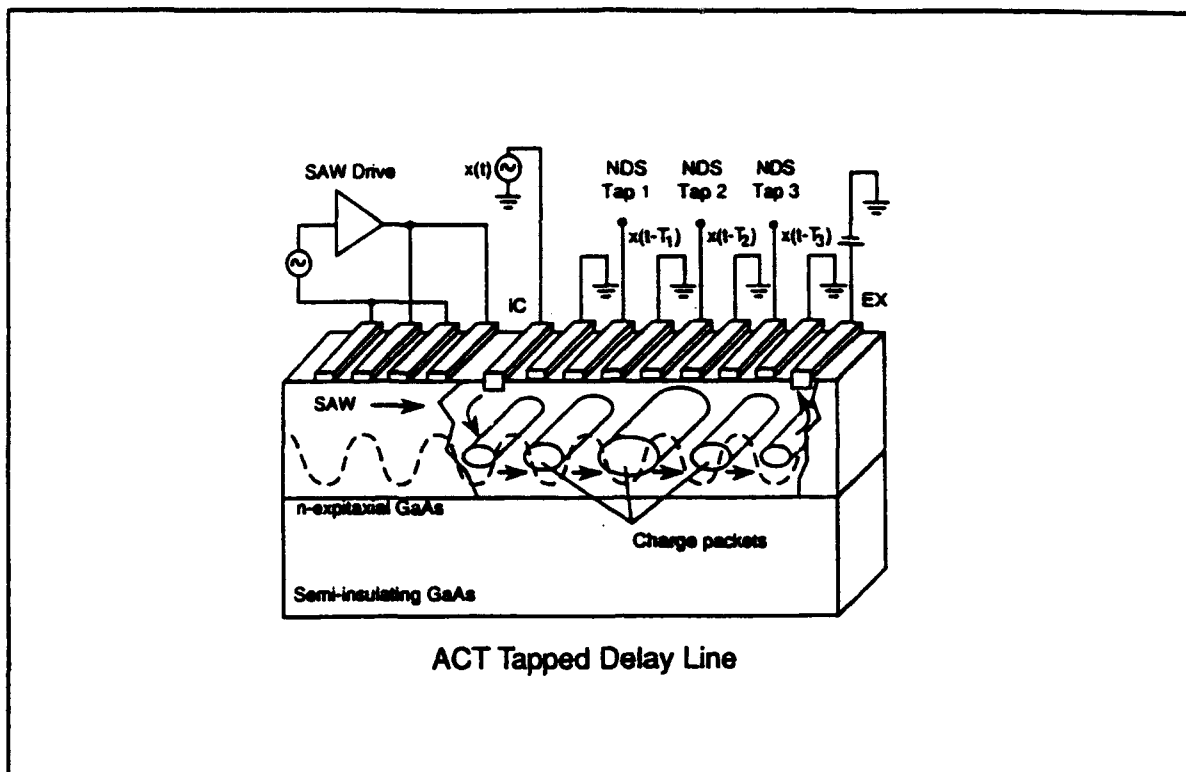
Figure 14 Simplified drawing of an ACT delay line [29].

(ACT) channel. The traveling surface wave produces electric fields via the piezoelectric coupling of the GaAs crystal which confine and transport charge injected into the depleted ACT channel at the input contact (IC) due to the input signal $x(t)$. The charge propagates along with the traveling surface wave and electric fields past nondestructive sense (NDS) electrodes at the characteristic GaAs SAW velocity, 2864 m/s, to the charge extraction contact (EX). Each NDS tap then provides a delayed replica, $x(t - T)$, of the input signal.

As already firmly suggested by now, the ACT device's basic structure is the programmable transversal filter function with adjustable tap weights and integral tap coefficient storage. Since the basic operation of the generic PTF has already been explained in Chapter 3, it will not be repeated here. Figure 15, however, shows a simplified schematic of the ACT PTF integrated circuit architecture to perform the PTF function. This figure additionally shows that the summing function is provided by parallel connection of the outputs of all the programmable attenuators to a tap summing node. The tap coefficient storage is performed by GaAs static random access memory (SRAM). Without going into details (see [27] for more), the programmable attenuators

4-3

are implemented by *C-2C* ladders (using only two values of capacitance) that act as multiplying digital-to-analog converters.
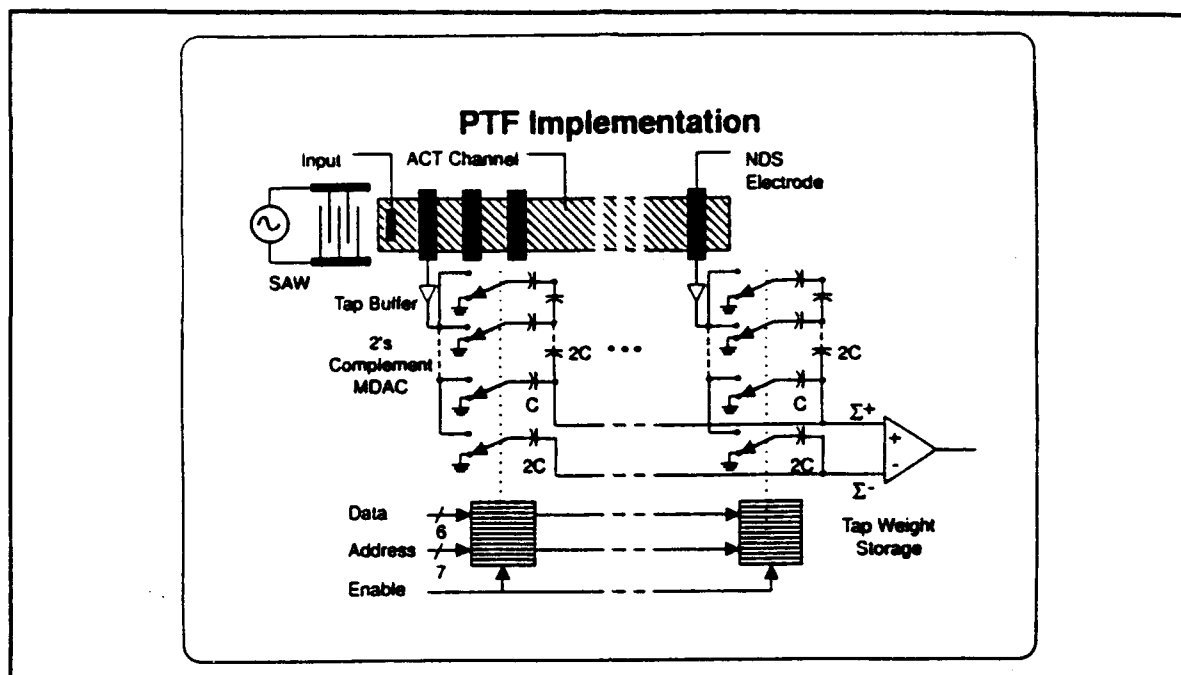
Figure 15 ACT PTF simplified schematic diagram [29].

4.2.2 Charge-coupled devices (CCDs)

Charge-coupled devices are an important class of semiconductor devices that are widely used today as imaging devices in portable video cameras. They are also useful in analog signal processing applications such as delay lines and filters.

The device operates by transferring packets of electrons along a semiconductor surface via a sequence of transfer electrodes controlled with a three-phase clocking mechanism. Other devices transfer the charge within a buried channel. These buried-channel devices can operate at higher frequencies than the previously mentioned CCDs and have some similarity to ACT devices. The biggest difference is that the ACT device is "self-clocking," because the acoustic wave sweeps the charge packets through the device without the need for the complex multiphase clocking electrode structure that CCDs require. ACTs do not need the transfer electrodes of CCDs, nor do they need multiphased clock waveforms or separate input gating pulses. An ACT device needs

4-4

only a single-frequency sinusoidal signal to drive the surface acoustic wave transducer that generates the acoustic carrier wave. One disadvantage of the self-clocking nature of ACT devices is that it is not easy to vary the rate of movement of charge packets in an ACT device. This may be done quite easily in a CCD by simultaneously varying the frequency of all of the clock phases.

The clock noise problem usually forces high-speed CCD transversal filters into "pipe-organ" structures, in which each tap has its own narrow delay line channel. This limits the total number of taps, and it also limits the dynamic range of each tap. Even a fixed (nonprogrammable) CCD transversal filter is a complicated structure, because each tap's channel must have a complete set of clocking electrodes.

The primary factor that tends to limit the maximum usable frequency range of a CCD is charge transfer inefficiency. Transfer inefficiency is a measure of how many electrons are left behind during the movement of a charge packet from one CCD transfer electrode to the next. For example, consider an input pulse which is originally narrow, corresponding to a higher frequency. As the charge is transfered down the channel some is left behind, effectively spreading the pulse and causing a frequency roll-off, thereby limiting the frequency range.

In summary, CCDs have been successful in applications as imagers and variable delay lines at low video frequencies. However. despite considerable development effort over the past two decades, CCDs have not made their mark as high-speed signal processors in the VHF range. Limited dynamic range and clock noise problems are the reasons most often cited by system designers.

4.2.3 Surface Acoustic Wave (SAW) Devices

The SAW device operates by transferring an electric signal to an acoustic signal via interdigital transducers (IDTs) placed on the surface of a piezoelectric substrate. The acoustic wave velocity is five orders of magnitude slower than the speed of light. Therefore, delays of approximately 5 μs can be obtained on materials 1 cm in dimension versus the 1 km of coaxial cable needed to obtain delays of the same magnitude.

SAW devices are in considerable demand for a variety of signal processing functions throughout the VHF and UHF bands. Nonprogrammable transversal filters, resonators, oscillators, delay lines (fixed, tapped, dispersive, nondispersive), and correlators are part of the SAW repertoire. These devices are appealing to system designers because they are simple, cheap, rugged, passive, and very repeatable.

Although fixed-tap ACT transversal filters look similar to SAW devices, there are many important differences. Both devices use a surface acoustic wave, but in the SAW device the acoustic wave is the signal itself. In the ACT, the wave is only a carrier for the signal. This has many important consequences. The wide bandwidth of an ACT device extends down to dc, whereas SAW is fundamentally a bandpass technology. Also, each tap of an output SAW PTF extracts some of the acoustic energy, and thus diminishes the signal that will be sensed by the other remaining taps. Signal sensing in an ACT tap array is nondestructive; the number of electrons in a charge packet are only nominally diminished by the presence of a tap. An ACT device can have thousands of fixed nondestructive sensing (NDS) taps.

Also, in SAW devices, there is the fundamental problem of insertion loss and triple-transit echoes which must be traded off; *i.e.*, a simple SAW filter can never be closely impedance matched at both input and output ports, or substantial triple-transit echoes occur. ACT devices do not have a triple-transit problem because the "charge transport mechanism is unidirectional, and therefore, not capable of supporting multiple reflections of transported charge between transducers or other reflective objects" [25].

The most important difference between ACT and SAW devices is integratability. ACT devices are made on GaAs, so they can be integrated with linear and nonlinear active circuits. SAWs are usually fabricated on insulating piezoelectric materials such as quartz and lithium niobate, and fabrication of active circuits directly on these substrates is not presently feasible.

Because of these differences, it seems unlikely that *fixed* ACTs and SAWs will compete much for applications. Because ACT devices are more complex to build and require large drive power, it is doubtful that they will find much application as nonprogrammable bandpass filters: SAW devices do the job more simply and

4-6

cheaply. *Programmable* ACT devices, however, probably will compete with SAW devices for reasons of versatility and cost.

4.2.4 Digital Signal Processors

Since signals in the real world are analog, digital signal processors require analog-to-digital (A/D) converters. However, ACT devices require no A/D converters since it is done naturally by the sweeping SAW. For high-speed signal processing, digital devices are usually quite costly in terms of money, speed, size, weight, and power consumption. These disadvantages are often perceived to be outweighed by two big advantages; namely, accuracy and programmability. Programmability is something that digital devices clearly have had over analog devices and has been lacking in high-speed analog signal processing systems. The ACT device attempts to reverse this deficiency. The power of ACT devices can be seen when signals undergo the processes of multiplication and addition. A typical ACT filter can perform at the equivalent of 45 GFlops (floating point operations) in the space required for one digital chip in a digital computer. This processing capability is over 50 times that of a Cray-2 supercomputer [28].

ACT devices need not necessarily compete with digital devices. Clearly, in the transversal filtering mode they are superior, especially when the frequencies are over, say, 50 MHz. But many times, ACTs work in concert with digital devices. ACTs can work at intermediate frequencies (IF) towards a final digital processing stage for further processing.

4.2.5 Active Filters

ACT devices can also be compared with active filters. Active filters realize a desired filter response by combining amplifiers with passive feedback elements such as resistors and capacitors. Moreover, active filters can have gain, whereas passive filters cannot. The high end of the usable frequency range for active filters is limited mainly by operational amplifier technology, which can be several hundred megahertz or more of bandwidth, thereby coinciding with SAWs and ACTs. Active filters, however, are mostly used below 1 MHz.

They are invariably infinite impulse response (IIR) or feedback recursive filters versus the FIR technology found in ACTs, SAWs, and CCDs. Therefore, with active circuits, designers must take special caution to prevent instability, a problem not inherent in FIR structures. IIR filters also have nonlinear phase responses which require multiple stages of active circuitry to alleviate. By contrast, ACT devices have precisely linear phase. Practically speaking, for those frequencies where ACT and active filters coexist, transversal filters with ACT can realize higher order filter responses in a smaller volume than active filters. If narrow bandwidths are desired (below 1 MHz), than active filters become advantageous.

4.3 ACT PTF Specifications

The performance parameters of the ACT PTF used in this thesis are provided in Table 1. The device is the commercially available ACT-202 enhanced performance PTF designed and developed by Electronic Decisions Division of Comlinear Corporation [29]. Programmable devices have 127 taps while fixed transversal filters have up to 2000 taps. Tap weight resolution for the ACT-202 is 6 bits: 5 bits for amplitude and one for the sign. Devices with 8 bits of resolution are also available. Although the frequency range of the device is listed as 160 MHz, the PTF supports only a 1-90 MHz bandwidth capability. This bandwidth is limited by the tap spacing of 5.6 ns. It should also be noted that the absolute maximum input power of the device is +10 dBm; therefore, sufficient input buffering is required so that the device is not overdriven and damaged.

Table I ACT Programmable Transversal Filter (ACT202) specifications.

Tap characteristics

Number of taps	127
Tap weighting	6 bits
Tap spacing	5.6 nsec
Tap Uniformity	±1 dB

RF Performance [a]

Insertion loss	0 dB
Dynamic range [b]	
Spurious-free	
2nd-order limited	35 dB
3rd-order limited	45 dB
Input	60 dB

Delay line characteristics

Frequency range	1-160 MHz
Sampling rate	358 MHz
Delay range	
Minimum delay	3 nsec (typical)
Maximum delay	708 nsec (typical)

RF input/output

Input level [c]	-5 dBm [d]
Absolute maximum input	+10 dBm
I/O impedance	50 ohms
SAW spurious output level	-40 dB

Digital input

Compatibility	IBM/PC parallel port
Programming time	55 μsec/tap

Temperature range

Operating (case)	0-50°C
Storage	0-70°C

Power

Input power supplies	
+12 V supply tolerance	5%
-5 V supply tolerance	5%
+12 V supply current	500 mA (typical)
-5 V supply current	200 mA (typical)
Power dissipation	7 watts (typical)

Physical characteristics

Size	
Length	8"
Width	5"
Height	1"
Weight	1.6 lb

[a] Measured with taps set for 45 MHz hanning-weighted filter
[b] Measured with 150 MHz noise bandwidth
[c] at 1 dB compression
[d] Optimal input level depends on tap setting

V. Hardware Experimental Configuration, Tests, and Results

This chapter describes the experimental set-up implemented in this thesis, including an explanation for the particularly chosen configuration. This is followed by details of the testing procedure and the results obtained from the tests. Finally, an analysis is provided of the results and how they relate to what was expected from theoretical derivations.

5.1 Configuration Options Described

It was initially desired to construct the interference rejection filter to implement the LMS adaptive algorithm using only *one* ACT PTF, as seen in Figure 16. However, as indicated in Equation (49), to update the PTF tap weights so that the gradient of the mean-square error is driven down the performance curve toward the optimal Wiener solution, the value of the delayed input sample signal at each tap is required. With the ACT PTF construction, this is not possible because the only interface to the ACT PTF is via an RF input signal port, an RF output signal port (which is the summation of all of the weighted and delayed input samples), and the 25-pin parallel RS-232 port which can only be used to *load* initial and updated tap values. Hence, implementation of the interference rejection subsystem with the conventional LMS adaptive algorithm is not possible using only *one* ACT PTF. However, an adaptive interference canceller could be constructed using only one ACT PTF if the linear random search (LRS) algorithm is used. As discussed in Chapter 3, the convergence time for this algorithm is much longer than that of an adaptive canceler using the LMS algorithm.

Two possibilities will be described for a solution using a *pair* of ACT PTFs. One of these solutions, called the "burst-processing" technique, was described in [8]. However, the signal samples in the burst-processing system are shifted at a rate *N* times the input sampling rate in order to facilitate the update of all the weights by a single multiplier, whereas with the conventional LMS adaptive system, the signal samples are shifted at a rate equal to the input sampling rate. For the input sampling rate of the ACT PTF, this would require a (127 taps X 356 MHz =) 45.2 GHz system bandwidth. Hence, it would be impossible to update the tap weights at each successive input sample. Also, the two devices must be precisely timed.
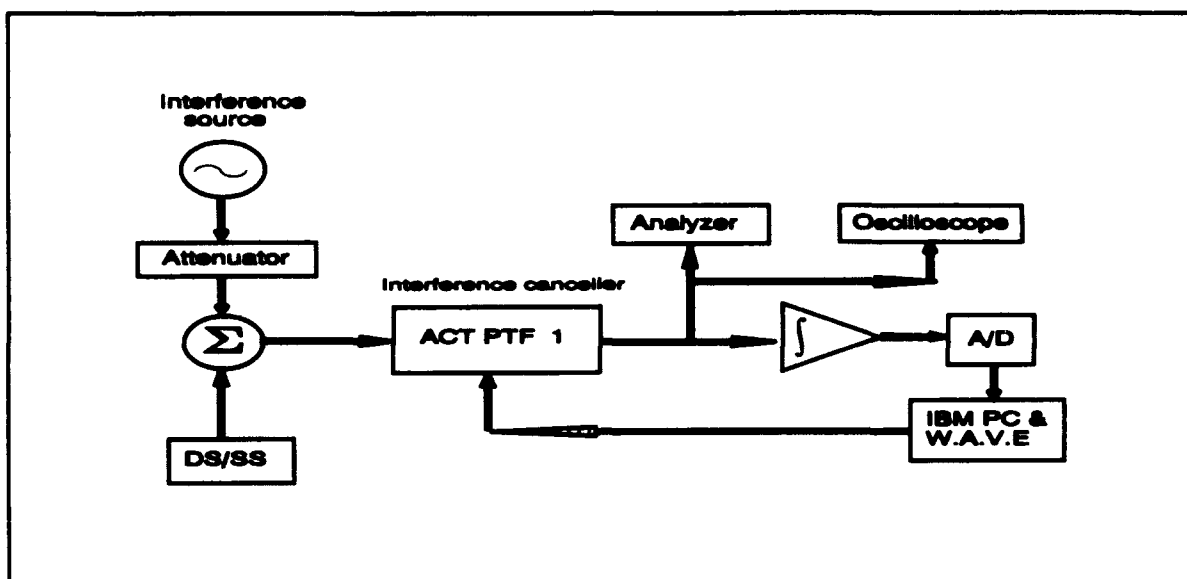
Figure 16 Originally desired AIS subsystem using only one ACT PTF.

Another possibility of implementing an adaptive interference rejection filter with two devices is as illustrated in Figure 17 [29]. PTF1 performs an autocorrelation of the signal plus noise which is followed by the taking the Fourier transform of this signal to determine the power spectral density (PSD). With this procedure the frequency component of the strongest signal is determined and the information forwarded to the second PTF which develops the notch. As descibed here, this adaptive interference rejection system does not actually implement an adap'ive algorithm, but is a transform-domain processor similar to that described by Ketchum and Proakis in [5]. This technique may seem simpler than the system which employs an adaptive algorithm; however, it exhibits stability problems. Also, it is not clear how to program the PTFs for multiple or variable (non-stationary) jamming signals.

5.2 Chosen Experimental Configuration

The configuration illustrated in Figures 18 and 19 is used for this thesis. This configuration implements a "modified" LMS algorithm. An ACT PTF establishes the notch (as desired) while another ACT PTF device, which is implemented as a selectable delay line (SDL), updates the tap weights one tap at a time by adjusting each tap in succession while setting the remaining taps to zero. This "modified" LMS algorithm is based on the

5-2
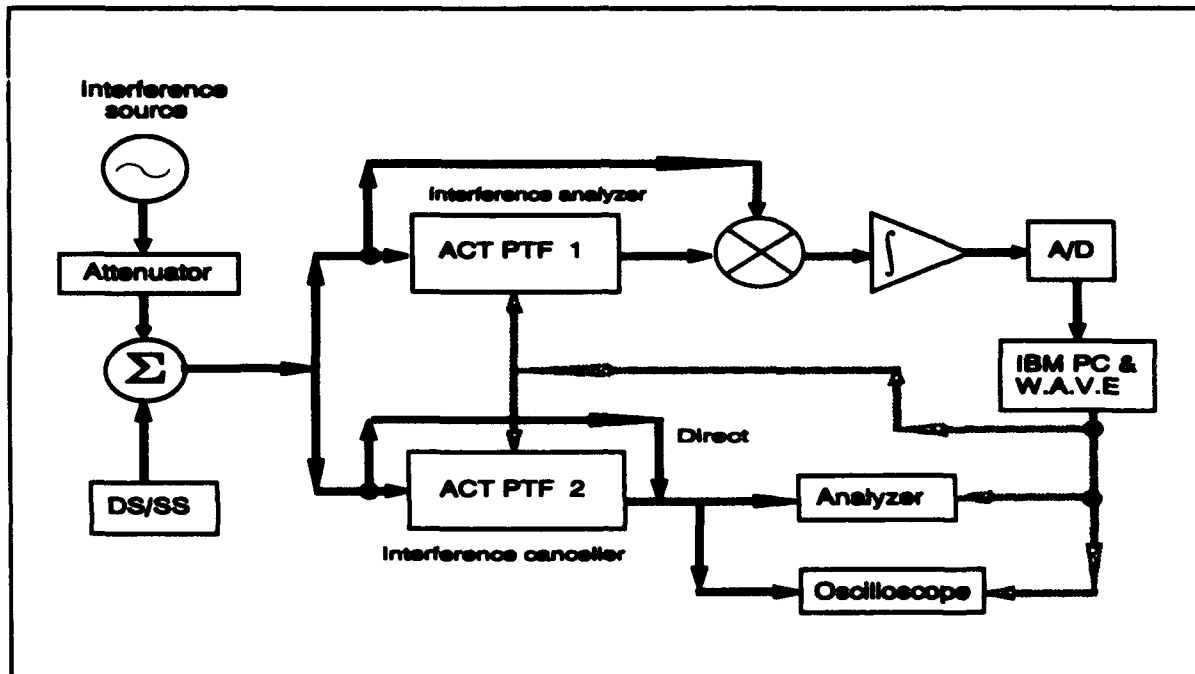
Figure 17 Block diagram of a transform domain interference suppression technique.

following constraints:

(1) It assumes the statistical properties of the system input remain constant over the adaptation time interval;

(2) It does not update the taps every kth sample (which is physically impossible because it implies a 500 ns update time), but rather in larger groupings (longer update intervals);

(3) It does not calculate the quantity $2\mu\varepsilon_k x_k$ for every kth sample but uses time-averages instead; hence

$$w_i(k + 1) = w_i(k) + \mu \overline{e(k)x(k - i\Delta T)} \tag{54}$$

where the overbar indicates a time-averaging of the cross-correlation between the error signal and the weighted sample values of the taps. This averaging is accomplished by feeding the output error signal through a LPF prior to A/D conversion for input to the software where the LMS algorithm is computed (see Figure 20).

Once the error signal is input into W.A.V.E. it is processed according to the description of the "modified" LMS. The required coding within W.A.V.E. is provided in Figure 21. Since each of the tap weights

5-3
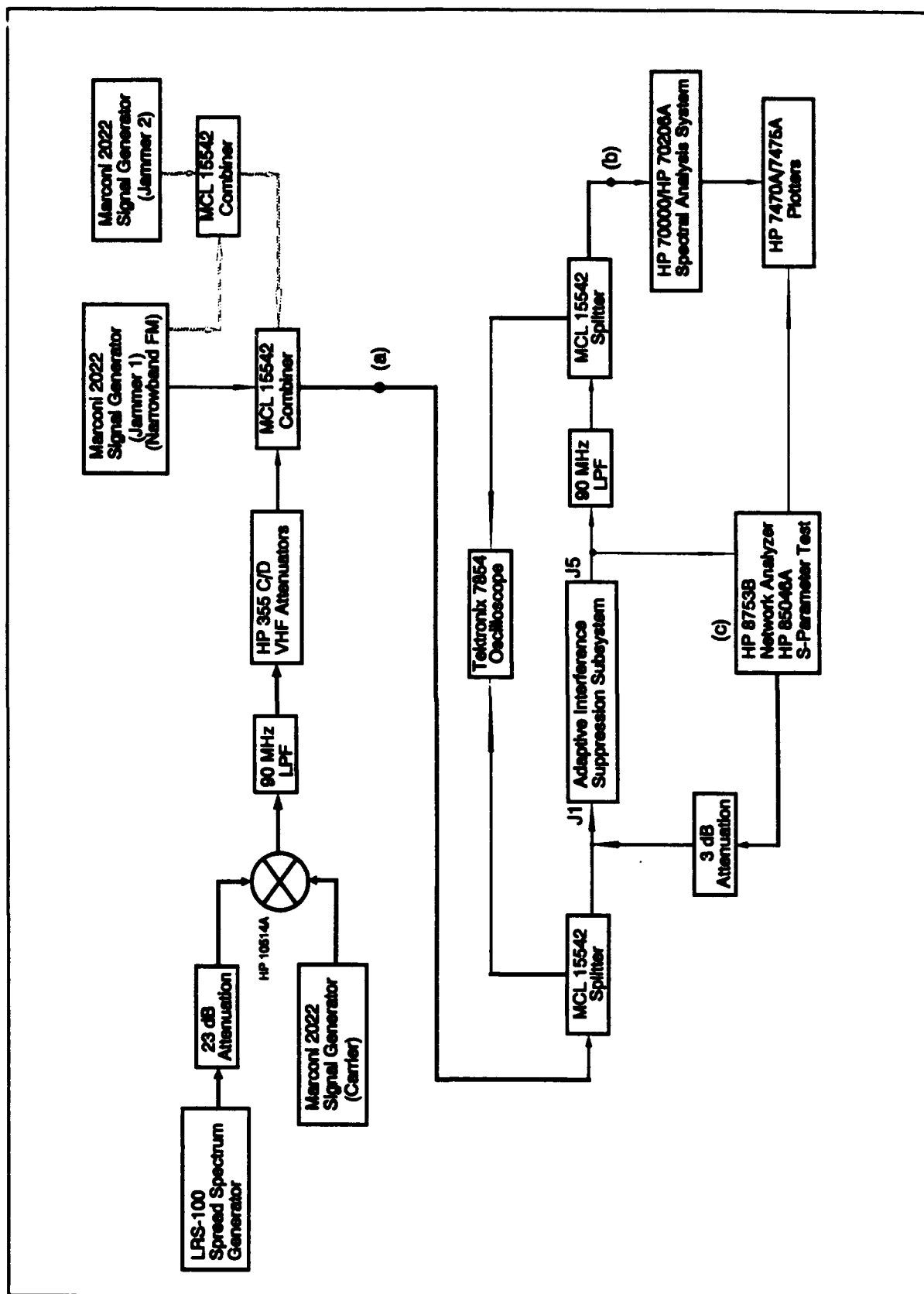
Figure 18 Experimental hardware configuration implemented in this study.
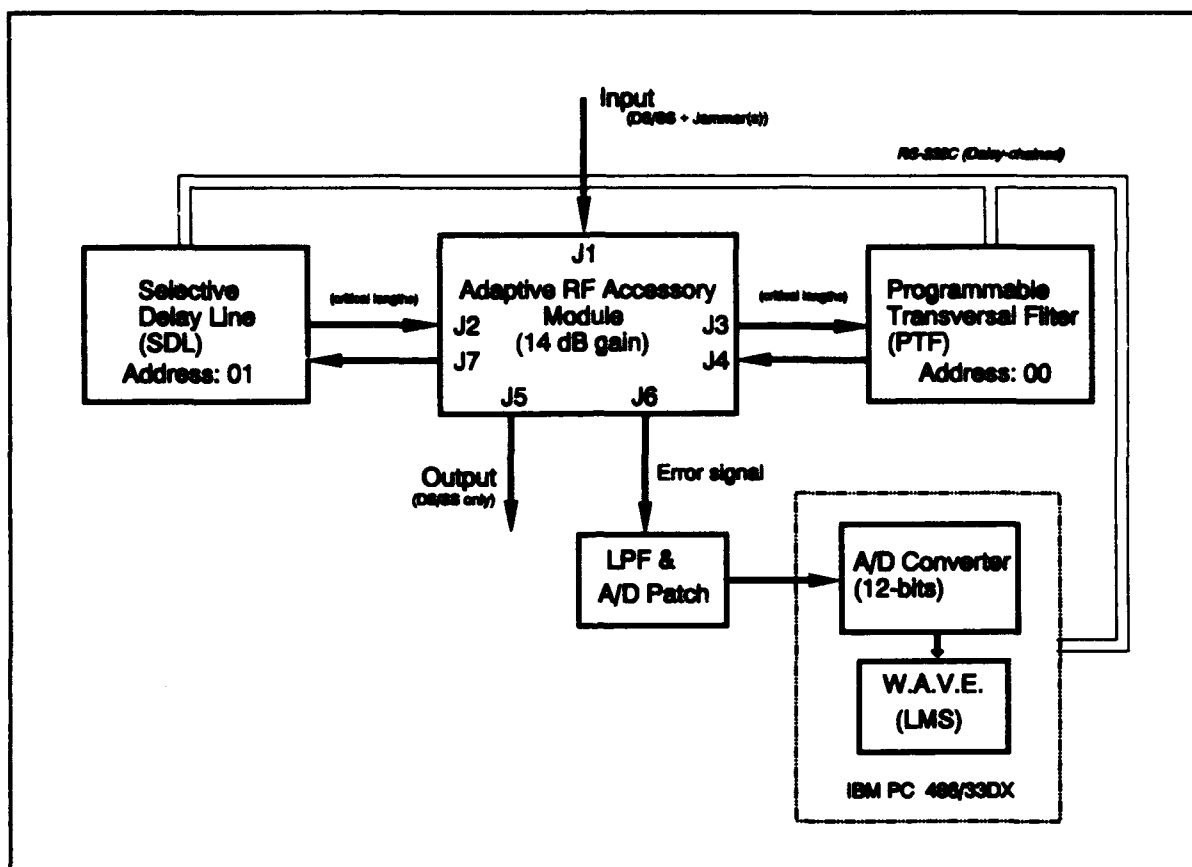
Figure 19 Configuration of the adaptive interference suppression (AIS) subsystem.

are updated individually, exact timing must be maintained between the PTF and the SDL with respect to the RF accessory module. This alignment is verified first. Next, key system parameters are initialized. The STARTTAP and ENDTAP variables can use any quantity of consecutive tap weights; 100 taps were typically used. To ensure a de-correlation of the DS/SS signal entering the PTF and SDL with that of the direct path, the delay, ΔT, is the duration of one chip in the PN sequence; 50 ns for the 20 Mcps case typically used for the experiments. Hence, by turning off the first 9 taps (5.6 ns x 9 = 50.4 ns) in the PTF and SDL (as a minimum), de-correlation is assured, since a PN sequence shifted by one or more chips with respect to itself is uncorrelated.
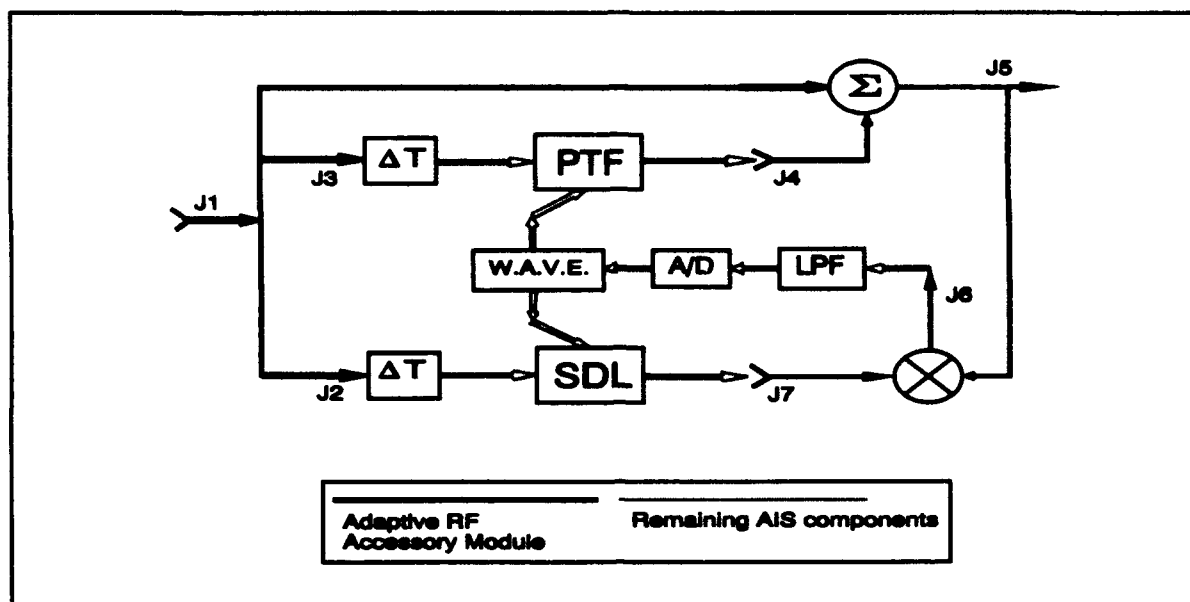
Figure 20 Internal operation of the Adaptive RF Accessory Module.

5.3 Test Factor Variations

The following factors, along with their corresponding parameters, were varied for the test cases conducted in this experimentation:

■ *Jammer-to-signal ratios* (JSRs)(dB): 10; 20; 30.

This parameter will test the adaptive systems ability to notch out jammers of varying relative strength to the DS signal.

■ *Jammer offset from carrier (single jammer)* (degrees): 0; 10; 45; 80.

This parameter will test the adaptive systems ability to notch jammers at different locations within the DS/SS's PSD, especially at the critical carrier frequency. To clarify, zero degrees offset is located at the carrier or center frequency and 90 degrees offset is at the null of the mainlobe of the BPSK waveform.

■ *Jammer offset (dual jammers)* (degrees): 0 & 45 ; –45 & 45.

Since there is much interest in determining the ability of an AIS suppression system in handling multiple jammer environments, this parameter is an extension of the single-jammer case. Also, a need exists to determine how the system handles jammers of varying strength.

5-6

```
####  CHECK TIME ALIGNMENT OF PTF AND SDL TAPS  ####
#  TAP 28 - 169 ns - BEGINNING
pf28 /00 dup(27,0) | [-31] | dup(100,0)
pf28 /01 dup(27,0) | [-31] | dup(100,0)


#  TAP 78 - 449 ns - MIDDLE
pf28 /00 dup(77,0) | [-31] | dup(50,0)
pf28 /01 dup(77,0) | [-31] | dup(50,0)


#  TAP 127 - 723 ns - END
pf28 /00 dup(126,0) | [-31] | [0]
pf28 /01 dup(126,0) | [-31] | [0]


###  INITIALIZE PARAMETERS  ###
ADGAIN = 10                        #/ Gain in the A/D converter
STARTTAP = 28                      #/ Varies number of taps used; (ΔT)
ENDTAP = 127                       #/ Specify last tap used in range
STEPSIZE = 0.9                     #/ Convergence parameter
LEAKAGE = .9995                    #/ Expected tap weight leakage
WAIT_TIME = .1                     #/ Time for LPF to settle (seconds)


##  CHECK MULTIPLIER POWER
adrecv(0,ADGAIN,YOE,100)           #/ Reading from A/D converter
YOE                                #/ Power levels of 100 samples


PTF_TAPS = dup(128,0)              #/ Initial PTF taps
pf28 /00 PTF_TAPS                  #/ Initial PTF load
pf28 /01 PTF_TAPS                  #/ Initial SDL load


#COUNT = 0
#while COUNT >= 0                   #/ Intialize looping of iterations


##  ADAPTIVE LOOP
TAP = STARTTAP                      #/ Start with first tap
pf28 /01 dup(128,0)                #/ Clear SDL
pf28 /01 31, TAP                   #/ SDL - 1st tap on
wait WAIT_TIME                     #/ Wait for LPF to settle out
adrecv(0,ADGAIN,YOE,100)             #/ Read A/D converter
RAW_ERROR = [mean(YOE)]              #/ Estimate error signal
for TAP = STARTTAP+1, ENDTAP, 1      #/ Loop through the rest of the taps
  pf28 /01 0, TAP-1                  #/ Turn previous SDL tap off
  pf28 /01 31, TAP                   #/ SDL - 1 tap on
  wait WAIT_TIME                     #/ Wait for LPF to settle out
  adrecv(0,ADGAIN,YOE,100)           #/ Read A/D converter
  RAW_ERROR = RAW_ERROR | [mean(YOE)]     #/ Estimate error signal
next TAP                           #/ End of loop
ERROR = RAW_ERROR - mean(RAW_ERROR)     #/ Subtract DC offset in error vector
UPDATE = -ERROR/2000                 #/ Normalize update
PTF_TAPS = LEAKAGE*PTF_TAPS +
dup(STARTTAP-1,0)|(31*STEPSIZE*UPDATE)|[0]
                              #/ Calculate new PTF tap weights
pf28 /00 PTF_TAPS                       #/ Load new PTF tap weights
#COUNT = COUNT + 1
#COUNT
#endwhile
```

Figure 21 W.A.V.E. coding to perform "modified" LMS algoritm.

- *Carrier frequency* (MHz): 45, 135.

The 45 MHz carrier is optimal in terms of the maximal allowable bandwidth the ACT device, so it will be chosen as the carrier frequency of the DS/SS signal. (The 45 MHz signal is in the center of the dc-90 MHz region of the ACT device which is limited by the 5.6 ns tap spacing). The 135 MHz carrier, which is in the ACT's second Nyquist interval (as a result of aliasing), could also be implemented so as to increase the intermediate frequencies for which the system is operated.

- *Chip sequence data rate, R_c* (Mcps): 10; 20.

Because of the intertap delays in the ACT PTF construction, these two chip sequence data rates will be examined in conjunction with the number of taps chosen.

- *PN Sequence length*: R4(4,1), R13(13,12,11,5,2,1).

These two PN sequence lengths will help determine the effects of having finite length repeated sequences and their relationship to the adaptive system's ability to predict them. This should affect the amount of the undesired notching of the DS/SS signal along with the notching of the narrowband jammers.

- *Processing gain, G_p* (dB): 20; 30; 40.

Although not of relevance to the SNR improvement factor tests, this parameter is, of course, pertinent to the P_e measurements.

- *PTF tap structure*: One-sided predictive filter; two-sided interpolating filter. This parameter should validate the superiority of the two-sided filter structure when the jammer is close (± 17 degrees) to the carrier frequency. Aside from these offsets, the two structures alternate as to which is better in terms of expected SNR improvement factor as indicated in Figure 42.

- *Number of taps, L*: 127 (100 actually used); 15; 7.

Because it is critical that the intertap delay be approximately equal to the chip duration so that the DS/SS signal is approximately uncorrelated at different taps (such that the AIS cannot predict and, henceforth, notch out the desired signal), the number of taps will be adjusted in conjunction to the chip rate. Below is shown the taps which will be used with the number of taps selected:

7 taps: 1,22,43,64,85,106,127

15 taps: 1,10,19,28,37,46,55,64,73,82,91,100,109,118,127

■ *Convergence parameter, μ* : vary according to signal level.

The value of μ must be < 0.1 of signal power. This parameter affects the speed of convergence as well as the accuracy (the closer it can achieve the optimal Wiener solution). Unfortunately, these two characteristics must be traded off.

5.4 Desired Measurements and Data Collection

The following measurements and data were gathered during the experimentation:

■ JSR before (or input to) the adaptive interference suppression (AIS) subsystem along with a plot of the corresponding spectrum (see point (a) in Figure 18). This is done by calculating the power of the jammer and the power of the DS/SS signal at the output of the respective generators and then recalculating the levels output from any mixers, splitters, etc. leading up to the AIS subsystem.

■ JSR after the AIS subsystem adaptation or at its final (convergent) setting of the tap weights along with the corresponding signal spectra (point (b) in Figure 18). The ratio of the JSR after adaptation to that before entering the AIS subsystem is the SNR improvement factor, G_I .

■ Plot of the frequency-domain response and time-domain response of the filter at its convergent values. This is accomplished by disconnecting the ACT PTF from the rest of the system with the tap weights set at the convergent solution and inputting a signal from network analyzer/S-parameter test set (point (c) in Figure 18).

■ Measurement of the squared-error signal after each iteration within each test case. These values will be used to derive learning curves for each case. These values were obtained in the W.A.V.E software program as seen in Figure 19.

■ Convergence time in terms of the total time it takes the AIS subsystem to reach its convergent value and in terms of the time and number of iterations of the adaptive algorithm. This measurement was also obtained in W.A.V.E.

■ Calculation of the SNR improvement factor, G_i. This value is determined by examining the amount the AIS notches the jammers from the before and after spectral plots.

■ Bandwidth of the resulting notch. This width is a function of the number of taps implemented in the PTF (and the total time delay of the PTF), *i.e.* more taps used yields a narrower notch—a desired effect so as not to overly disrupt the reception of the desired signal. This value is obtained from the ACT PTF frequency response curves for those cases in which it was generated.

5.5 SNR Improvement Tests

The SNR improvement factors can be described as the ratio of the SNR with the adaptive system in place to the SNR with no adaptive system. The above analysis is especially straightforward because it corresponds to SNR at the output of the suppression filter rather than the SNR at the output of the final detection filter. Table 2 lists the test cases that were run in the experimentation.

Case 1 involves a tone jammer at the carrier with a JSR of 10 dB, which equates to a peak signal 27 dB above the peak value of the DS/SS signal. The power level of the sinusoid can be found directly from the spectral plot as seen in Figure 22; the power of the DS/SS signal can calculated from the same plot as follows:

$$P_{DS/SS}(dBm) = Peak\ value(dBm) + 10\log\left(\frac{W_{ss}/2}{ResolutionBW}\right) \qquad (55)$$

In all the cases, the JSR is adjusted (via the HP 355 C/D attenuators) by reducing the DS/SS power level and keeping the tone jammer power constant. This makes it possible to determine the amount of SNR improvement obtained in the experimentation from the spectral plots taken after the adaptations. This SNR improvement is equal to the amount of the notching of the tone jamming signal. From Figure 22, it is evident that the adaptive

Table 2 Test Cases Run in the Experimentation.

Predictive filter; 100 taps; R13 code length; 20 Mcps; 45 MHz carrier; single jammer.

$\delta\omega = 0$

Case 1: JSR = 10 dB
Case 2: JSR = 20 dB
Case 3: JSR = 30 dB

JSR = 30 dB

Case 4: $\delta\omega = 10°$
Case 5: $\delta\omega = 45°$
Case 6: $\delta\omega = 80°$

JSR = 20 dB

Case 7: $\delta\omega = -45°$

Dual Jammers

Case 8: $\delta\omega = 0°$ (JSR: 17 dB) & 45° (JSR: 27 dB)

Case 9: $\delta\omega = -45°$(JSR: 17 dB) & 45° (JSR: 27 dB)

Case 10: $\delta\omega = -45°$(JSR: 27 dB) & 45° (JSR: 17 dB)

Case 11: Case 10 with different convergence rate

R5(5,4,2,1) PN Sequence

Case 12: JSR = 20 dB; $\delta\omega = 0$

R13(13,12,11,5,2,1) with 15 consecutive taps

Case 13: JSR = 20 dB; $\delta\omega = 0$

Narrowband FM jammers:

Case 14: 300 kHz deviation FM jammer

Case 15: 10 kHz deviation FM jammer

---

interference rejection system notched the tone jammer by 38 dB. This was accomplished within 13 iterations as seen from the learning curve derived for this case in Figure 27.

Each iteration for the cases using 100 taps took approximately 35 seconds to complete; the iteration times for 15 taps and 7 taps would be about 5.25 seconds and 2.45 seconds respectively. This relatively long
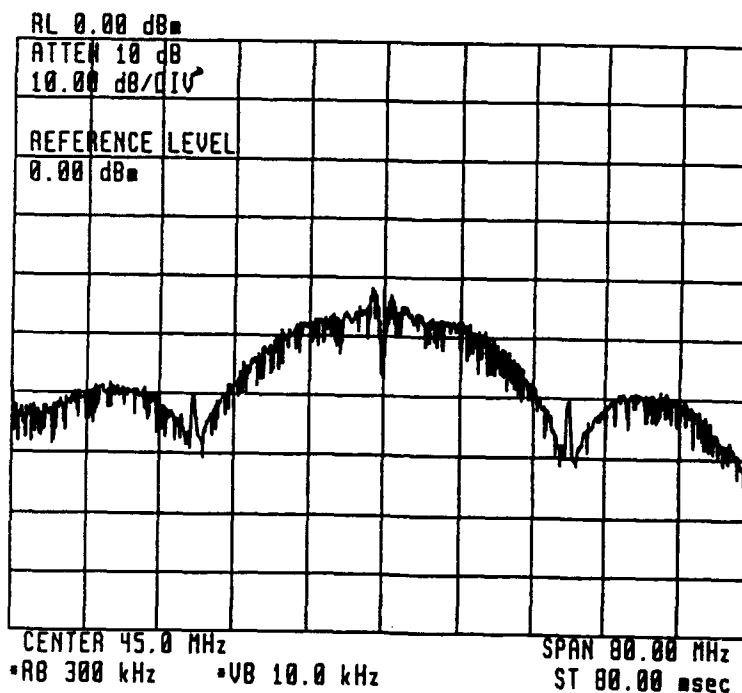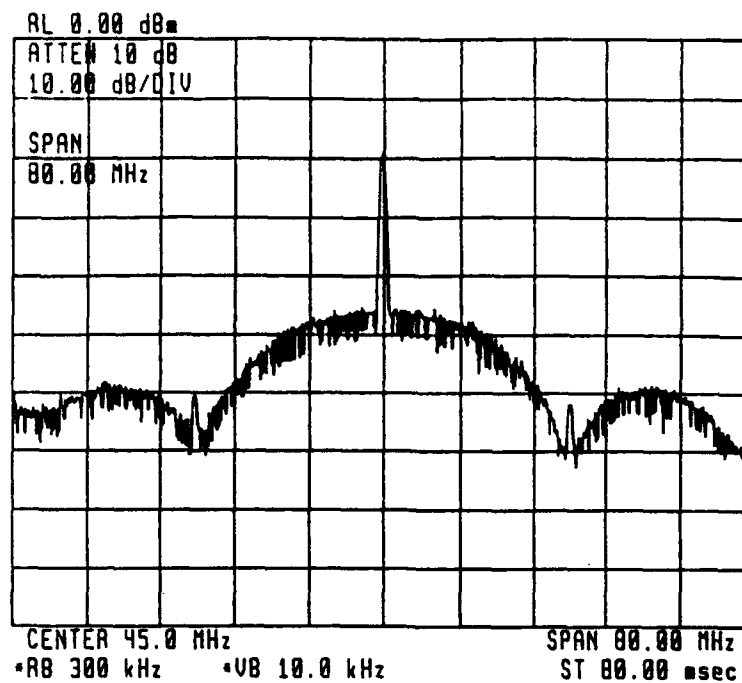
Figure 22 Case 1 (10 dB JSR, δω = 0) before and after spectra. The notch is 38 dB.

period of time for an iteration can be attributed to the following conditions:

(1) the use of 100 taps greatly surpassed the number of taps used in other experimental systems investigated [5-11];

(2) because of the need to use two ACT PTFs, and the way in which the taps are updated (sequentially), the time is, henceforth, increased;

(3) the wait-time for the LPF to settle was conservatively set 1-2 orders of magnitude longer than required (0.1 s as seen in W.A.V.E. coding of Figure 21);

(4) W.A.V.E is an interpretive software package; the use of a dedicated digital signal processor to perform the LMS would decrease the time greatly;

(5) the convergence parameter was not set at the optimal value for every test case; the requirement to do so would have added excessive difficulty within the time available to conduct the experiments.

Figure 23 contains the frequency and impulse responses of the ACT PTF at convergence. Notice the approximately 38 dB of notch at 45 MHz. Also, the 3-dB bandwidth of the notch is approximately 400 kHz, bettering the 1 MHz goal, and the frequency response is flat outside the vicinity of the notch. This explains why the DS/SS signal is minimally affected during the adaptive process, thereby maintaining transmission integrity.

Case 2 is depicted in Figure 24. The only difference in this case from Case 1 is that the JSR is increased to 20 dB such that the peak of the jammer is 37 dB above the DS/SS signal. The adaptive system again notched the signal sufficiently, about 43 dB. In Case 3 (Figure 25), the JSR is increased to 30 dB (peak value of jammer is 47 dB above the DS/SS signal). The amount of notch or SNR improvement can be seen to be about 56 dB. As was also demonstrated in Cases 1 and 2, there is minimal degradation to the desired spread spectrum signal. The frequency response of the ACT PTF at convergence is illustrated in Figure 26, where 55+ dB of notching is evident. The 3-dB notch bandwidth is approximately 500 kHz.

The learning curves for Cases 1-3 are given in Figure 27. Other than the spurious phenomena with Case 1 at iteration 2, the curves are strikingly similar. It will be shown for the upcoming cases that their learning curves are, likewise, consistent with those found in Figure 27. This condition resulted because the jamming

5-13

CH1 S$_{21}$ log MAG   10 dB/   REF -56.63 dB   1 -47.257 dB

FREQUENCY RESPONSE OF ACT PTF - CASE 45.012 000 MHz

CH1 CENTER   45.000 000 MHz   SPAN   10.000 000 MHz

CH2 S$_{21}$ Re   100 mU/   REF 0 U   1 170.87 mU

19.6 ns

MARKER 1
19.6 ns
5.3759 n

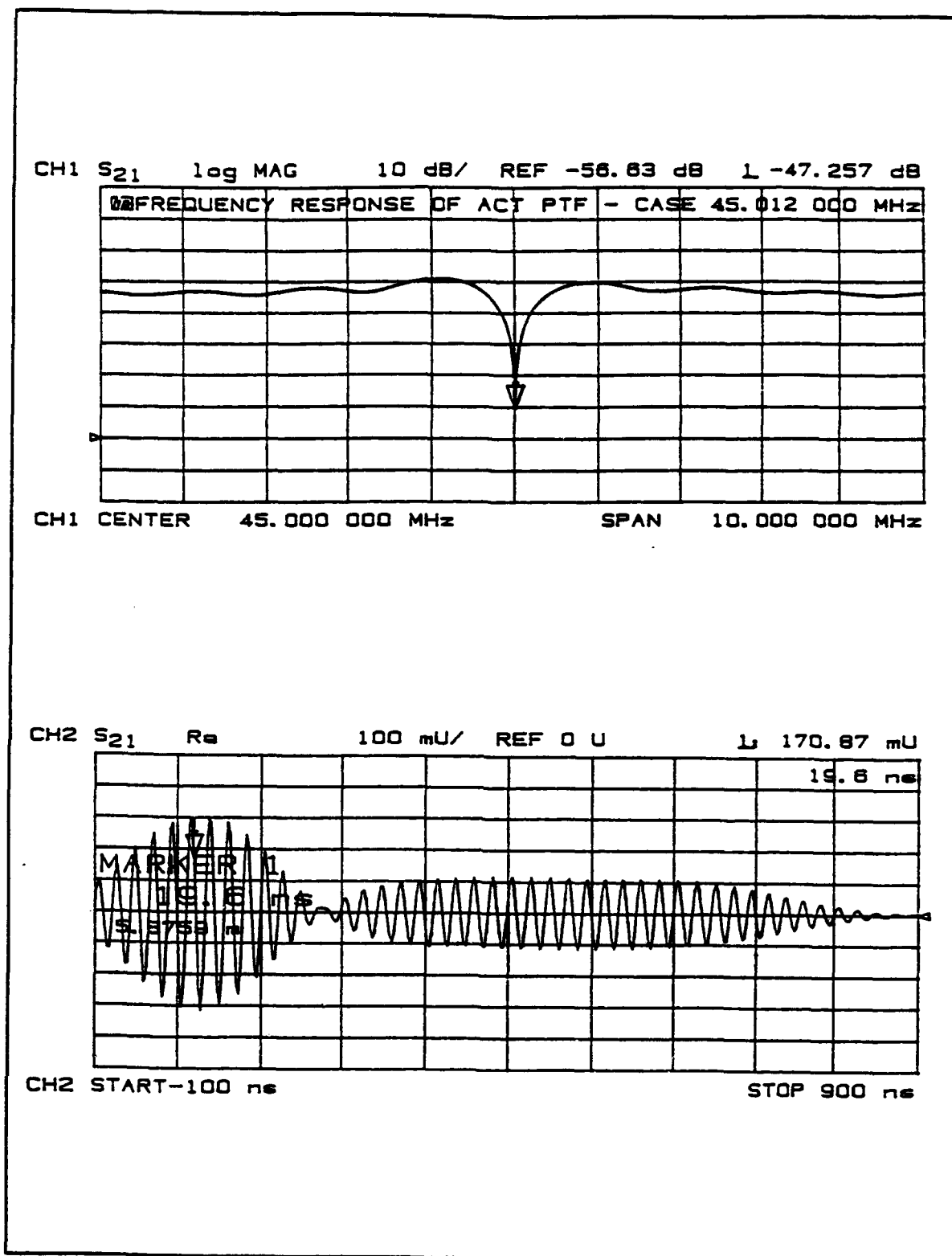CH2 START-100 ns   STOP 900 ns

Figure 23 Frequency and impulse responses for Case 1.

5-14
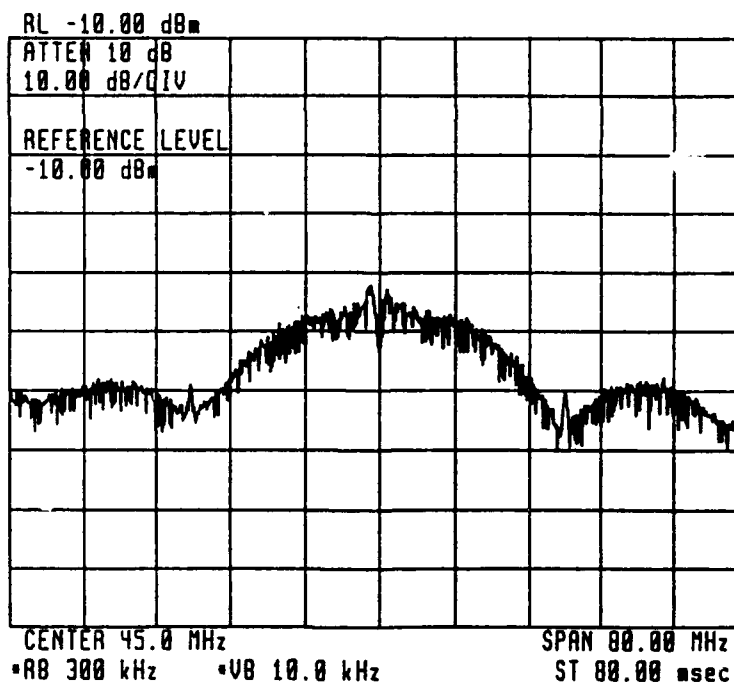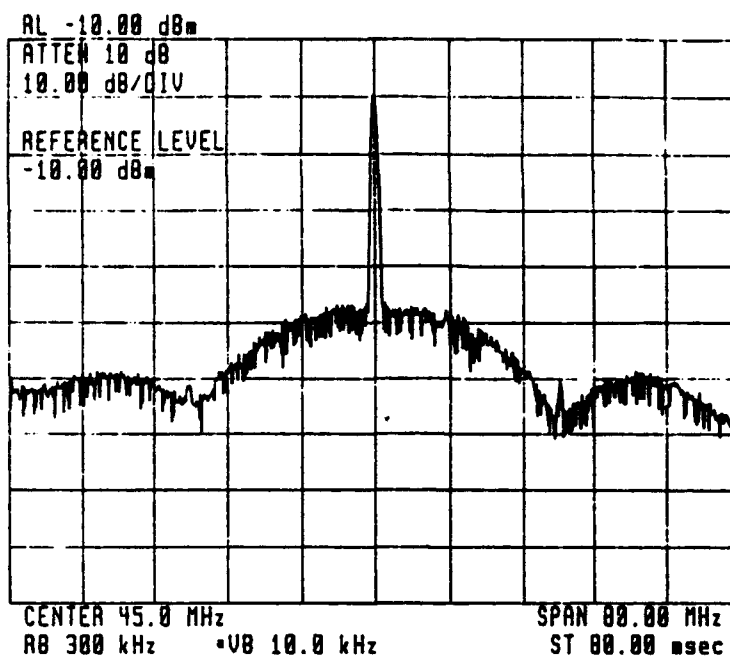
Figure 24 Before and after spectra for Case 2 (20 dB JSR, $\delta\omega = 0$). The notch is 43 dB.
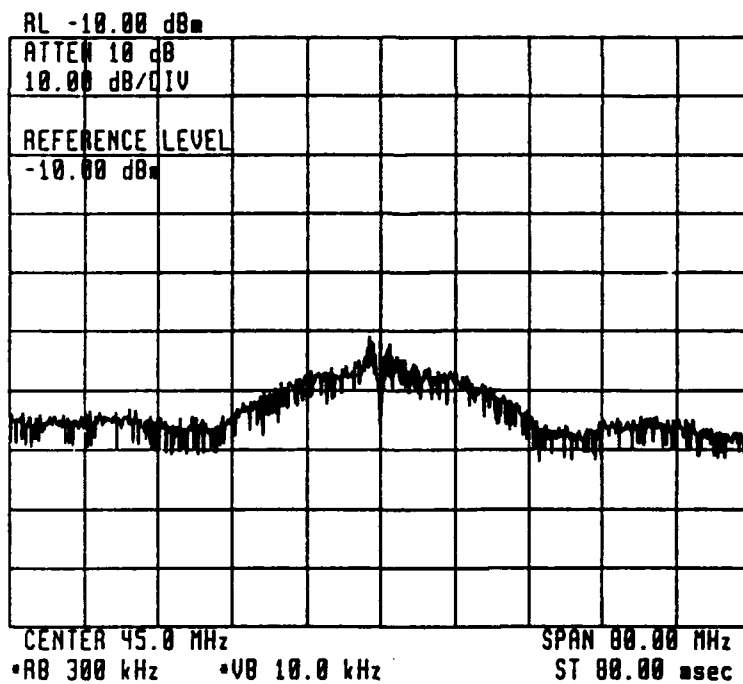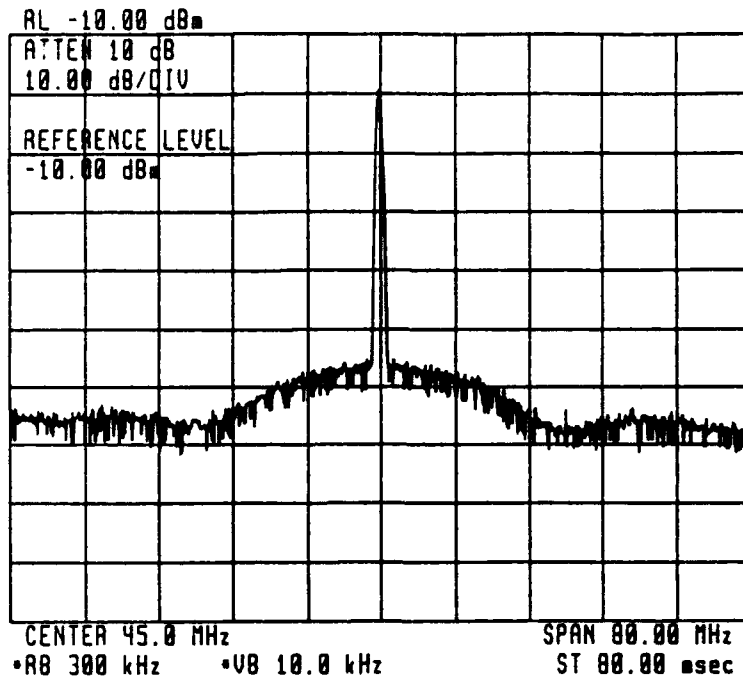
Figure 25 Case 3 (30 dB JSR, δω = 0) before and after adaptation spectra. The resulting notch is 56 dB.
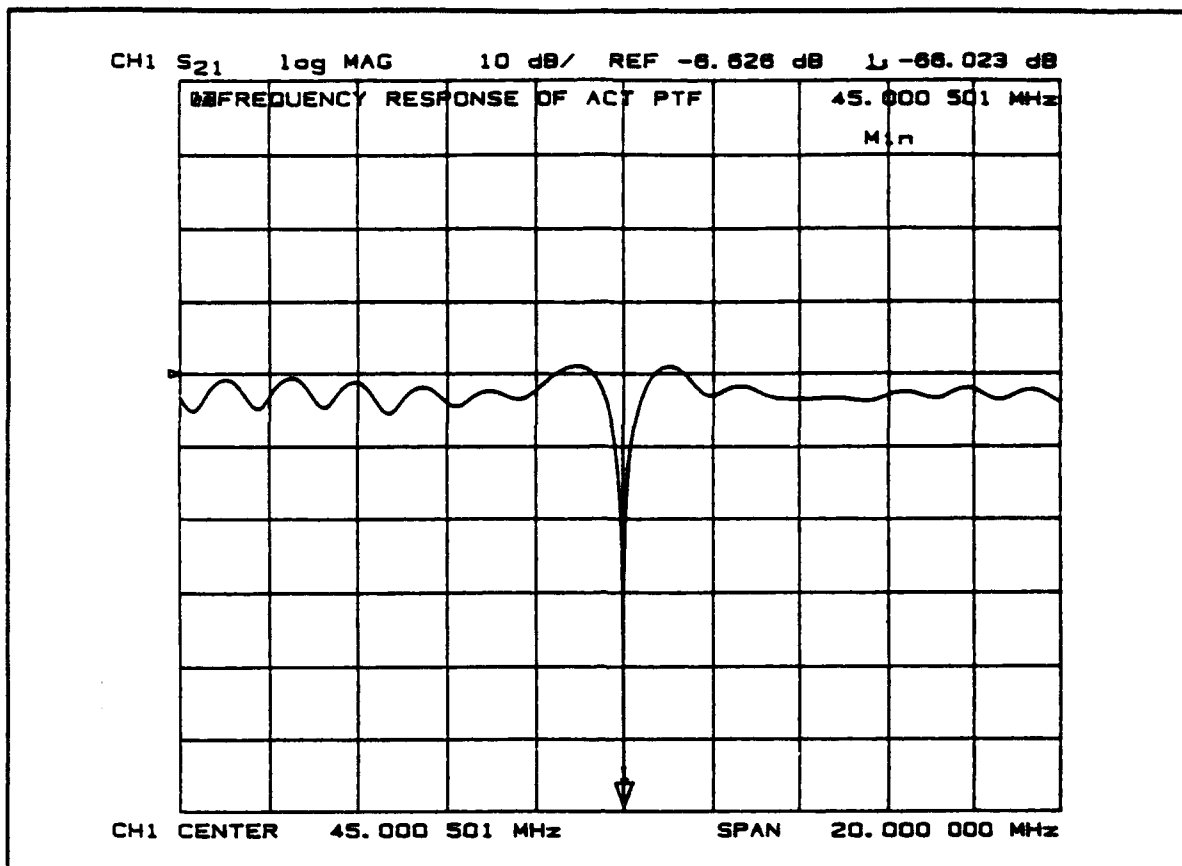
Figure 26 The frequency response of the ACT PTF after adaptation for Case 3.

signal was chosen to be constant at the start of the adaptive process for each case, even though the JSR's were different.

Starting with Case 4 the location of the jamming tone is shifted within the spread spectrum bandwidth. While maintaining the same 30 dB JSR as in Case 3, the jammer is moved to an offset of 10° from the carrier, or to 47.222 MHz. However, as seen from Figure 28, the jammer is nonetheless notched by 55 dB. Even when the jamming tone is moved to an offset of 45° from the carrier (55 MHz), as demonstrated with Case 5, the jammer is, again, notched by 55 dB (Figure 28). This serves to show that the adaptive interference system counters power levels regardless of the frequency location within the spread spectrum bandwidth. This point will be reinforced in later cases.

Learning Curves for Cases 1-3

Iteration	1	2	3	4	5	6	7	8	9	10	11	12	13	14	15
■ Case 1	178.27	51.39	88.21	55.12	33.31	23.93	12.18	6.92	5.52	4.13	2.5	1.78	1.76		
◇ Case 2	167.27	102.92	66.23	41.96	27.85	16.71	10.88	5.88	3.46	3.12	2.36	1.94	1.57	2.02	2.36
▲ Case 3	166.92	102.67	67.61	41.73	26.33	16.65	11.69	6.32	4.06	2.71	1.51	1.59	1.74	1.97	1.23
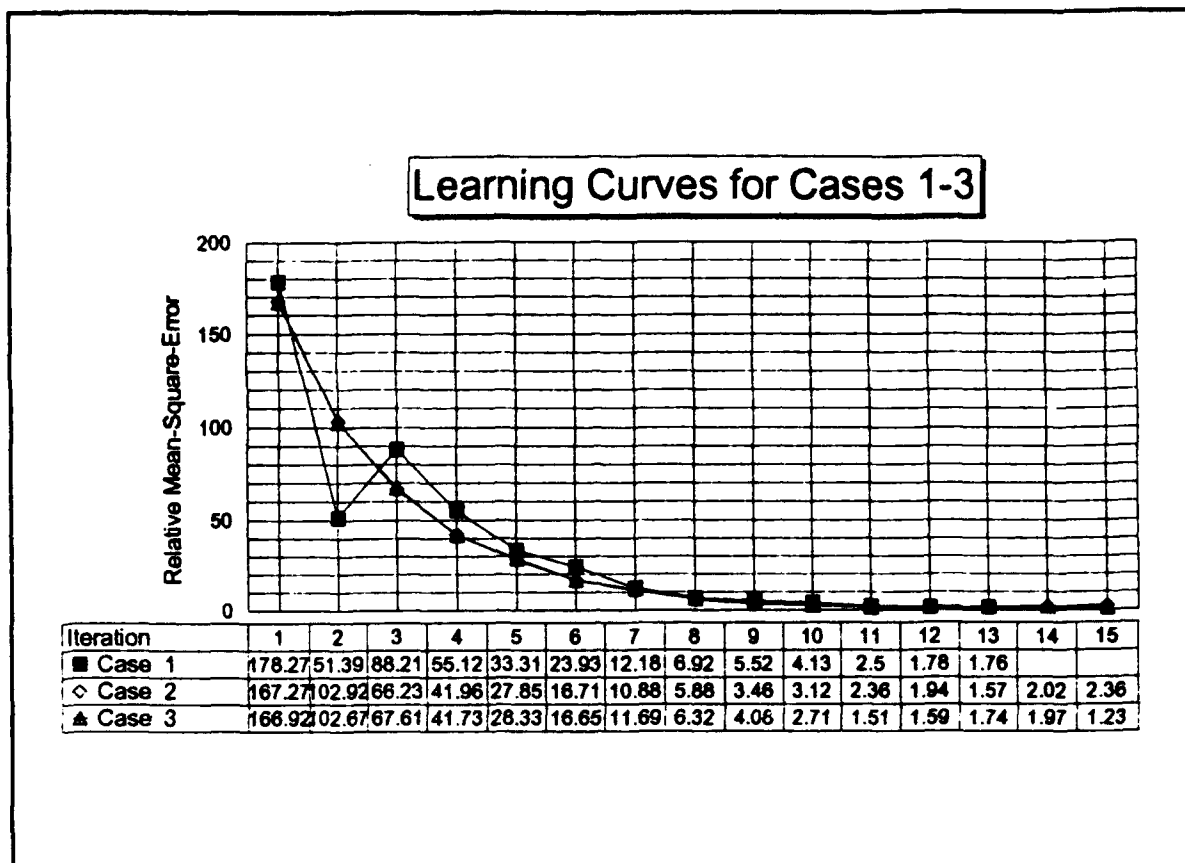
Figure 27 Learning curves for Cases 1-3.

With Case 6, the tone is relocated to 62.778 MHz (or 80° offset). Still maintaining a 30 dB JSR, the jammer is 57 dB abov: the DS/SS signal at this frequency. However, with this case a 56 dB notch is obtained as viewed in Figure 30.

Learning curves for Cases 4-6 are shown in Figure 31. Again notice a consistent process of adaptation even when the jamming signal is shifted with respect to the carrier.

With Case 7, the jammer is moved to the lower-frequency side of the DS/SS mainlobe (at a −45° offset or 35 MHz). This case was run to demonstrate that the adaptive interference cancelling system counteracts the jamming tone's power level regardless of frequency. Figure 32 shows Case 7 in which a 20 dB JSR is encountered. The amount of notch or SNR improvement is 52 dB. Of interest is the spurious signal (obviously a harmonic of the jamming signal) at approximately 70 MHz. This is a result of the squaring operation within

5-18

RL -10.00 dBm
ATTEN 10 dB
10.00 dB/DIV

REFERENCE LEVEL
-10.00 dBm

CENTER 45.0 MHz   SPAN 80.00 MHz
•RB 300 kHz   •VB 10.0 kHz   ST 80.00 msec

RL -10.00 dBm
ATTEN 10 dB
10.00 dB/DIV

REFERENCE LEVEL
-10.00 dBm

CENTER 45.0 MHz   SPAN 80.00 MHz
RB 300 kHz   •VB 10.0 kHz   ST 80.00 msec
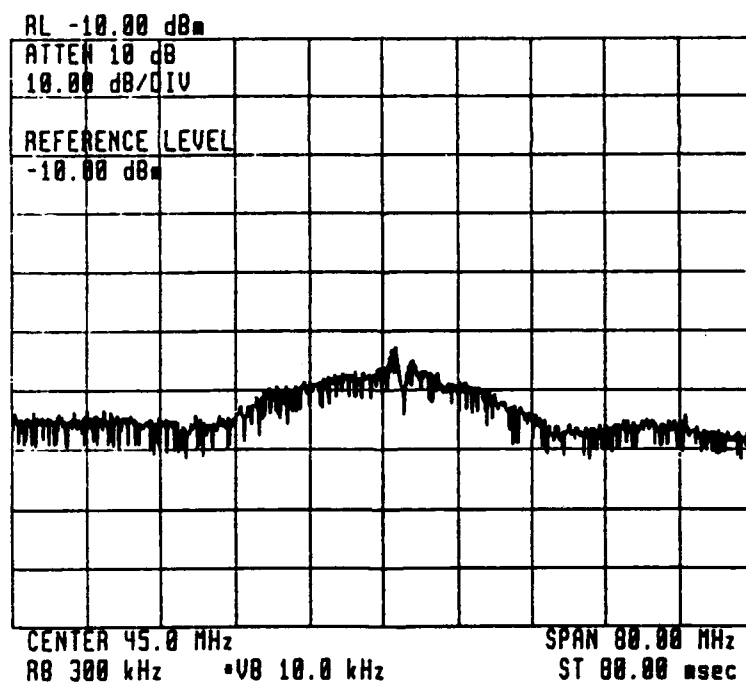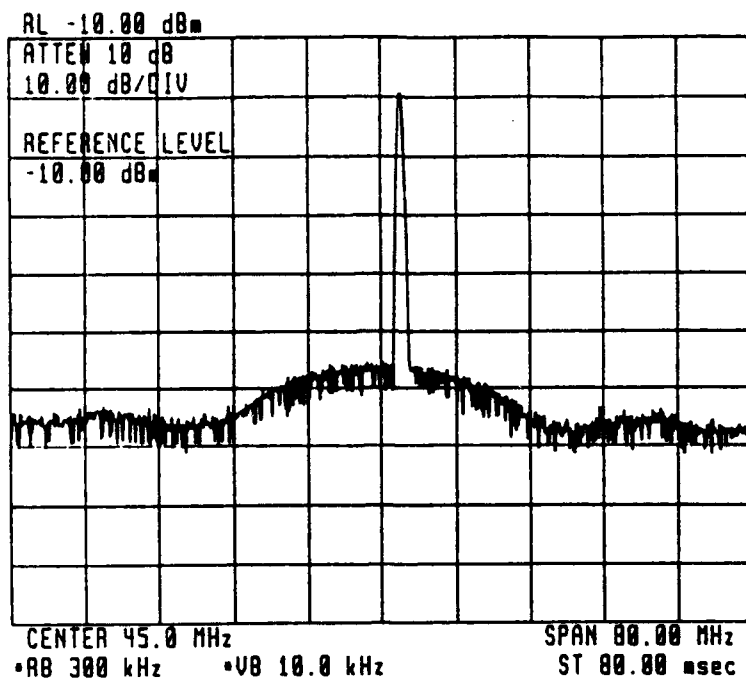
Figure 28 Before and after adaptation spectra for Case 4 (JSR = 30 dB, $\delta\omega = 10°$). The resulting notch is 55 dB.

RL -10.00 dBm
ATTEN 10 dB
10.00 dB/DIV

REFERENCE LEVEL
-10.00 dBm

CENTER 45.0 MHz   SPAN 80.00 MHz
RB 300 kHz   •VB 10.0 kHz   ST 80.00 msec

RL -10.00 dBm
ATTEN 10 dB
10.00 dB/DIV

REFERENCE LEVEL
-10.00 dBm

CENTER 45.0 MHz   SPAN 80.00 MHz
RB 300 kHz   •VB 10.0 kHz   ST 80.00 msec
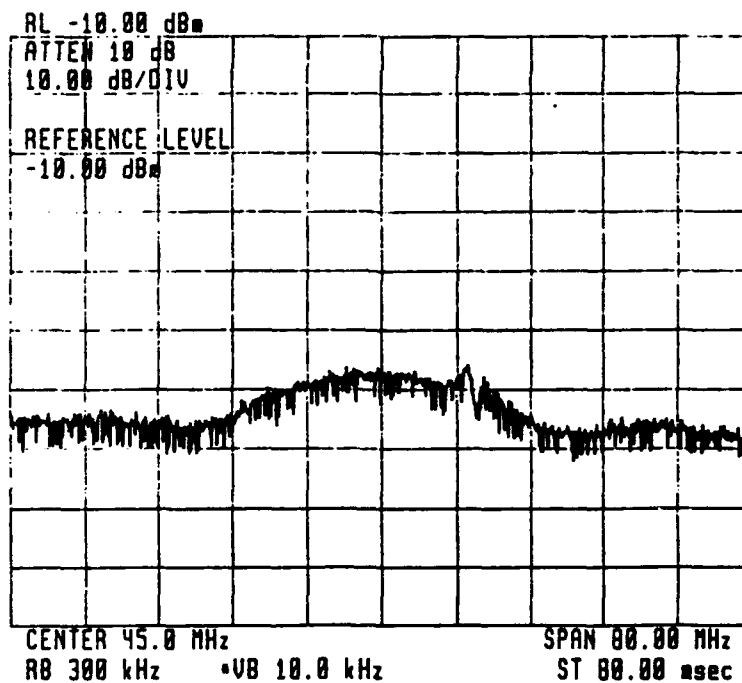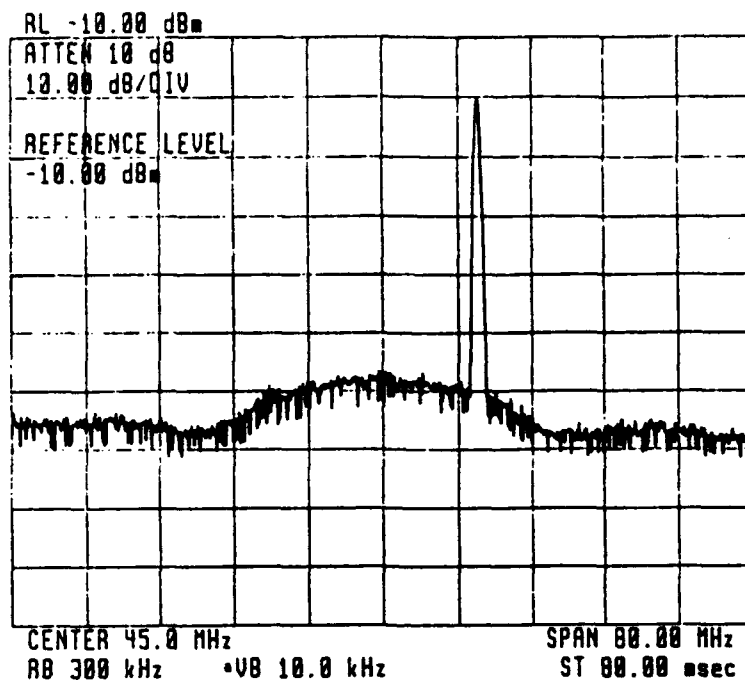
Figure 29 Case 5 spectra. JSR = 30 dB, $\delta\omega$ = 45°. The resulting notch is 55 dB.

5-20

RL -10.00 dBm
ATTEN 10 dB
10.00 dB/DIV

REFERENCE LEVEL
-10.00 dBm

CENTER 45.0 MHz
RB 300 kHz   *VB 10.0 kHz

SPAN 80.00 MHz
ST 80.00 msec

RL -10.00 dBm
ATTEN 10 dB
10.00 dB/DIV

REFERENCE LEVEL
-10.00 dBm

CENTER 45.0 MHz
RB 300 kHz   *VB 10.0 kHz

SPAN 80.00 MHz
ST 80.00 msec

Figure 30 Case 6 with 30 dB JSR and $\delta\omega = 80°$. The jammer is notched 56 dB.

5-21
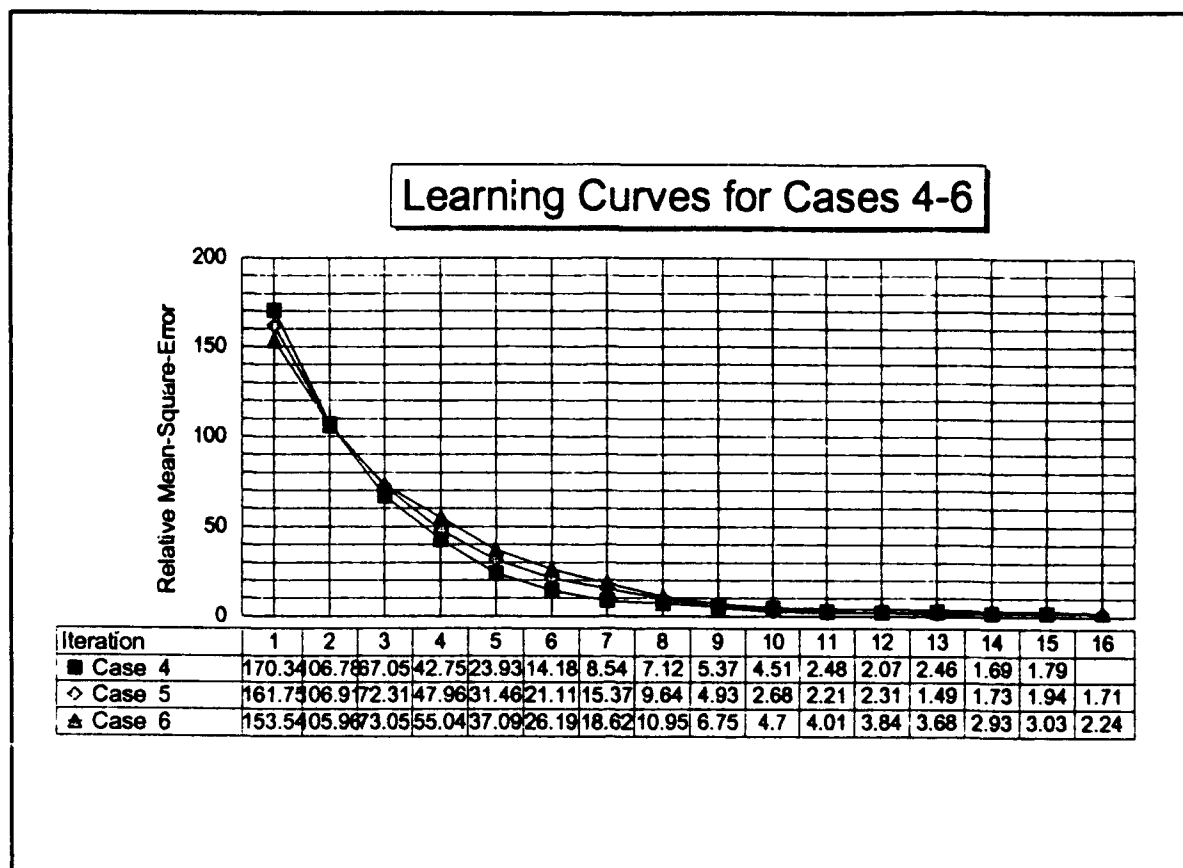
Figure 31 Learning curves for Cases 4-6.

Iteration	1	2	3	4	5	6	7	8	9	10	11	12	13	14	15	16
■ Case 4	170.34	06.78	67.05	42.75	23.93	14.18	8.54	7.12	5.37	4.51	2.48	2.07	2.46	1.69	1.79	
◇ Case 5	161.73	06.9	72.31	47.96	31.46	21.11	15.37	9.64	4.93	2.68	2.21	2.31	1.49	1.73	1.94	1.71
▲ Case 6	153.54	05.96	73.05	55.04	37.09	26.19	18.62	10.95	6.75	4.7	4.01	3.84	3.68	2.93	3.03	2.24

the spectrum analyzer since the analyzer displays power signals. Making use of the trigonometric identity, $\cos^2\theta = \tfrac{1}{2}(1 - \cos 2\theta)$, the double-frequency harmonic becomes evident. Two trials were carried out for Case 7, and their learning curves are provided in Figure 33.
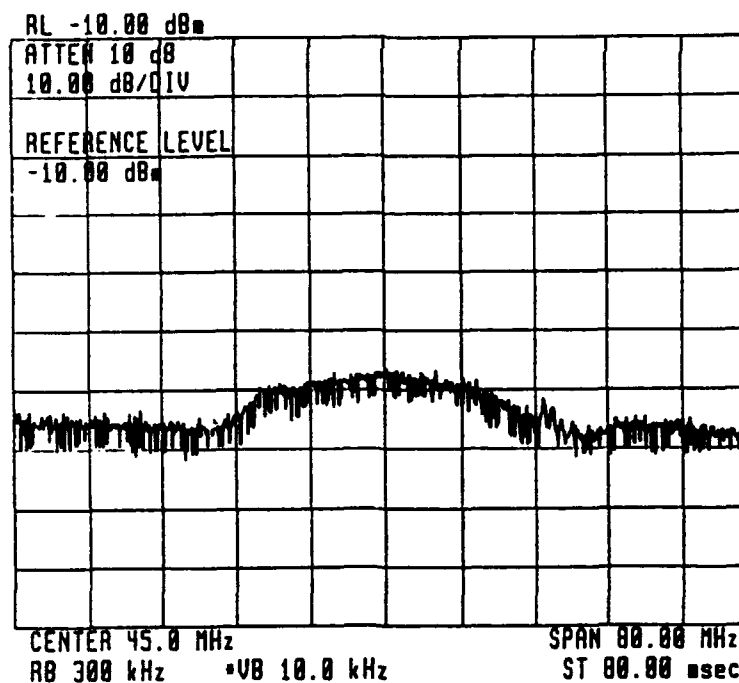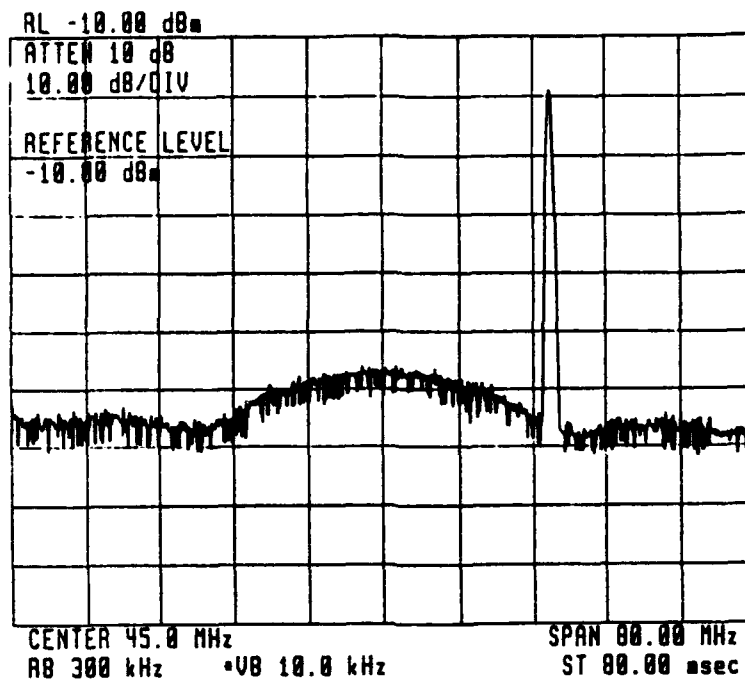
In Cases 8-11 a critical capability of the adaptive interference system is examined: that of notching jammers in a multiple-jammer scenario. Hardware restrictions, however, limit the number of jammers, practically, to two. Case 8 involved a tone at the carrier with a JSR of 17 dB and a stronger jammer (JSR of 27 dB) located at 55 MHz (45° offset). When two jammers of unequal power were input to the system, it took substantially longer to notch them relative to a single jammer at either location. The W.A.V.E. algorithm was setup to perform looping after each iteration because of the larger number of iterations it took to notch the jammers. Figure 34 (which comprises four separate plots shows that after 10 iterations, the tone at 55 MHz was
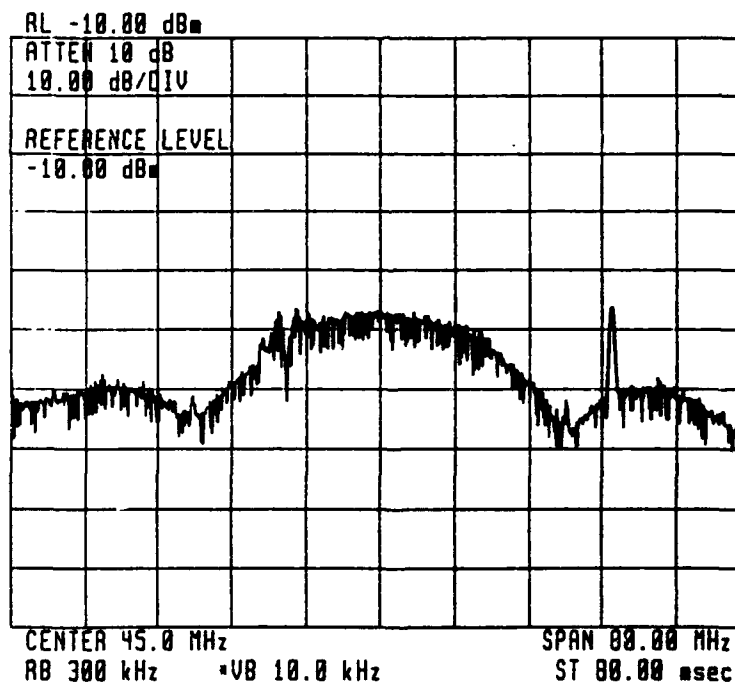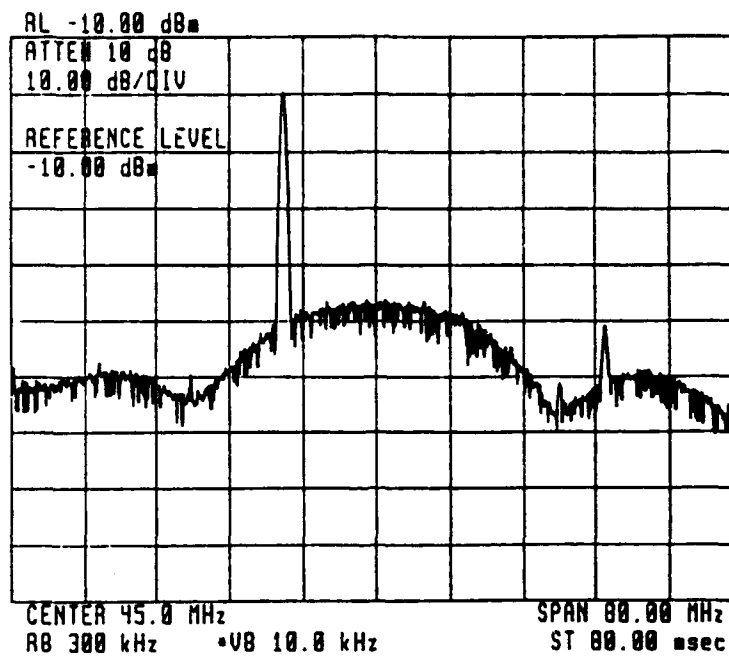
Figure 32 Case 7 before and after spectra. JSR = 20 dB, δω = -45°. The tone is notched by 52 dB.

Learning Curves for Case 7

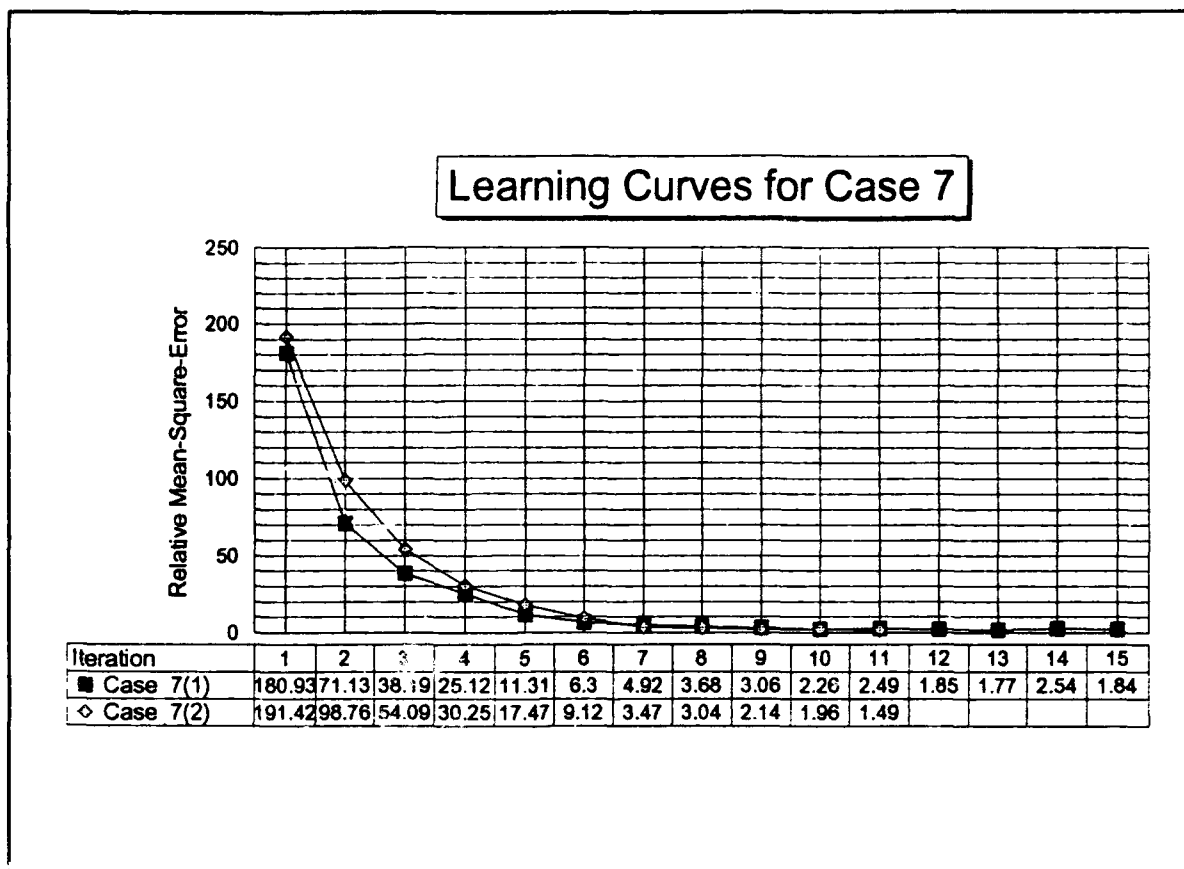| Iteration	1	2	3	4	5	6	7	8	9	10	11	12	13	14	15
■ Case 7(1)	180.93	71.13	38.19	25.12	11.31	6.3	4.92	3.68	3.06	2.26	2.49	1.85	1.77	2.54	1.84
◇ Case 7(2)	191.42	98.76	54.09	30.25	17.47	9.12	3.47	3.04	2.14	1.96	1.49				

Figure 33 Learning curves for two trials of Case 7.

notched by 39 dB and the tone at the carrier by 20 dB. After 20 iterations, the notch levels are 45 dB and 25 dB, respectively. Finally, after 30 iterations, the notches are much the same: 45 dB and 27 dB. Clearly, it takes longer to notch two jammers; furthermore, the amount of the notching is not as much as with the single jammer cases.

Case 9 considers jammers on either side of the carrier: the same tone at 55 MHz (JSR = 27 dB), and a weaker tone at 35 MHz (JSR = 17 dB). Although no spectral plots were generated for this case, from the learning curves generated in Figure 37 one can conclude that similar results should arise with this case as with Case 8.

In Case 10, the jamming tones of Case 9 are reversed. This case is the most telling as to whether the adaptive interference rejection system responds by notching jammers based on their power or based on their
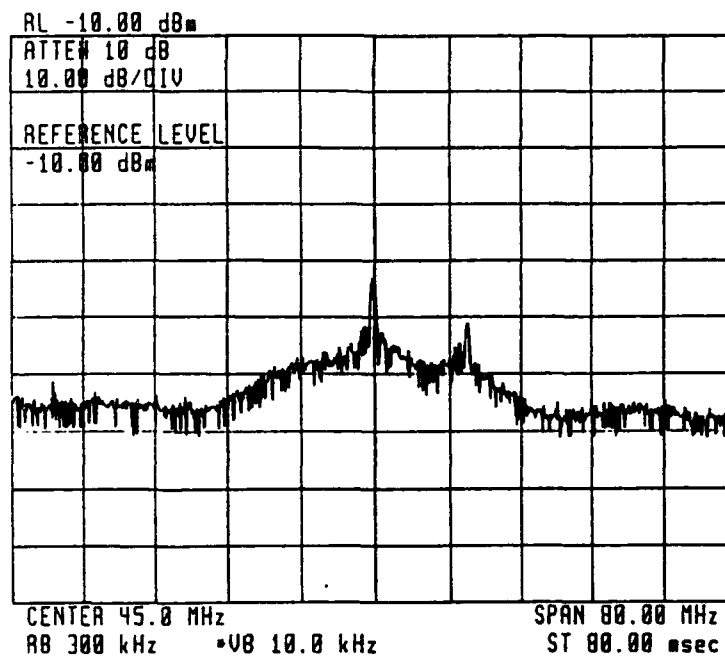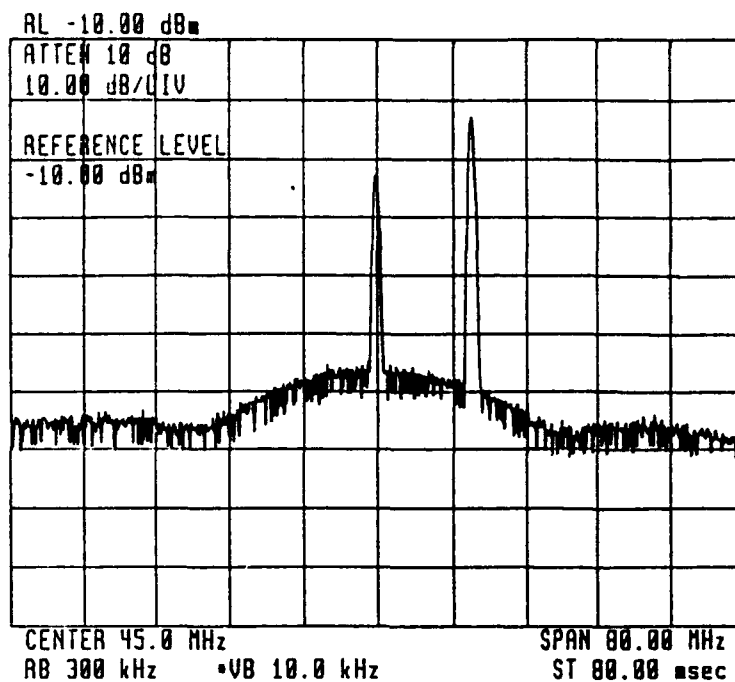
Figure 34 Case 8 with two jammers (JSR 17 dB @ $\delta\omega = 0$; JSR 27 dB @ $\delta\omega = 45°$), (a) before adaptation, (b) after 10 iterations.
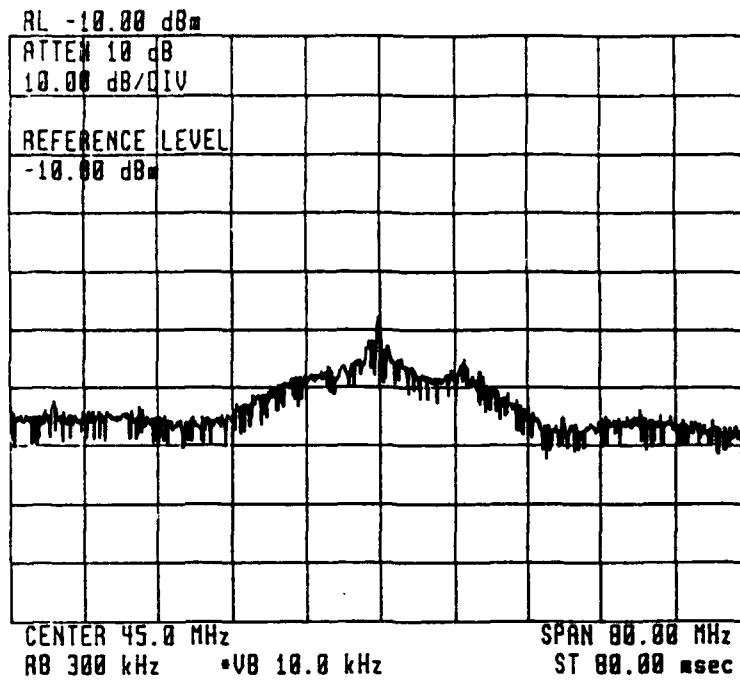
Figure 34 (cont'd) Case 8 (c) after 20 iterations, (d) after 30 iterations.

RL -10.00 dBm
ATTEN 10 dB
10.00 dB/DIV

REFERENCE LEVEL
-10.00 dBm

CENTER 45.0 MHz   SPAN 80.00 MHz
RB 300 kHz   •VB 10.0 kHz   ST 80.00 msec

RL -10.00 dBm
ATTEN 10 dB
10.00 dB/DIV

REFERENCE LEVEL
-10.00 dBm

CENTER 45.0 MHz   SPAN 80.00 MHz
RB 300 kHz   •VB 10.0 kHz   ST 80.00 msec
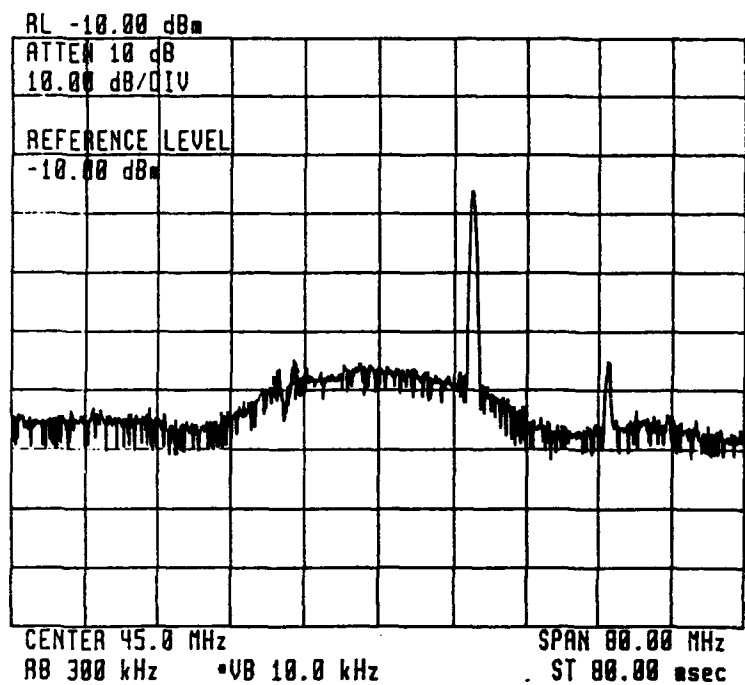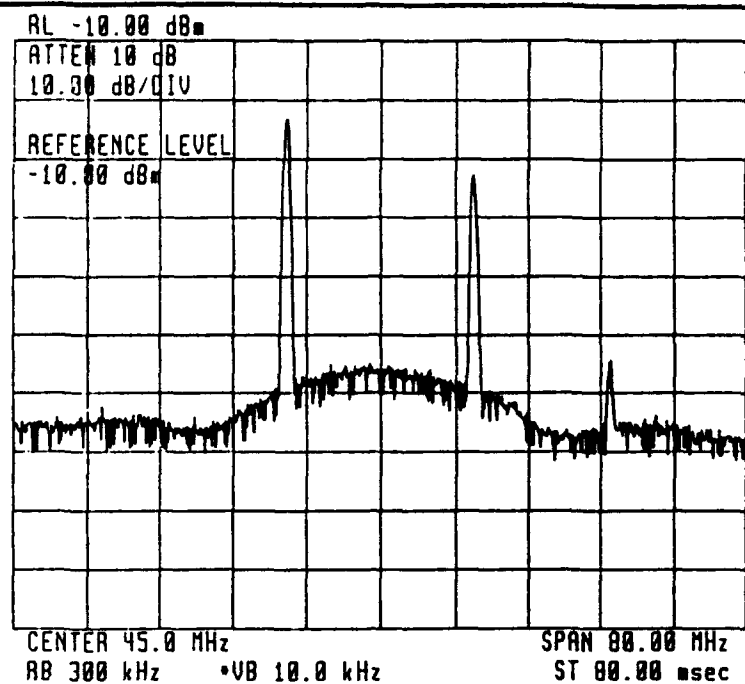
Figure 35 Case 10 with two jammers (JSR = 27 dB @ 35 MHz; JSR = 17 dB @ 55 MHz) (a) before adaptation, (b) after 10 iterations.

RL -10.00 dBm
ATTEN 10 dB
10.00 dB/DIV

REFERENCE LEVEL
-10.00 dBm

CENTER 45.0 MHz   SPAN 80.00 MHz
RB 300 kHz   •VB 10.0 kHz   ST 80.00 msec

RL -10.00 dBm
ATTEN 10 dB
10.00 dB/DIV

REFERENCE LEVEL
-10.00 dBm

CENTER 45.0 MHz   SPAN 80.00 MHz
RB 300 kHz   •VB 10.0 kHz   ST 80.00 msec

Figure 35 (cont'd) Case 10 (c) after 100 iterations, (d) after 110 iterations.

Figure 36 Frequency response of ACT PTF for Case 10.

5-29

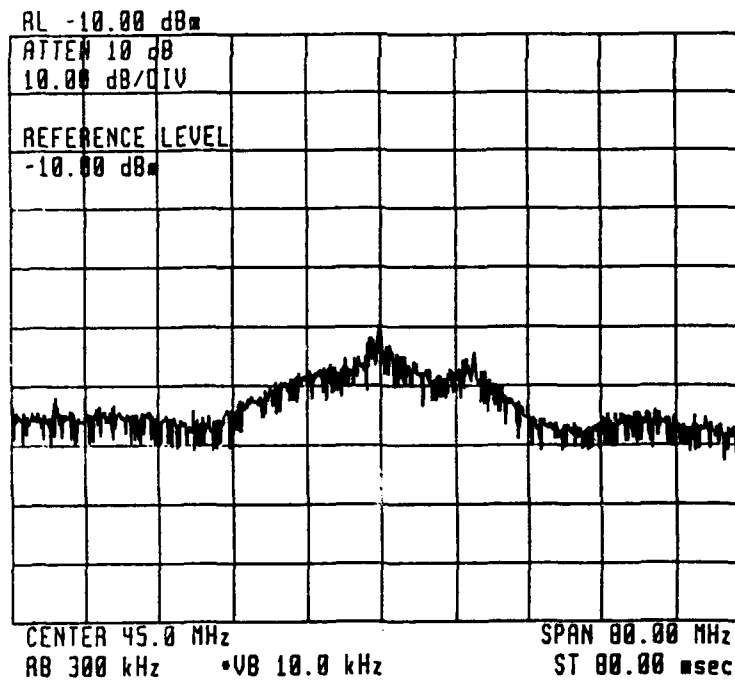frequency. Two separate trials were performed with Case 10. The results contained in the learning curves of Figure 37 were from the non-looping case, where only 10 iterations were conducted. Again, the 70 MHz harmonic within the first side-band is present in Case 7. From the results, one can conclude that, again, power levels are the subject of interest, not frequencies. The before and after spectra in Figure 35 were derived from the looping case. From the plots, one finds that after 10 iterations, the stronger powered signal is all but completely removed (notched by 52 dB), while the weaker signal is only reduced by about 3 dB. This is because of the larger gradient value of the stronger 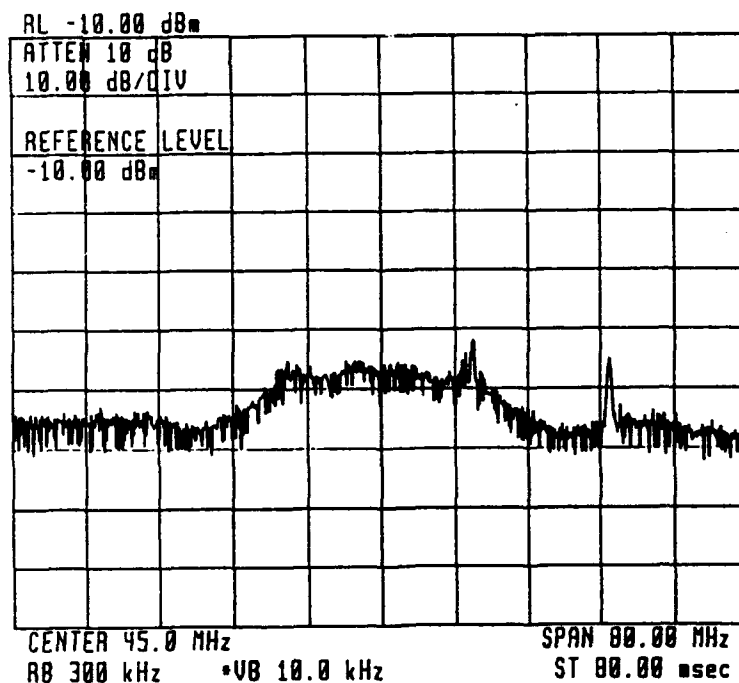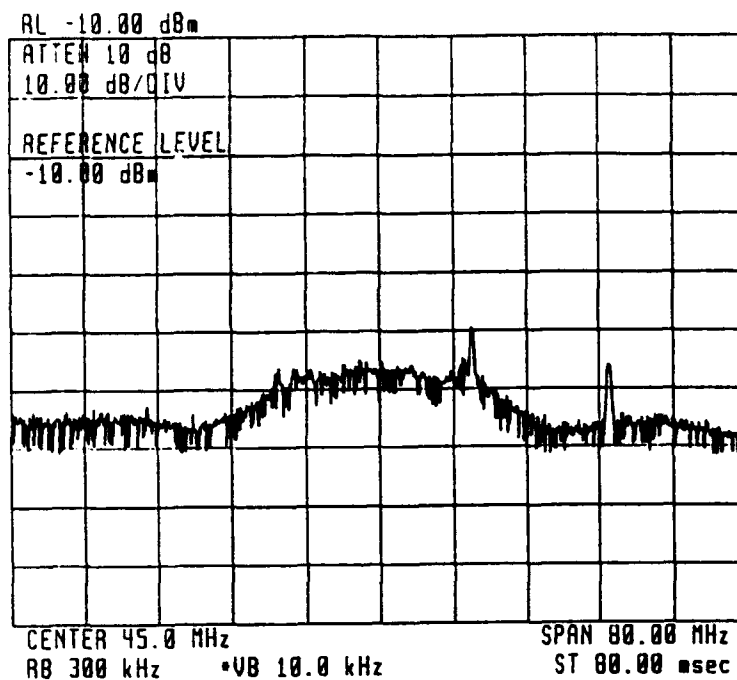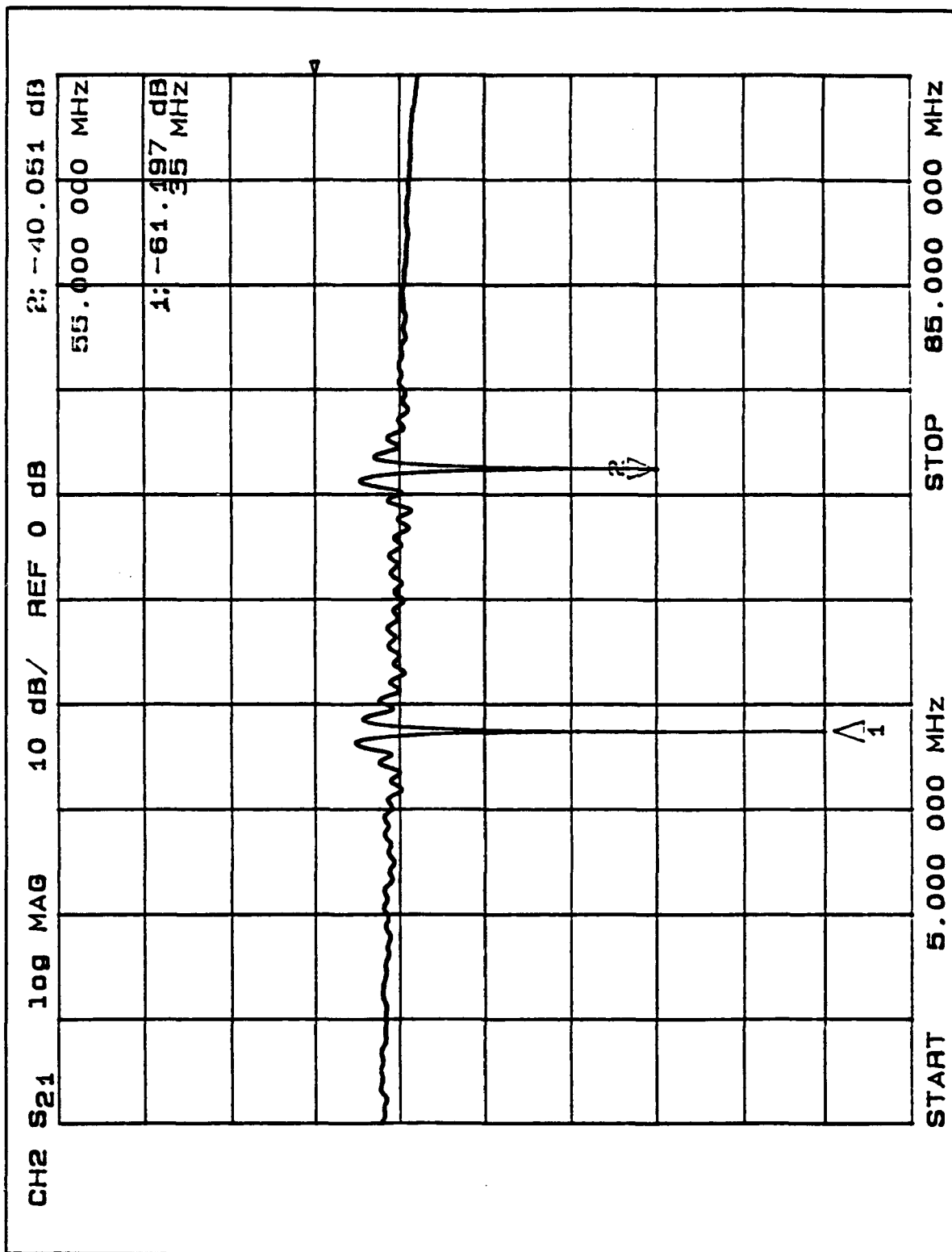jamming tone input into the AIS system. Therefore, the adaptive system responds proportionally to these stronger signals to minimize the mean-square error.

Figure 35(c) is a plot of Case 10 after 100 iterations were conducted. It is now seen that the tone at 55 MHz is rejected by 26 dB. After 110 iterations (Figure 35(d)), the notch is 29 dB. It is apparent, then, that because the weaker tone is 10 dB less than the stronger tone, it took approximately 10 times longer to notch (100 iterations versus 10 iterations). Even when the AIS system had notched the stronger jamming signal at 35 MHz below the level of the weaker jammer at 55 MHz, it continued to work on the stronger jammer because its input signal strength to the AIS system is still larger then the weaker jammers' input. It only appears that adaptive system notched the stronger jammer completely before notching the weaker signal. It was simply the result of the relative time the system took to notch the 10-dB weaker signal. Figure 36 illustrates the frequency response of the ACT PTF after 110 iterations. The notches agree precisely with those found in the spectral plots of Figure 35. The 3-dB bandwidths in this case appear to be approximately 1 MHz. In addition, the rest of the spectrum is relatively free from obstruction. As already alluded to, Figure 37 contains the learning curves for Case 8-10. Again, consistency in the level of the relative mean-square error verses iteration is demonstrated.

Case 11 is a repeat of Case 10 except that a faster convergence parameter was selected to perform the iterations. Although no spectral plots were obtained, the learning curves in Figure 38 clearly show the effect of more finely tuning this parameter to enable a faster convergence.

Case 12 repeats Case 2 using a different length PN sequence in the DS/SS signal. The R13 (8095 bits long) sequence was replaced with an R5 (31 bits long) to ascertain whether shorter-length repeating PN
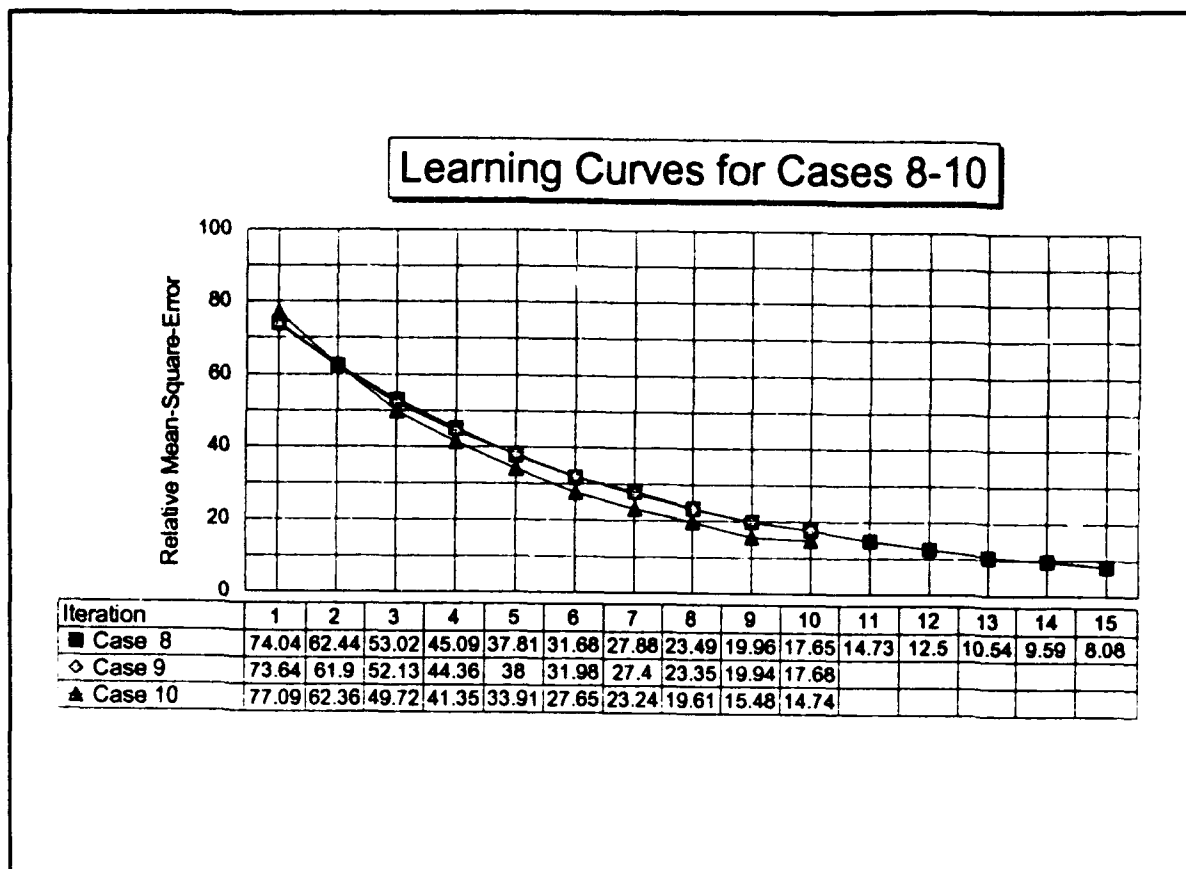
Figure 37 Learning curves for Cases 8-10.

sequences could be predicted by the adaptive filter any easier than the longer code. From the plots in Figure 39, the answer is no. The notch produced in Case 12 was 42 dB compared with 43 dB in Case 2. One can also see from a plot of the learning curves (Figure 40) that the two practically overlay each other.

Case 13 examines the effect of using fewer taps in the PTF's. Case 13 repeats Case 2 except the number of taps was reduced from 100 to 15 (taps 113 to 127). It was expected that the adaptive process would be much slower, which the learning curves in Figure 41 confirm. It is concluded that even though the time for an iteration with 15 taps is significantly less (5.25 seconds versus 35 seconds), the relatively accomplishment of each iteration towards rejecting the tone interferer was correspondingly less successful. It is presumed from extending out the error signals resulting from each iteration with the 15-tap case, that the 100-tap adaptive filter

5-31

Learning Curves for Cases 10 & 11

Iteration	1	2	3	4	5	6	7	8	9	10	11	12	13	14	15
■ Case 10	77.09	62.36	49.72	41.35	33.91	27.65	23.24	19.61	15.48	14.74					
◇ Case 11	77.18	47.54	30.27	20.96	13.99	10.01	7.36	7.05	6.34	5.97	5.7	5.76	5.39	5.84	4.94
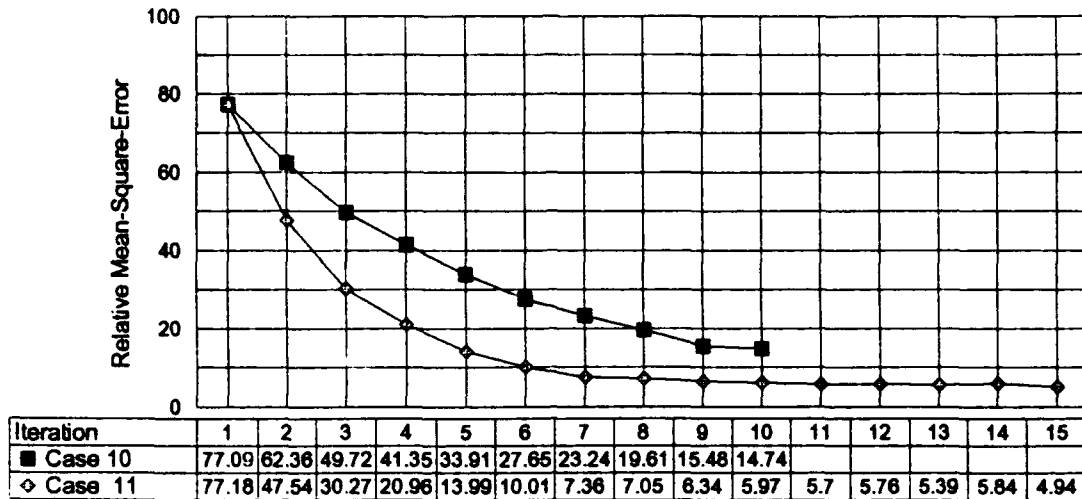
Figure 38 Learning curves comparing Cases 10 & 11 with two different convergence parameters.

would be faster (overall) than the 15-tap comparable system. Additionally, a narrower notch bandwidth and a deeper null can be achieved by using more taps (with the same tap spacing).

Table 3 is a summary of the values representing the learning curves for each case. The value indicated at each iteration is the RMS value of 100 samples of the squared-error signal output from the four-quadrant multiplier, one sample for each of the 100 taps. To explain what *relative* mean-square error denotes, it is first pointed out that the signal output from the summer (at J5) in Figure 20 is the error signal (eventually the remaining desired signal), while the output from the 4-quadrant multiplier is the squared-error. The A/D converter reads the power signal output from the 4-quadrant multiplier, then quantizes this squared-error signal using 12 bits (4096 levels or ± 2048 levels) with a full-scale voltage level of ± 10 V. Obtaining the precise error signal for these learning curves must also take into consideration the 10 dB of gain from the A/D

Figure 39 Case 12 before and after adaptation spectra (JSR = 20 dB, δω = 0). The prevailing notch is 42 dB.
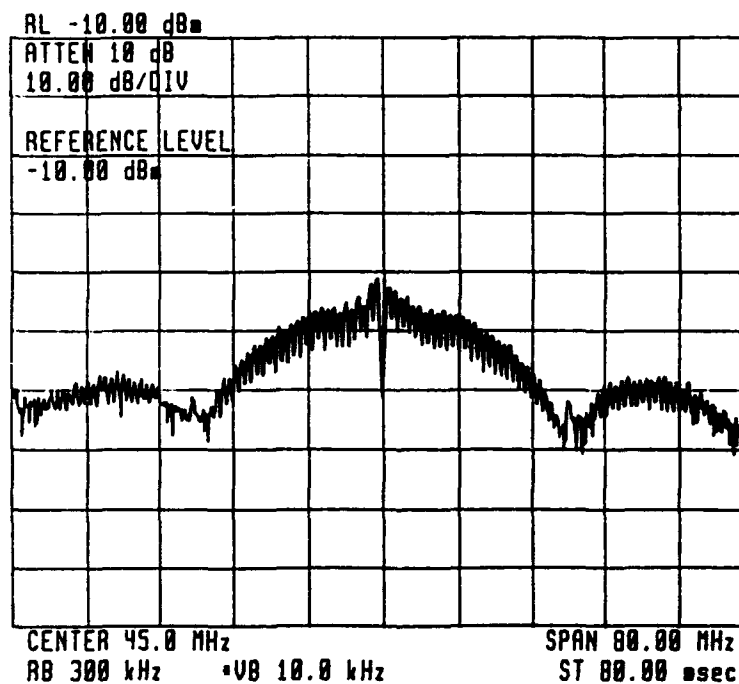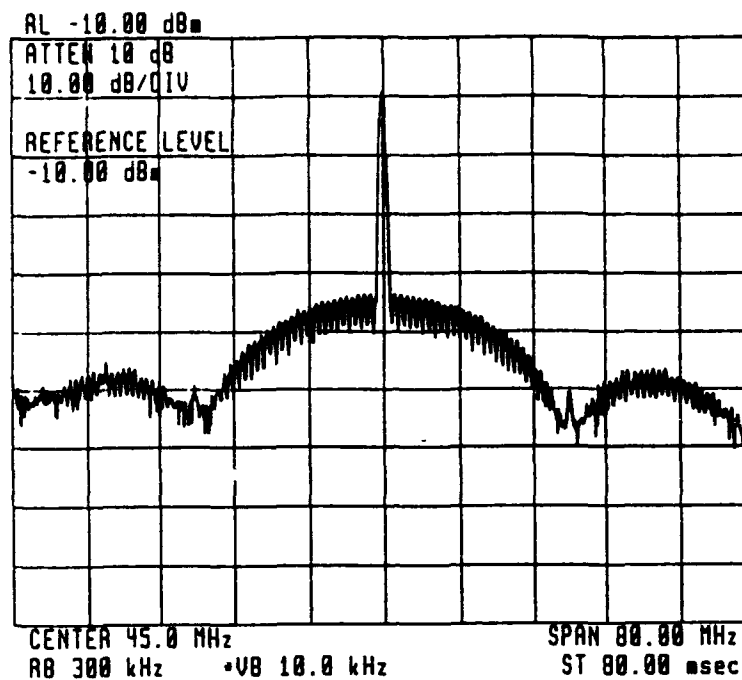
Learning Curves for Cases 2 & 12

Iteration	1	2	3	4	5	6	7	8	9	10	11	12	13	14	15
■ Case 2	167.27	102.92	66.23	41.96	27.85	16.71	10.88	5.88	3.46	3.12	2.36	1.94	1.57	2.02	2.36
◇ Case 12	174.64	105.81	66.11	39.6	26.59	15.3	10.47	6.07	3.39	2.33	1.59	1.6	1.49	1.39	
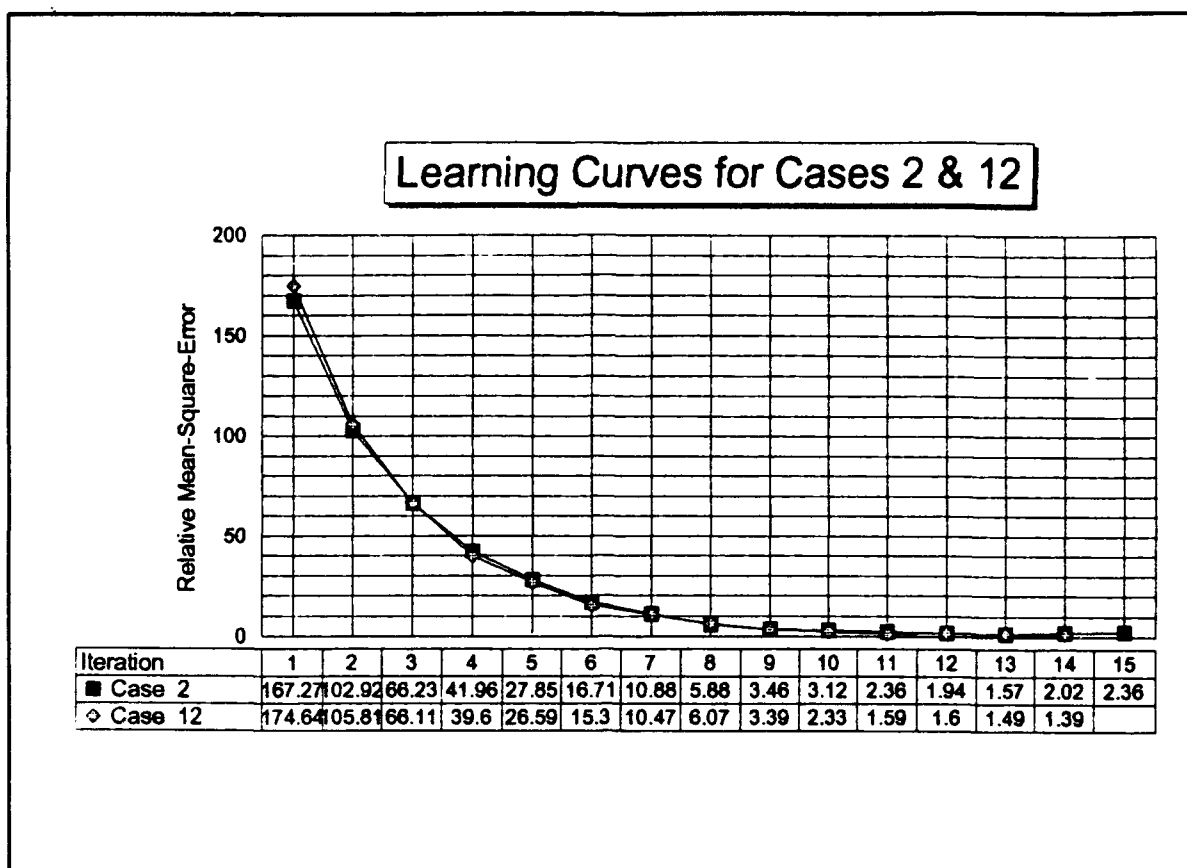
Figure 40 Learning curves comparing Cases 2 & 12.

converter. Hence, for simplicity, relative values determined within W.A.V.E. were used to represent the mean-square-errors as depicted in the learning curves. Furthermore, it is seen from the coding in Figure 21 that the squared-error signal is normalized by subtracting out the mean value; a near zero relative mean-square error could not result otherwise since the desired DS/SS signal remains after the adaptation.

Cases 14 and 15 involved an attempt for the adaptive interference suppression system to counter narrowband FM jammers. In Case 14, a 10 kHz bandwidth FM signal centered at 48 MHz was notched completely (45 dB) by the AIS system. This is not surprising considering the the 3-dB bandwidth of the notches created by the ACT PTF in the sinusoidal jamming cases varied from 300 kHz to about 1 MHz. However, in Case 15 a 300 kHz bandwidth signal was generated at the carrier. Figure 42 reveals that after 10 iterations the PTF had created a notch that did not completely eliminate the narrowband jammer. Since no further iterations

Learning Curves for Cases 2 & 13

Iteration	1	2	3	4	5	6	7	8	9	10
■ Case 2	167.27	102.92	66.23	41.96	27.85	16.71	10.88	5.88	3.46	3.12
◇ Case 13	173.26	163	152.02	142.71	133.23	125.92	118.46	111.02	104.56	96.18
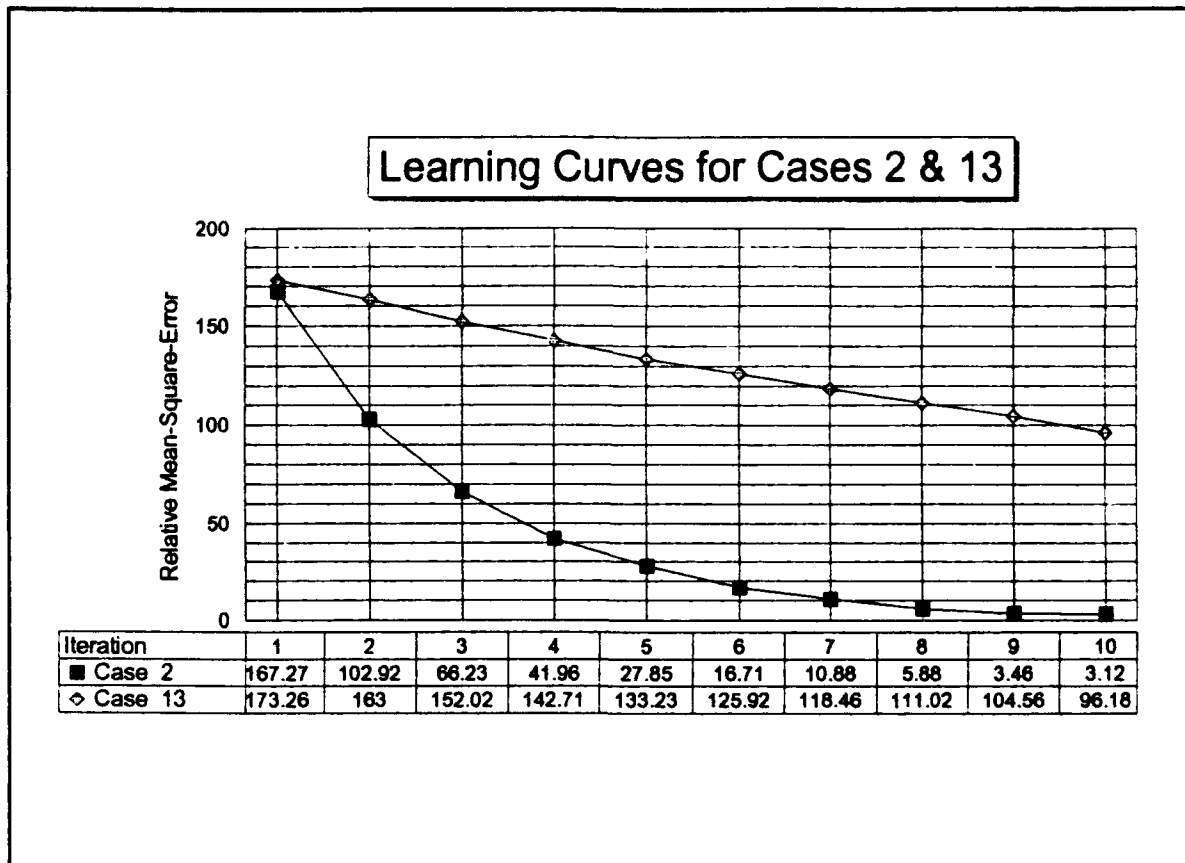
Figure 41 Comparison of learning curves for Case 2 & 13.

were carried out, it can only be presumed that the notch would have developed such that it would have eventually elimated the jammer. Unfortunately, the power levels of the FM jammers were not recorded.

To compare the theoretical improvement factors of a comparable system model of [6] to that obtained by experimentation, the following analysis is made. From Equation (28) in Chapter 3, when the jammer is located at the carrier of the DS/SS signal, $\Omega T = 0$, and Equation (28) can be solved simply for G_I. Applying l'Hospital's rule, the terms sin $(L\Omega T)/\sin(\Omega T)$ reduce to L; therefore, the solution to Equation (28) can be derived as

Table 3 RMS Error Signals for Each Case at Each Iteration

| Iteration	Case 1	Case 2	Case 3	Case 4	Case 5	Case 6	Case 7	Case 8	Case 9	Case 10	Case 11	Case 12	Case 13
1	178.27	167.27	166.92	170.34	161.75	153.54	191.42	74.04	73.64	77.09	77.18	174.64	173.26
2	51.39	102.92	102.67	106.78	106.91	105.96	98.76	62.44	61.9	62.36	47.54	105.81	163
3	88.21	66.23	67.61	67.05	72.31	73.05	54.09	53.02	52.13	49.72	30.27	66.11	152.02
4	55.12	41.96	41.73	42.75	47.96	55.04	30.25	45.09	44.36	41.35	20.96	39.6	142.71
5	33.31	27.85	28.33	23.93	31.46	37.09	17.47	37.81	38	33.91	13.99	26.59	133.23
6	23.93	16.71	16.65	14.18	21.11	26.19	9.12	31.68	31.98	27.65	10.01	15.3	125.92
7	12.18	10.88	11.69	8.54	15.37	18.62	3.47	27.88	27.4	23.24	7.36	10.47	118.46
8	6.92	5.88	6.32	7.12	9.64	10.95	3.04	23.49	23.35	19.61	7.05	6.07	111.02
9	5.52	3.46	4.08	5.37	4.93	6.75	2.14	19.96	19.94	15.48	6.34	3.39	104.56
10	4.13	3.12	2.71	4.51	2.68	4.7	1.96	17.65	17.68	14.74	5.97	2.33	96.18
11	2.5	2.36	1.51	2.48	2.21	4.01	1.49	14.73			5.7	1.59	
12	1.78	1.94	1.59	2.07	2.31	3.84		12.5			5.76	1.6	
13	1.76	1.57	1.74	2.46	1.49	3.68		10.54			5.39	1.49	
14		2.02	1.97	1.69	1.73	2.93		9.59			5.84	1.39	
15		2.36	1.23	1.79	1.94	3.03		8.08			4.94		
16					1.71	2.24							
17													
18													
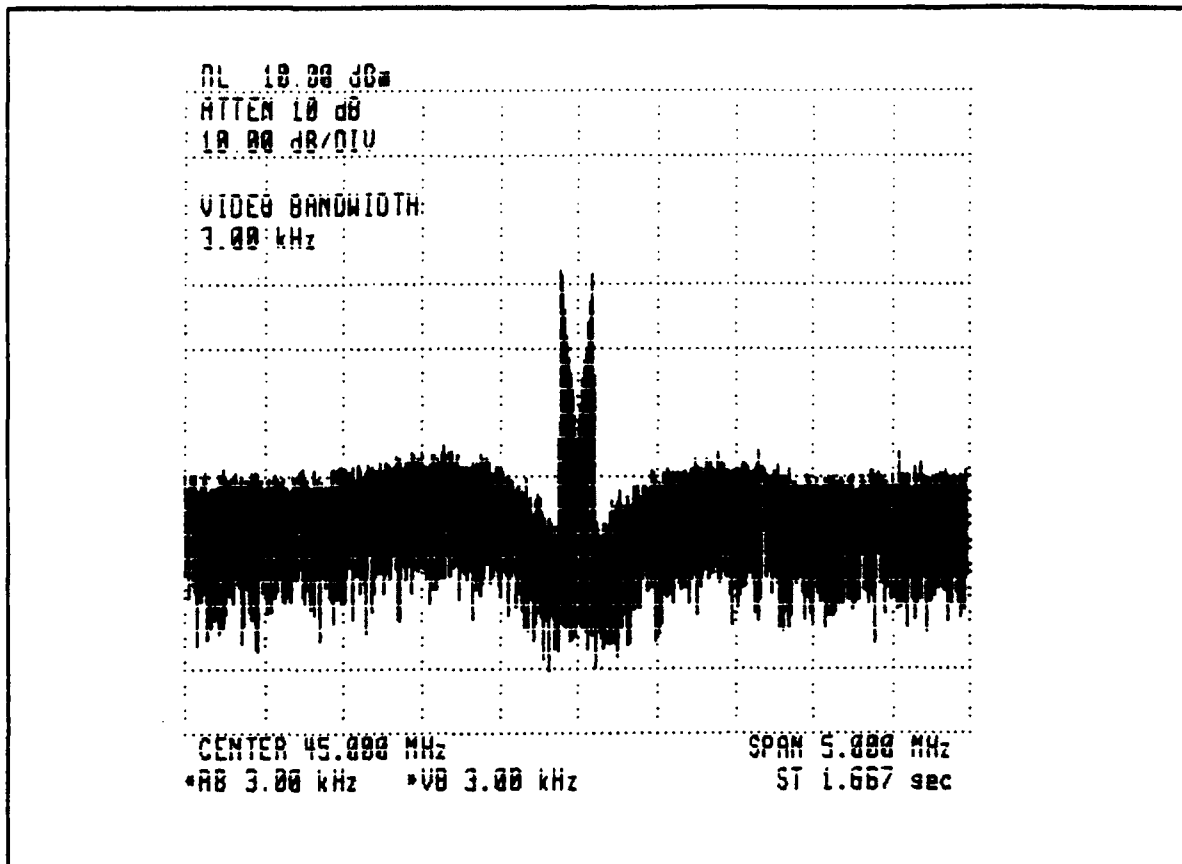
Figure 42 Case 15: The notch created after 10 iterations on a 300 kHz bandwidth FM jammer centered at the carrier frequency.

$$G_1 = \left[1 + \frac{J}{2S}(L + L) \right] \frac{L + \frac{2S}{J} - L}{L + \frac{2S}{J} - L\cos0}$$

$$= 1 + \frac{JL}{S}$$

(56)

Since J/S is usually much greater than one (not to mention the additional effect that the number of taps provides in Equation (56)),

$$G_1 \approx \left(\frac{J}{S}\right)L$$

(57)

Therefore, one can see that the expected comparable SNR improvement should exceed the JSR by an amount equal to the number of taps in the PTF. For example, if L = 100, it is seen that for a 30 dB JSR at the carrier,

5-37

we can expect to achieve approximately 50 dB of suppression (assuming the tap weight resolution of the PTF would allow for such a notch depth). Also, from Equation (30), it is found that for the two-sided interpolating filter structure at the carrier that

$$G_2 = 1 + \frac{J}{2S}\left[2N - 1 + 2N + 1\right] = 1 + \frac{J}{S}(2N)$$
$$\approx \frac{J}{S}(2N); \qquad \text{where } 2N = L - 1.$$

(58)

Essentially, the two filter structures yield equivalent results when the jammer is located at the carrier. Figure 43 is a plot of the theoretical SNR improvement expected for the two filter structures for L = 10 and frequency offsets from the carrier up to 90°.

Table 4 contains the results of applying Equation (28) to Cases 1-7 and compares the results to those obtained through experimentation. The conclusion is that the system implemented in this thesis worked better than the calculated results from the system model in [6]. The reason for this situation may reside in the fact that this system does not conform rigidly to the framework for which Equations (28) and (30) were derived [6]. The differences in the systems can be summarized as follows:

(1) Their system utilized only one PTF in the conventional implementation of the LMS adaptive interference canceler, and this at baseband; ours uses two PTF's with a "modified" LMS configuration at IF;

(2) Their system set the tap spacing of the PTF equal to both the chip duration of the PN sequence and the sampling interval in order to assure a de-correlation of the PN sequence amoung the taps such that the PTF could not predict the DS/SS signal; our system did not attempt to set the tap spacing equal to the chip duration but simply introduced a shift of one chip for the signals entering the PTF and SDL with respect to the direct path to obtain decorrelation.

(3) Their system was updated with each successive input signal sample; ours was updated after receiving a large number of input samples because of the sequential method of updating the taps and because of the high input sampling rate of the ACT PTF. Hence, in out system, the chip duration T_c (= 50 ns) is not equal to the sampling interval T_s (= 1/358 MHz = 2.8 ns); therefore, their frequency offset as seen in Figure 42,

which was equal ΩT_c, is not the same as our definition of the frequency offset. For example, in their framework $\Omega = 0$ represents a jammer located at the carrier frequency of the DS/SS signal. In our case, a jammer located at the carrier, using their framework, yields a $\Omega T_c = 14°$ and a $\Omega T_s = 0.79°$.
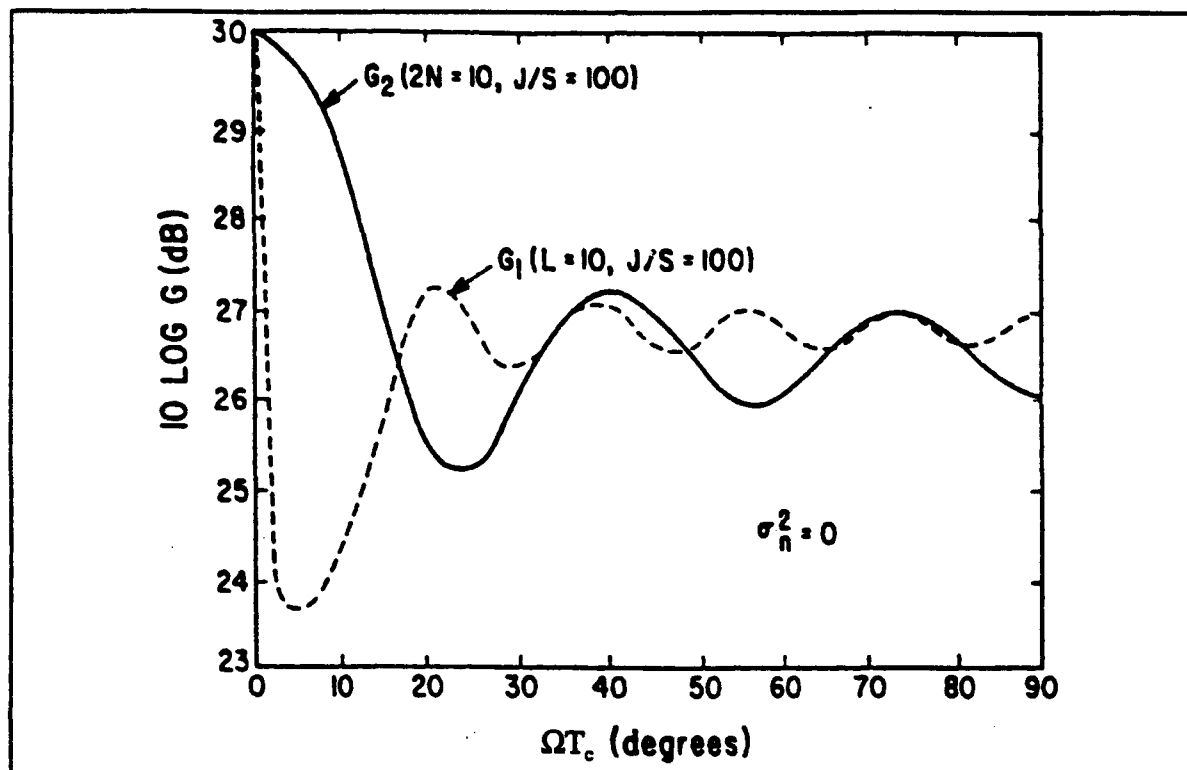

Figure 43 Theoretical SNR improvements for the two LMS PTF filter structures for an arbitrary filter length and JSR when $\sigma_n^2 = 0$ [6].

Table 4 Comparison of Predicted and Resulting SNR Improvement Factors

	Case 1	Case 2	Case 3	Case 4	Case 5	Case 6	Case 7
G_t according to Eq. (28) (dB)	30	40	50	46.89	46.99	46.95	36.99
G_t from experiments (dB)	38	43	56	55	55	56	52

VI. Conclusions and Recommendations for Further Study

6.1 Conclusions

The adaptive interference suppression system tested in this research performed admirably in a number of respects. First, the system was able to successfully notch single-tone jammers anywhere within the DS/SS passband, including jammers located at the critical carrier frequency. The depth of the resulting notches was as high as 56 dB. Second, in all cases, the achieved SNR improvement with the ACT adaptive interference system in place exceeded what was expected from the theoretical calculations of a similar LMS adaptive interference suppression configuration. The 3-dB notch bandwidths obtained were as low as 300 kHz and never exceeded approximately 1 MHz. These narrow notch bandwidths helped to spare the DS/SS signal from excessive degradation. Finally, it was also determined from frequency response plots of the PTF after adaptation that minimal degradation was inflicted upon the spread spectrum system outside the notch vicinity. Based on these results, and from results obtained in [10], it is estimated that if the complete SS receiver were built and probability of bit error measurements taken, that the results would have been close to that of a SS system where no jamming were present and no adaptive interference system were in place.

It was also found that the number of iterations needed for convergence was remarkably low for a system employing the LMS adaptive algorithm. For all single-jammer cases, convergence was met within 10-15 iterations. Dual jammer cases took somewhat longer, depending on the power levels of the jammers. The number of iterations ranged from approximately 20 to 100. The main system performance factor that could have used substantial improvement was the time per iteration (35 seconds for 100 taps). Chapter 5 contains a discussion as to why this was so and how it could be improved. The ultimate solution was brought up in a discussion with Dr Vigil from EDI, Inc. The long term solution is to build a dedicated ACT PTF that incorporated, on chip, the LMS algorithm. In this case, a parallel updating of the tap weights via only one ACT PTF with the LMS algorithm built right onto the chip would provide superior results. Combined with the 8-bit tap weight resolutions of the latest ACT technology, a highly versatile and successful adaptive interference rejection subsystem is envisioned.

6-1

6.2 Recommendations for Further Study

It is recommended that another adaptive algorithm, although more difficult to implement than the LMS, be adopted such that adequate results can be obtained from using only one ACT PTF (or any other PTF-type). A viable candidate algorithm is the *random search algorithm.*

Another possible research suggestion is to find some other device technology which could provide more dynamic range or greater notch depths, *i.e.* fiber-optic PTFs [33]. These PTFs have already demonstrated 70+ dB of notch depth.

A more practical follow-on topic to this work would be to either build the spread spectrum receiver (correlator) or use some spread spectrum modems in order to take probability of error (P_b) measurements for the system tested in this research. This is in addition to the steps that should be taken to optimize the convergence times as mentioned in Chapter 5. The system should be further tested against other jamming signals such as swept tones, pulse tones, narrow-band Gaussian noise jammers, or combinations thereof.

The primary performance criteria for the P_b tests is the P_b verses E_b/N_o curves. The following curves should be generated for comparison purposes:

(1) *Theoretical BPSK;*

(2) *Adaptive system off* (all weights set to "0" with no jammer);

(3) *Adaptive system on* (with no jammer);

(4) 10-dB JSR;

(5) 20-dB JSR;

(6) 30-dB JSR;

(7) *Jammer on with no adaptive system* (all three JSRs should cause a P_b of 0.5).

For P_b tests AWGN must be added to the input of the AIS system so that E_b/N_o can be calculated and the corresponding curves generated. It would also be necessary to add an attenuator to adjust E_b/N_o by leaving the noise constant and adjusting E_b. This is necessary in order to derive the P_b versus E_b/N_o curves. Of course,

it is necessary to coherently demodulate the spread spectrum signal to baseband (or to an IF frequency), synchronously despread the recovered PN sequence with a correlator to extract the message sequence, and then perform comparisons of received versus generated data to calculate P_b .

References

1. Lawrence L. Gutman and Glenn E. Prescott, "System Quality Factors for LPI Communications," *1989 International Conference on Systems Engineering*, 26 August 1989.

2. Laurence B. Milstein and Ronald A. Iltis, "Signal Processing for Interference Rejection in Spread Spectrum Communications," *IEEE ASSP Magazine*, pp. 18-31, March 1986.

3. Laurence B. Milstein, "Interference Rejection Techniques in Spread Spectrum Communications," *Proceedings of the IEEE*, Vol. 76, No. 6, pp. 657-671, June 1988.

4. Frank M. Hsu and Arthur A. Giordano, "Digital Whitening Techniques for Improving Spread-Spectrum Communications Performance in the Presence of Narrow-Band Jamming and Interference," *IEEE Trans. on Comm.*, Vol. COM-26, No.2, pp. 209-216, February 1978.

5. John W. Ketchum and John G. Proakis, "Adaptive Algorithms for Estimating and Suppressing Narrow-Band Interference in PN Spread-Spectrum Systems," *IEEE Trans. on Comm.*, Vol. COM-30, No.5, pp. 913-924, May 1982.

6. Loh-Ming Li and Laurence B. Milstein, "Rejection of Narrow-Band Interference in PN Spread-Spectrum Systems Using Transversal Filters," *IEEE Trans. on Comm.*, Vol. COM-30, No.5, pp. 925-928, May 1982.

7. Ronald A. Iltis and Laurence B. Milstein, "Performance Analysis of Narrow-Band Interference Rejection Techniques in DS Spread-Spectrum Systems," *IEEE Trans. on Comm.*, Vol. Com-32, No.11, pp.1169-1177, November 1984.

8. Gary J. Saulnier, P.K. Das, and Laurence B. Milstein, "Suppression of Narrow-Band Interference in a PN Spread-Spectrum Receiver Using a CTD-Based Adaptive Filter," *IEEE Trans. on Comm.*, Vol. COM-32, No.11, pp.1227-1232, November 1984.

9. ____, "An Adaptive Digital Suppression Filter for Direct-Sequence Spread-Spectrum Communications," *IEEE Journal on Sel. Areas in Comm.*, Vol. SAC-3, No.5, pp.676-685, September 1985.

10. Gary J. Saulnier, "Interference Suppression Using a SAW-Based Adaptive Filter," *Conference Record IEEE MILCOM '90*, Monterey, CA, Sep 30-Oct 3, 1990, pp.970-974.

11. ____, "Suppression of Narrowband Jammers in a Spread-Spectrum Receiver Using Transform-Domain Adaptive Filtering," *IEEE Journal on Sel. Areas in Comm.*, Vol. SAC-10, No.4, pp.742-749, May 1992.

12. John Gevargiz, P.K. Das, and Laurence B. Milstein, "Adaptive Narrow-Band Interference Rejection in a DS Spread-Spectrum Intercept Receiver Using Transform Domain Signal Processing Techniques," *IEEE Trans. on Comm*, Vol. 37, No.12, pp.1359-1366, December 1989.

13. Sorin Davidovici and Emmanuel G. Kanterakis, "Narrow-Band Interference Rejection Using Real-Time Fourier Transforms," *IEEE Trans. on Comm.*, Vol. 37, No.7, pp.713-722, July 1989.

14. Laurence B. Milstein and P.K. Das, "An Analysis of a Real-Time Transform Domain Filtering Digital Communication System--Part I: Narrow-Band Interference Rejection," *IEEE Trans. on Comm.*, Vol. COM-28, No.6, pp.816-824, June 1980.

15. Francis A. Reed and Paul L. Feintuch, "A Comparison of LMS Adaptive Cancellers Implemented in the Frequency Domain and the Time Domain," *IEEE Trans. on Acoustics, Speech, and Signal Processing,* Vol. ASSP-29, No.3, pp.770-775, June 1981.

16. Michael M. Shepard, *The Performance of a PN Spread Spectrum Receiver Preceded by an Adaptive Interference Suppression Filter.* MS Thesis, AFIT/GE/EE/82-62. School of Engineering, Air Force Institute of Technology (AU), Wright-Patterson AFB OH, December 1982.

17. John R. Way, Jr, *The Performance of a New Adaptive Filter For Digital Communications.* MS Thesis, AFIT/GE/EE/84S-12. School of Engineeriing, Air Force Institute of Technology (AU), Wright-Patterson AFB OH, June 1984, AAJ-3819.

18. George S. Mikulanicz, *Performance of an Acoustic Charge Transport (ACT) Programmable Tapped Delay Line (PTDL) for Signal Processing Applications.* MS Thesis, AFIT/EN/GE90D-40. School of Engineering, Air Force Institute of Technology (AU), Wright-Patterson AFB OH, December 1990.

19. Robert C. Dixon, *Spread Spectrum Systems,* 2nd Ed., John Wiley & Sons, New York, 1984.

20. George R. Cooper and Clare D. McGillem, *Modern Communications and Spread Spectrum,* McGraw-Hill, New York, 1986.

21. Don J. Torrieri, *Principles of Secure Communication Systems,* 2nd Ed., Artech House, Norwood, MA, 1992.

22. Bernard Widrow and Samuel D. Stearns, *Adaptive Signal Processing,* Prentice-Hall, Inc., Englewood Cliffs, N.J., 1985.

23. Samuel D. Stearns and Ruth A. David, *Signal Processing Algorithms,* Prentice-Hall, Inc., Englewood Cliffs, N.J., 1988.

24. Simon Haykin, *Introduction to Adaptive Filters,* MacMillan Publishing Co., New York, 1984.

25. Robert L. Miller, Carl E. Nothnick, and Dana S. Bailey, *Acoustic Charge Transport: Device Technology and Applications,* Artech House, Norwood, MA, 1992.

26. John H. Cafarella, "Programmable Transversal Filters: Appliications and Capabilities," *1987 IEEE Ultrasonics Symposium Proceedings,* New York: IEEE, 1987, pp.31-42.

27. Rick W. Miller and Robert J. Kansy, "Acoustic Charge Transport Digitally Programmable Transversal Filter Development," *1990 IEEE MTT-S Symposium Proceedings,* Vol. 3, pp. 1111-1114, May 1990.

28. Frank Goodenough, "IC Signal Processor Runs 45 Billion MACs/s," *Electronic Design,* July 23, 1992.

29. Seminar notes, "Acoustic Charge Transport Technology: Principles and Applications," Comlinear Corp., Urbana, Il., Oct.-Nov. 1992.

30. Bernard Widrow and John M. McCool, "A Comparison of Adaptive Algorithms Based on the Methods of Steepest Descent and Random Search," *IEEE Trans. on Antennas and Propagation,* Vol. AP-24, No. 5, pp. 615-637, Sept 1976.

31. Herbert Taub and Donald L. Schilling, *Principles of Communications Systems*, 2nd Ed., McGraw-Hill, New York, 1986.

32. Bernard Sklar, *Digital Communication: Fundamentals and Applications*, Prentice-Hall, Inc, Englewood, NJ, 1988.

33. M.H. Berry and D.M. Gookin, "2.0 GHz Sampling Rate Transversal Filter," *Proceedings of the 23rd Annual Asilomar Conference on Circuits, Systems, and Computers*, Pacific Grove, CA, Oct 30-Nov 1, 1989, v1, Maple Press, San Jose, CA, pp. 294-296.

Vita

Capt Michael S. Mills was born on 29 January 1961, at Eglin Air Force Base, Florida. He graduated from Ben Davis Senior High School in Indianapolis, Indiana and is an alumni of the Southern Illinois University at Edwardsville (SIU-E). Upon graduation from SIU-E, he was assigned to the Foreign Technology Division (FTD) of Air Force Material Command (now known as the Foreign Aerospace Science and Technology Center (FASTC)), as an electronic warfare technology analyst until entering the Graduate School of Engineering, Air Force Institute of Technology, in May 1992.

Permanent address: 1042 S. Prairie Depot
                         Indianapolis, Indiana 46234

REPORT DOCUMENTATION PAGE

Form Approved
OMB No 0704-0188

1. AGENCY USE ONLY (Leave blank)	2. REPORT DATE December 1993	3. REPORT TYPE AND DATES COVERED Master's Thesis

4. TITLE AND SUBTITLE
EVALUATION OF AN ACOUSTIC CHARGE TRANSPORT (ACT) DEVICE FOR ADAPTIVE INTERFERENCE SUPPRESSION IN SPREAD SPECTRUM COMMUNICATIONS SYSTEMS

5. FUNDING NUMBERS

6. AUTHOR(S)
Michael S. Mills, Capt, USAF

7. PERFORMING ORGANIZATION NAME(S) AND ADDRESS(ES)
Air Force Institute of Technology, WPAFB OH 45433-6583

8. PERFORMING ORGANIZATION REPORT NUMBER
AFIT/GE/ENG/93D-27

9. SPONSORING / MONITORING AGENCY NAME(S) AND ADDRESS(ES)
Lawrence Gutman, WL/AAAI, Wright-Patterson AFB OH 45433

10. SPONSORING / MONITORING AGENCY REPORT NUMBER

11. SUPPLEMENTARY NOTES

12a. DISTRIBUTION / AVAILABILITY STATEMENT

Approved for public release; distribution unlimited

12b. DISTRIBUTION CODE

13. ABSTRACT (Maximum 200 words)
Analytical results have shown that adaptive filtering can be a powerful tool for the rejection of narrowband interference in a direct sequence spread spectrum receiver. However, the complexity of adaptive filtering hardware has hindered the experimental validation of these results. This theseis describes a unique adaptive filter architecture for implementing the Widrow-Hoff Least-Mean-Square (LMS) algorithm using two state-of-the-art Acoustic Charge Transport (ACT) Programmable Transversal Filters (PTFs). Signal-to-noise ratio improvement measurements demonstrate the effectiveness of the adaptive filter for suppressing single- and dual-tone jammers at jammer-to-signal ratios (JSRs) of up to 30 dB. It is shown that the ACT adaptive interference rejection system can consistently produce 55 dB notch depths with 3-dB bandwidths as low as 300 kHz with minimal degradation to the spread spectrum signal. It is also shown that the adaptive system can eliminate single tone jammers at any frequency within the spread spectrum bandwidth at any of 10, 20, or 30 dB JSRs within 10-15 iterations of the adaptive algorithm. The only drawback with the adaptive system as tested is the amount of time taken to perform an iteration because of the requirement to update the PTF tap weights sequentially. Suggestions are given as to how this particular parameter of the adaptive interference system could be optimized.

14. SUBJECT TERMS
Adaptive interference suppression, adaptive interference rejection, Least-Mean-Square (LMS) algorithm, acoustic charge transport (ACT), direct sequence spread spectrum, narrowband jammers, CW jammers

15. NUMBER OF PAGES
106

16. PRICE CODE

17. SECURITY CLASSIFICATION OF REPORT UNCLASSIFIED	18. SECURITY CLASSIFICATION OF THIS PAGE UNCLASSIFIED	19. SECURITY CLASSIFICATION OF ABSTRACT UNCLASSIFIED	20. LIMITATION OF ABSTRACT UL

NSN 7540-01-280-5500

Standard Form 298 (Rev 2-89)